

STABILITY OF AMORPHOUS PHARMACEUTICALS: CALORIMETRIC STUDIES



NAZIHA ALEM

**A THESIS SUBMITTED IN PARTIAL FULFILMENT OF THE
REQUIREMENTS FOR THE DEGREE OF DOCTOR OF PHILOSOPHY**

UNIVERSITY OF LONDON SCHOOL OF PHARMACY

29-39 BRUNSWICK SQUARE

LONDON

WC1 1AX

2010



ProQuest Number: 10104702

All rights reserved

INFORMATION TO ALL USERS

The quality of this reproduction is dependent upon the quality of the copy submitted.

In the unlikely event that the author did not send a complete manuscript and there are missing pages, these will be noted. Also, if material had to be removed, a note will indicate the deletion.



ProQuest 10104702

Published by ProQuest LLC(2016). Copyright of the Dissertation is held by the Author.

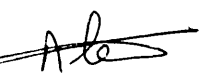
All rights reserved.

This work is protected against unauthorized copying under Title 17, United States Code.
Microform Edition © ProQuest LLC.

ProQuest LLC
789 East Eisenhower Parkway
P.O. Box 1346
Ann Arbor, MI 48106-1346

Plagiarism Statement

This thesis describes research conducted in the School of Pharmacy, University of London between Oct/2006 and Aug/2009 under the supervision of Dr Simon Gaisford and Prof Anthony Beezer. I certify that the research described is original and that any parts of the work that have been conducted by collaboration are clearly indicated. I also certify that I have written all the text herein and have clearly indicated by suitable citation any part of this dissertation that has already appeared in publication.

Signature: 

Date: 06/12/2010

Publications

Some parts of this thesis were published in the following articles:

- Alem, N., Beezer, A.E., Gaisford, S. 2010. *Quantifying the rates of relaxation of binary mixtures of amorphous pharmaceuticals with isothermal calorimetry*. International Journal of Pharmaceutics, 399, 12-18.
- Almeida e Sousa, L., Alem, N., Beezer, A. E., O'Neill, M. A. A., Clapham, D., Gaisford, S. 2010. *Quantitative Analysis of Solid-State Processes Studied With Isothermal Microcalorimetry*. Journal of Physical Chemistry A, 114, 13173-13178.

Abstract

The amorphous form can offer a solution to poor solubility of BCS Class II drugs thanks to its higher apparent solubility compared with the crystalline form. However, this advantage is severely compromised by the inherent instability of the amorphous state. The understanding and prediction of the behaviour of this solid form can offer a good strategy towards the rational development of stable amorphous formulations. The work undertaken in this thesis aimed at exploring certain aspects of amorphous form stability using mainly isothermal microcalorimetry (IMC).

The first area explored was the feasibility of using IMC to assess enthalpy relaxation of amorphous pharmaceutical materials. In the first study, relaxation profiles for amorphous indomethacin obtained by differential scanning calorimetry (DSC) and IMC were compared. The results showed that the two techniques measure the same molecular mobility as similar relaxation profiles were obtained.

In the second study, IMC was used to assess the enthalpy relaxation of two-component amorphous pharmaceutical systems. Simulated and real calorimetric data for pre-characterised 2-phase systems were fitted to 2- Kohlrausch-Williams-Watts (KWW) and 2- modified stretched exponential (MSE) models. The 2- KWW model was able to recover the correct relaxation parameters for simulated data but not for real calorimetric data due to inherent noise. The sensitivity of the MSE model seemed less prone to the effect of noise and any failings of this model to recover the expected values was taken as a sign of the two consisting components behaving differently from when they were aged individually.

In the second section of the thesis, the dynamic behaviours of amorphous α and β lactose were compared. Enthalpy relaxation of the two milled anomers was assessed by IMC. Glass transition (T_g) width measurements were conducted using DSC. Moisture-solid interactions were also assessed using dynamic vapour sorption (DVS). The two anomers showed different enthalpy relaxation profiles. T_g width was the same for both anomers and this could be due to significant mutarotation during DSC measurements. Water sorption isotherms revealed that the anomeric configuration can only affect the physical stability of amorphous lactose above the T_g .

In the last section, crystallisation from the amorphous state was explored using IMC. In the first study, the use of calculation methods based on the universal Sestak-Berggren equation to extract crystallisation parameters was examined. Calculation results were compared to those obtained by model-fitting approach. Simulated data revealed that a minimum of 15% data coverage is needed to recover the correct crystallisation parameters. Real data were obtained for crystallisation of indomethacin below its T_g ; no trend was observed in terms of the success of the calculation method. This could be attributed to inherent noise in real calorimetric data.

The second study of the last section examined the use of IMC to extract crystallisation kinetics of indomethacin above its T_g (60°C). Amorphous indomethacin was prepared either as film-like (AFI) or bulk (ABI) samples. Power-time profiles for two sample types were different reflecting differences in the crystallisation behaviours. This was speculated to be partly due to differences in the free surface areas between the two sample-types. AFI samples crystallisation at 60°C was also assessed with X-ray powder diffraction (XRPD) and polarised light microscopy (PLM). Quantitative analysis carried out with the Lorentzian model to deconvolute the calorimetric signal was reasonably consistent with the analysis undertaken with PLM and XRPD.

Acknowledgement

I would like to thank my supervisors Dr Simon Gaisford and Professor Anthony Beezer for their guidance throughout my PhD.

I would also like to thank:

- David McCarthy for PLM
- Dr Gary Parkinson for XRPD
- Dr Jeremy Cockcroft, UCL, for his helpful discussion
- Dr Paul Royall, King's College, for his helpful discussion
- Algerian Ministry for High Education and Research for funding the project

Many thanks go to my colleagues in the pharmaceuticals department: Peng, Mohammed, Hisham, Sulaf, Meena, Sunny, Katerina and Matthew.

I am also grateful to Hanene, the Burney family and my family for their constant help and support.

In the name of God, Most Gracious, Most Merciful.

“Proclaim! (or Read!) In the name of thy Lord and Cherisher, Who created, Created man, out of a (mere) clot of congealed blood, Proclaim! and thy Lord is Most Bountiful, He Who taught (the use of) the Pen, Taught man that which he knew not” The Quran 96, 1-5.

Table of Content

Plagiarism Statement	2
Publications.....	3
Abstract	4
Acknowledgement	5
Table of Content	6
List of figures.....	11
List of Tables	15
List of Abbreviations	17
<i>1) Chapter 1: Introduction</i>	<i>19</i>
1.1. Background.....	20
1.2. The crystalline state	21
1.3. Amorphous state	22
1.4. Advantages and disadvantages of amorphous form from a pharmaceutical perspective	22
1.4.1. Advantages.....	22
1.4.2. Disadvantages	24
1.5. Basic concepts of thermodynamics relating to the crystalline and amorphous states.	25
1.6. Properties of the amorphous state	27
1.6.1. The glass transition temperature (T_g).....	27
1.6.2. Fragility.....	28
1.6.3. Thermodynamic properties	29
1.7. Amorphous state formation.....	29
1.8. Relaxation phenomenon of amorphous state	32
1.9. Assessment of relaxation rate	32
1.9.1. Enthalpy relaxation measurement with DSC	34
1.9.2. Enthalpy relaxation measurement by IMC	36
1.10. Polyamorphism	38
1.11. Water interaction with the amorphous state.....	38
1.12. Water as a plasticiser.....	39
1.13. Crystallisation from the amorphous state.....	41
1.14. Factors affecting crystallisation from the amorphous state.....	46

1.14.1.	Thermodynamic factors	46
1.14.2.	Effect of additives	47
1.14.3.	Kinetic factors (molecular mobility).....	47
1.14.4.	Effect of sample preparation method	48
1.15.	Aims.....	48
2)	<i>Chapter 2: Materials and Methods</i>	52
2.1	Materials	53
2.2.	Methods.....	53
2.2.1.	Preparation of amorphous lactose and sucrose using spray-drying	53
2.2.1.1.	Introduction.....	53
2.2.1.2.	Experimental	54
2.2.2.	Preparation of amorphous lactose with ball milling	55
2.2.2.1.	Introduction.....	55
2.2.2.2.	Experimental	56
2.2.3.	Isothermal microcalorimetry	57
2.2.3.1.	Introduction.....	57
2.2.3.2.	Operating principle of heat conduction microcalorimetry	58
2.2.3.3.	Quantitative analysis of calorimetric data.....	60
2.2.3.4.	Experimental	61
2.2.4.	Calorimetric data analysis.....	62
2.2.5	Differential scanning calorimetry (DSC).....	62
2.2.5.1.	Introduction:.....	62
2.2.5.2.	Experimental	64
2.2.6.	Modulated temperature DSC (MTDSC)	65
2.2.6.1.	Introduction.....	65
2.2.6.2.	Experimental	66
2.2.7.	X-ray powder diffraction (XRPD)	67
2.2.7.1.	Introduction.....	67
2.2.7.2.	Experimental	68
2.2.8.	Dynamic vapour sorption (DVS)	68
2.2.8.1.	Introduction.....	68
2.2.8.2.	Experimental	69
2.2.9.	Other methods	70
2.2.9.1.	Thermal gravimetric analysis (TGA)	70

2.2.9.2. Polarised light microscopy	70
2.2.9.3. High performance liquid chromatography (HPLC)	70
2.2.9.4. Nuclear magnetic resonance (NMR)	71
3) <i>Chapter 3: Isothermal microcalorimetry as a tool to study enthalpy relaxation of pharmaceuticals.</i>	72
3.1. Introduction	73
3.2. Aims & Objectives	76
3.2.1. Section I	76
3.2.2. Section II	76
3.3. Experimental	77
3.3.1. Materials and methods	77
3.3.1.1. Section I	77
3.3.1.2 Section II	78
3.4. Results & Discussion	82
3.4.1 Section I	82
3.4.1.1. Effect of preparation method on thermal history	82
3.4.1.2. Enthalpy relaxation with IMC	84
3.4.1.3. Enthalpy relaxation by DSC	86
3.4.2. Section II	93
3.4.2.1. Simulated data	93
3.4.2.2. Experimental calorimetric data	94
3.4.2.3. General discussion	99
3.5. Summary	105
4) <i>Chapter 4: Effect of the anomeric form on the physical stability of amorphous lactose.</i> ..	107
4.1. Introduction	108
4.2. Aims and objectives	110
4.3. Experimental	110
4.3.1. Preparation of amorphous lactose	110
4.3.2. Characterisation of lactose samples	111
4.3.3. Structural relaxation with IMC	111
4.3.4. T _g width measurement with DSC	111
4.3.5. Dynamic Vapour Sorption	112
4.3.6. Statistical analysis	112
4.4. Results and discussion	112

4.4.1.	Characterisation of ball milled samples	112
4.4.1.1.	Amorphocity	112
4.4.1.2.	Anomeric composition.....	113
4.4.2.	Structural relaxation with IMC	114
4.4.3.	T _g width study	116
4.4.4.	Other thermal characteristics of amorphous lactose anomers	121
4.4.5.	Pre-T _g exothermic event.....	123
4.4.6.	Moisture-solid interactions	128
4.4.7.	Summary	135
5)	<i>Chapter 5: Crystallisation Studies with IMC-Development of a Calculation Method</i>	137
5.1.	Introduction.....	138
5.2.	Aims and objectives	141
5.3.	Materials and methods	141
5.3.1.	Preparation of amorphous indomethacin	141
5.3.2.	Isothermal microcalorimetric measurements	142
5.3.3.	Simulation of calorimetric data for solid-state reactions	142
5.3.4.	Theoretical development.....	144
5.4.	Results and Discussion.....	148
5.4.1.	Application of calculation method to simulated data.....	148
5.4.2.	Application of calculation method to real calorimetric data	151
5.4.2.1.	Characterisation of crystallised indomethacin with XRPD.....	151
5.4.2.2.	Determination of crystallisation kinetics with model fitting approach	152
5.4.2.3.	Determination of crystallisation kinetics with the calculation method	157
5.5.	Summary	160
6)	<i>Chapter 6: Complex crystallisation studies with IMC: amorphous indomethacin crystallisation at 60°C.....</i>	162
6.1.	Introduction.....	163
6.2.	Aims and objectives	164
6.3.	Experimental	164
6.3.1.	Materials	164
6.3.1.1.	Preparation of amorphous indomethacin	164
6.3.1.2.	Preparation of α and δ indomethacin polymorphs	165
6.3.2.	Methods.....	166
6.3.2.1.	Isothermal microcalorimetry.....	166

6.3.2.2.	X-ray powder diffraction (XRPD)	166
6.3.2.3.	Differential scanning calorimetry (DSC)	166
6.3.2.4.	Polarised light microscopy	167
6.4.	Results and discussion	167
6.4.1.	Qualitative analysis of calorimetric signal for ABI and AFI samples	167
6.4.2.	Characterisation of TAM samples	173
6.4.2.1.	XRPD	173
6.4.2.2.	DSC	176
6.4.3.	Characterisation of AFI samples with PLM	180
6.4.4.	Characterisation of AFI samples with XRPD	181
6.4.5.	Quantitative analysis of calorimetric signal	189
6.4.5.1.	AFI samples	189
6.4.5.2.	ABI samples	195
6.5.	General discussion	197
6.6.	Summary	200
<i>Chapter 7: Conclusion and future work</i>		201
<i>References</i>		209

List of figures

<i>Figure 1.1: Schematic representation of the structure of amorphous (left) and crystalline (right) solids (reproduced from: http://math.ucr.edu/home/baez/physics/General/Glass/glass.html).</i>	22
<i>Figure 1.2: Enthalpy or specific volume change with temperature for a solid material. T_m is the melting point, T_g is the glass transition temperature, T_a is the annealing temperature and T_k is the Kauzmann temperature. (a) corresponds to structural relaxation, (b) heating during a DSC scan and (c) the enthalpy recovery at T_g (reproduced from Ref [23]).</i>	30
<i>Figure 1.4: Schematic illustration of the effect of water on the T_g of an amorphous material (reproduced from Ref [30]).</i>	41
<i>Figure 1.5: Isothermal da/dt as a function of time for solid-state reactions: data simulated with a rate constant of 0.049 min^{-1} (a) acceleratory; (b-d) deceleratory; (e) constant; (f) sigmoidal (reproduced from Ref[37]).</i>	44
<i>Figure 2.1: Schematic for an open-mode spray dryer (adapted from [46]).</i>	54
<i>Figure 2.2: Principle of a planetary ball mill (reproduced from manual of Pulverisette 5, Fritsch).</i>	56
<i>Figure 2.3: A schematic diagram of a heat flux DSC. A = furnace, B = thermocouple (reproduced from Ref [57]).</i>	63
<i>Figure 2.4: A schematic diagram for power compensation DSC. A = furnaces, B = sample and reference crucibles, C = sample and reference platinum resistance thermometers (reproduced from Ref [57]).</i>	64
<i>Figure 2.5: Illustration of temperature as a function of time for conventional DSC and modulated temperature DSC (reproduced from Ref [57]).</i>	66
<i>Figure 2.6: Schematic diagram for an X-ray powder diffractometer (reproduced from PANanalytical manual)</i>	67
<i>Figure 2.7: Schematic diagram for a DVS instrument (reproduced from Ref [60]).</i>	69
<i>Figure 3.1: DSC scans for annealed DSC in-situ (solid line), DSC ex-situ (dash-dotted line) and TAM samples (dashed line).</i>	83
<i>Figure 3.2: DSC scans for DSC in-situ samples: one cooled at $20^\circ\text{C}/\text{min}$ (solid line) and the other at $100^\circ\text{C}/\text{min}$ (dashed line).</i>	83
<i>Figure 3.3: Power-time data for three different samples of the same batch of amorphous indomethacin.</i>	84
<i>Figure 3.4: Glass transition temperature (T_g) as a function of heating rate. Line represents linear fit to the data.</i>	89
<i>Figure 3.5: The relaxation functions Φ and their fit to the KWW equation for indomethacin at 25°C determined using A) T_g (onset), B) T_g (mid) and C) T_g (0). Solid lines represent best fit to the KWW equation.</i>	91
<i>Figure 3.6: Simulated calorimetric data for relaxation of a 2-phase system produced by summing data for two single-phase systems having time constants A) of the same order of magnitude and B) different by one order of magnitude.</i>	94

Figure 3.7: Power-time traces resulting from relaxation of sucrose (●), lactose (○), experimental sucrose-lactose binary system (▲) and theoretical sucrose-lactose binary system (Δ). Solid line for sucrose and lactose data represents fit to KWW equation. ...	95
Figure 3.8: Power-time traces resulting from relaxation of sucrose (○), indomethacin (●), experimental sucrose-indomethacin binary system (Δ) and theoretical sucrose-indomethacin binary system (▲). Solid line for sucrose and lactose data represents fit to KWW equation.	97
Figure 3.9: Calorimetric signal for relaxation of indomethacin. Closed circle (●) represent experimental signal of 400mg indomethacin sample, whereas open circles (○) represent summation of two 200mg experimental data.	101
Figure 3.10: Deconvoluted calorimetric signal for a representative sucrose-lactose system as obtained from 2-KWW fit (●: component 1, ○: component 2) as compared to experimental calorimetric signal for relaxation of individual sucrose (▲) and lactose (Δ) samples.	102
Figure 3.11: Deconvoluted calorimetric signal for a representative sucrose-indomethacin system as obtained from 2-MSE fit (-●-: component 1, -○-: component 2) as compared to calorimetric signal for relaxation of individual sucrose (-▲-) and indomethacin (-Δ-) samples.	103
Figure 4.1: Chemical structure of α and β lactose anomers.	108
Figure 4.2: X-ray diffractogram for ball milled α-lactose and β-lactose.	113
Figure 4.3: Representative power-time data for relaxing amorphous α-lactose and β-lactose.	115
Figure 4.4: Percentage of α anomer in ball-milled β-lactose as it is heated in the DSC at different heating rates. Solid line and equation represent linear fit.	119
Figure 4.5: Glass transition for amorphous β-lactose measured at 30 ⁰ C/min (dashed line) and 50 ⁰ C/min (solid line).	119
Figure 4.6: Clarification of the method used to determine T_g^{onset} and T_g^{end} to measure ΔT_g	120
Figure 4.7: Melting endotherms for recrystallised amorphous α-lactose (solid line) and recrystallised amorphous β-lactose (dashed line).	122
Figure 4.8: DSC scans for amorphous β-lactose samples: top (red) shows a typical thermal events for an amorphous material, bottom (blue) shows an extra pre- T_g exotherm.	123
Figure 4.9: Illustration of correlation of pre- T_g exotherm enthalpy with re-crystallisation enthalpy (A) and ΔC_p (B). Lines represent best linear fits.	124
Figure 4.10: Illustration of correlation between pre- T_g exotherm enthalpy and β anomer content (β%).	126
Figure 4.11: Typical water sorption profile for amorphous lactose.	128
Figure 4.12: Water sorption profiles for amorphous α-lactose (A) and β-lactose (B).	130
Figure 4.13: Pseudo-equilibrium water sorption isotherms for amorphous α-lactose and β-lactose.	131
Figure 4.14: Water sorption isotherm for amorphous α-lactose. Line and equation represent linear fit.	134

<i>Figure 4.15: Water sorption isotherm for amorphous β-lactose. Line and equation represent linear fit.</i>	135
<i>Figure 5.1: Simulated power-time data for crystallisation process. “a” represents the area under the curve used to carry out the calculation as described in Eq.5.13</i>	145
<i>Figure 5.2: XRPD pattern for γ indomethacin, α indomethacin and for crystallised indomethacin at 30⁰C and 35⁰C.</i>	152
<i>Figure 5.3: Power-time signal for amorphous indomethacin at 25⁰C. Red line represents simulated relaxation curve.</i>	154
<i>Figure 5.4: Power-time signal (A) and corresponding crystallisation rate as a function of reacted fraction (B) for amorphous indomethacin at 25, 30 and 35⁰C. Red curves in (B) represent fit to the reduced Sestak-Berggren equation (eq.5.5).</i>	156
<i>Figure 5.5: Arrhenius plot for c.k as a function of temperature for the crystallisation process of amorphous indomethacin below T_g.</i>	157
<i>Figure 6.1: Power-time signal for three ABI samples as they crystallised at 60⁰C.</i>	168
<i>Figure 6.2: Power-time signal for three AFI samples as they crystallised at 60⁰C.</i>	168
<i>Figure 6.3: Illustration of the power-time signal for an ABI sample and an AFI sample.</i>	168
<i>Figure 6.4: Power-time signal for a representative ABI sample, AFI sample and NAFI sample.</i>	170
<i>Figure 6.5: Power-time signal for powdered indomethacin samples as they crystallised in the TAM at 60⁰C using glass (solid line) and stainless steel ampoules (dashed line). Inset shows the power signal of the same samples at the beginning of the reaction. ...</i>	172
<i>Figure 6.6: XRPD pattern for ABI (solid line) and AFI (dashed line) after microcalorimetric measurements at 60⁰C.</i>	174
<i>Figure 6.7: Illustration of peak positions for crystallised indomethacin samples (top black) and for gamma indomethacin (bottom red).</i>	175
<i>Figure 6.8: Illustration of peak positions for crystallised indomethacin samples (top black) and for alpha indomethacin (bottom red).</i>	175
<i>Figure 6.9: Illustration of peak positions for crystallised indomethacin samples (top black) and for delta indomethacin (bottom red).</i>	175
<i>Figure 6.10: DSC scans for AFI samples after microcalorimetric measurements heated at 5, 40 and 100⁰C/min.</i>	177
<i>Figure 6.11: DSC scan for indomethacin δ-form at 100⁰C/min.</i>	178
<i>Figure 6.12: DSC scan for a 1:1 mixture of α and δ polymorphs scanned at 200⁰C/min.</i>	179
<i>Figure 6.13: DSC scan for a gamma seeded AFI sample scanned at 200⁰C/min.</i>	179
<i>Figure 6.14: Polarised light microscope pictures for AFI samples stored at 60⁰C for different time periods as designated on top of each picture.</i>	181
<i>Figure 6.15: Illustration of progress of XRPD pattern for AFI samples stored at 60⁰C over 9 days.</i>	182
<i>Figure 6.16: The evolution of intensity of characteristic peaks over time for AFI samples stored at 60⁰C.</i>	183
<i>Figure 6.17: Illustration of peak positions for crystallised AFI sample after 4 days storage at 60⁰C (top black) and for γ indomethacin (bottom red).</i>	183

<i>Figure 6.18: Illustration of peak positions for crystallised AFI sample after 4 days storage at 60⁰C (top black) and for α indomethacin (bottom red).</i>	184
<i>Figure 6.19: Illustration of peak positions for crystallised AFI sample after 4 days storage at 60⁰C (top black) and for δ indomethacin (bottom red).</i>	184
<i>Figure 6.20: Illustration of peak positions for crystallised AFI sample after 6 days storage at 60⁰C (top black) and for α indomethacin (bottom red).</i>	184
<i>Figure 6.21: “(a and b) Typical appearances of δ IMC crystals. Both were grown at 70 °C.” Figure reproduced from Wu et al [101].</i>	186
<i>Figure 6.22: Relative crystallinity at diffraction angles 9.28⁰, 13.92⁰, 18.71⁰ and 21.61⁰ for AFI samples at 60⁰C. Solid lines represent fit lines to Avrami model.</i>	188
<i>Figure 6.23: Power-time data for a typical AFI sample and the fit lines obtained by fitting to a 2-Lorentzian model.</i>	191
<i>Figure 6.24: Power-time data for a typical AFI sample and the fit lines obtained by fitting to a 3-Lorentzian model.</i>	191
<i>Figure 6.25: Power-time data for a typical AFI sample and the fit lines obtained by fitting to a 4-Lorentzian model.</i>	192
<i>Figure 6.26: Relative crystallinity as a function of time for AFI samples (three phases) at 60⁰C and the fit lines obtained by fitting to the Avrami model between 0.1 and 0.8 relative crystallinity as demonstrated between the two dashed vertical lines.</i>	193
<i>Figure 6.27: Calorimetric signal for a representative ABI sample fitted to Lorentzian models as illustrated in the legends.</i>	196

List of Tables

<i>Table 1.1: Methods of manufacturing amorphous pharmaceutical materials (reproduced from Ref[24]).</i>	31
<i>Table 1.2: Summary of solid-state reaction models (reproduced from Ref [37]).</i>	45
<i>Table 2.1: List of materials used with supplier and grade.</i>	53
<i>Table 3.1: Estimated values for relaxation parameters used for iteration process to fit simulated data to the 2-KWW model.</i>	81
<i>Table 3.2: Relaxation parameters obtained by fitting IMC data for amorphous indomethacin at 25⁰C to MSE and KWW equations. SD refers to standard deviation.</i>	85
<i>Table 3.3: Effect of modulation parameters on glass properties of amorphous indomethacin.</i>	86
<i>Table 3.4: T_g, ΔH_r (∞) (J/g) and relaxation parameters obtained for indomethacin at 25⁰C using DSC.</i>	90
<i>Table 3.5: Comparison between calorimetric relaxation times obtained from isothermal microcalorimetry and modulated DSC (in hours) along with enthalpic relaxation and recovery obtained at two temperatures for indomethacin for the study reported by Bhugra et al (adapted from Ref [64]).</i>	92
<i>Table 3.6: Fit values for relaxation parameters obtained by fitting simulated data to 2-KWW model.</i>	93
<i>Table 3.7: Relaxation parameters for individual sucrose and lactose samples obtained by fitting power-time data to KWW and MSE equations. (Standard deviation values in parentheses, n = 3).</i>	95
<i>Table 3.8: Fit values for relaxation parameters returned by 2-KWW and 2-MSE models for binary sucrose-lactose samples. Standard deviation values in parentheses, n = 3.</i>	96
<i>Table 3.9: Relaxation parameters for individual sucrose and indomethacin samples obtained by fitting power-time data to KWW and MSE equations. Standard deviation values in parentheses, n = 3.</i>	98
<i>Table 3.10: Fit values for relaxation parameters returned by 2-KWW and 2-MSE models for binary sucrose-indomethacin samples. Standard deviation values in parentheses, n = 3.</i>	99
<i>Table 4.1: Anomeric composition of lactose samples after ball-milling. n = 4 for each anomer.</i>	114
<i>Table 4.2: Relaxation parameters for amorphous α-lactose and β-lactose as obtained by fitting power-time data to KWW equation. Standard deviation is shown between parentheses.</i>	116
<i>Table 4.3: Glass transition temperature width (ΔT_g) for amorphous α-lactose and β-lactose as measured by DSC at 30⁰C/min.</i>	121
<i>Table 4.4: Thermal characteristics (T_g, ΔC_p, T_c: crystallisation temperature, T_m: melting temperature) of amorphous α-lactose and β-lactose based on DSC scans at 30⁰C/min.</i>	121
<i>Table 4.5: Anomeric composition for β-lactose before and after exothermic events (re-crystallisation at 167⁰C and pre-T_g event).</i>	125

Table 5.1: “Algebraic expressions for the $f(\alpha)$ functions for the most common mechanisms in solid-state reactions and their corresponding equivalent reduced Sestak-Berggren equations”. Reproduced from Ref [38].	140
Table 5.2: Summary of n and m values used to construct simulated calorimetric data for solid-state reactions.	144
Table 5.3: Summary of calculation results for simulated dataset 1 ($c.k: 5.10^{-6}$, $Q: 20J$, $n: 0.8$, $m: 0.5$).	149
Table 5.4: Summary of calculation results for simulated dataset 2 ($Cck: 5.10^{-6}$, $Q: 20J$, $n: 0.5$, $m: 0.8$).	149
Table 5.5: Summary of calculation results for simulated dataset 3 ($c.k: 5.10^{-6}$, $Q: 20J$, $n: 0.8$, $m: 0.8$).	150
Table 5.6: Summary of calculation results for simulated dataset 3 ($c.k: 5.10^{-6}$, $Q: 20J$, $n: 0.5$, $m: 0.5$).	150
Table 5.7: Crystallisation kinetic parameters for indomethacin at $25^{\circ}C$ determined by fitting data to reduced Sestak-Berggren model (Eq. 5.5) and by applying calculation method.	159
Table 5.8: Crystallisation kinetic parameters for indomethacin at $30^{\circ}C$ determined by fitting data to reduced Sestak-Berggren model (Eq. 5.5) and by applying calculation method.	159
Table 5.9: Crystallisation kinetic parameters for indomethacin at $35^{\circ}C$ determined by fitting data to reduced Sestak-Berggren model (Eq. 5.5) and by applying calculation method using three different values for α (0.3, 0.5 and 0.8).	160
Table 6.1: Mean total heat output from crystallisation of powdered indomethacin (300mg) (at $60^{\circ}C$) loaded either in glass or stainless steel ampoules. Standard deviation is in presented in parentheses.	172
Table 6.2: Crystallisation kinetic parameters for AFI samples at $60^{\circ}C$ obtained by fitting XRPD data at diffraction angles (9.28° , 13.92° , 18.71° and 21.61°) to the Avrami model using least squares minimisation. Standard deviation is shown between parentheses.	189
Table 6.3: Kinetic parameters obtained by fitting the crystallisation data for AFI samples (three phases) at $60^{\circ}C$ to the Avrami model with least squares minimization.	194
Table 6.4: Onset time to crystallisation determined for peaks deconvoluted by 3-Lorentzian model for AFI samples at $60^{\circ}C$	195

List of Abbreviations

% w/w	Percentage weight in weight
A	Pre-exponential factor
ABI	Amorphous Bulk Indomethacin
AFI	Amorphous Film Indomethacin
α	Fraction of material crystallised at time = t
API	Active Pharmaceutical Ingredient
B	A material parameter related to its fragility
β	Stretch Power
BCS	Biopharmaceutics Classification System
ΔC_p	Change in Heat Capacity
$\Delta_r H$	Relaxation Enthalpy
$\Delta_{rec} H$	Recovery Enthalpy
$\Delta \mu$	Difference in the chemical potential
DSC	Differential Scanning Calorimetry
DVS	Dynamic Vapour Sorption
E_a	Activation Energy
G	Gibbs Free Energy
g_i	Weighting Factor
H	Enthalpy
HPLC	High Performance Liquid Chromatography
IMC	Isothermal Microcalorimetry
k_w	Henry's Law constant
KWW	Kohlrash-Williams-Watts
MTDSC	Modulated Temperature DSC
MSE	Modified Stretched Exponential
NMR	Nuclear Magnetic Resonance
P	Power
PLM	Polarised Light Microscopy

q	Total heat evolved or absorbed at time t
Q	Total Heat evolved or absorbed by a process
R	Gas Constant
RH	Relative Humidity
RSD	Relative standard deviation
RSE	Relative standard error
S	Entropy
τ	Time constant
τ_0	Shortest possible relaxation time of VTF equation
t	Time
T	Temperature
T_a	Annealing Temperature
TAM	Thermal Activity Monitor
τ^β	Relaxation time constant on the stretched time scale
T_g	Glass Transition Temperature
TGA	Thermal Gravimetric Analysis
T_m	Melting Temperature
T_k	Kauzmann Temperature
T_∞	Temperature of longest relaxation time
U	Internal Energy
V	Volume
VTF	Vogel-Tammann-Fulcher
w	Work or weight fraction
$XRPD$	X-ray Powder Diffraction

1) Chapter 1: Introduction

1.1. Background

The solid dosage form offers various advantages over other drug delivery systems such as stability and ease of manufacture, and hence it is the most widely used form for pharmaceutical products including tablets, capsules, powder inhalers and lyophilised products.

A solid material can exist in either the crystalline or amorphous state. From a stability perspective, the most stable crystalline form of the active pharmaceutical ingredient (API) and excipients should ideally be used. However, for other reasons, usually poor bioavailability, the amorphous form might be intentionally used to enhance product performance. If the molecular weight is very high, the pharmaceutical material may not be purified in the crystalline form and only exists in the amorphous form. In a third scenario, the amorphous form is introduced to crystalline pharmaceutical material unintentionally during processing, which can result in detrimental consequences in product performance.

A good understanding of the amorphous state focussing specifically on stability is therefore a crucial aspect of the pharmaceutical field. Research into amorphous pharmaceuticals is a relatively young field but it has witnessed great progress in the past three decades [1]. This thesis is another contribution to this field. Some major theoretical aspects of the amorphous state should therefore be introduced.

1.2. The crystalline state

A crystal can be defined as a solid consisting of elements arranged in a highly ordered manner. This order extends over a long-range three-dimensional structure. The highly ordered arrays of structural motifs (atoms, groups of atoms, ions or molecules) are held together by either ionic or non-covalent bonds to form what is referred to as the crystal lattice [2]. The latter consists of a collection of unit cells which represent the smallest three-dimensional volume elements. All unit cells have the same size and same arrangement of structural motifs and are held with the same binding energy [2]. This gives a crystal its unique thermal, mechanical and optical properties. Unit cells break and the material transforms to the liquid state at a defined energy level (or temperature). Structural motifs of a crystal can arrange or pack in different orders leading to the formation of different crystalline forms [3]. These are known as polymorphs and, in principle, have different physical properties (eg. melting point, density and dissolution rate) [3].

Some materials, as they crystallise, entrap solvent or water molecules within the crystal lattice to form a solvate or hydrate. Solvates are referred to as pseudopolymorphs as they also have different properties from the non-solvated crystal forms [3].

Crystals are also characterised by their external shape known as the crystal habit [3]. Different polymorphs and pseudopolymorphs tend to show different crystal habits but crystals of the same internal packing can also have different crystal habits that can result in different properties [2, 3].

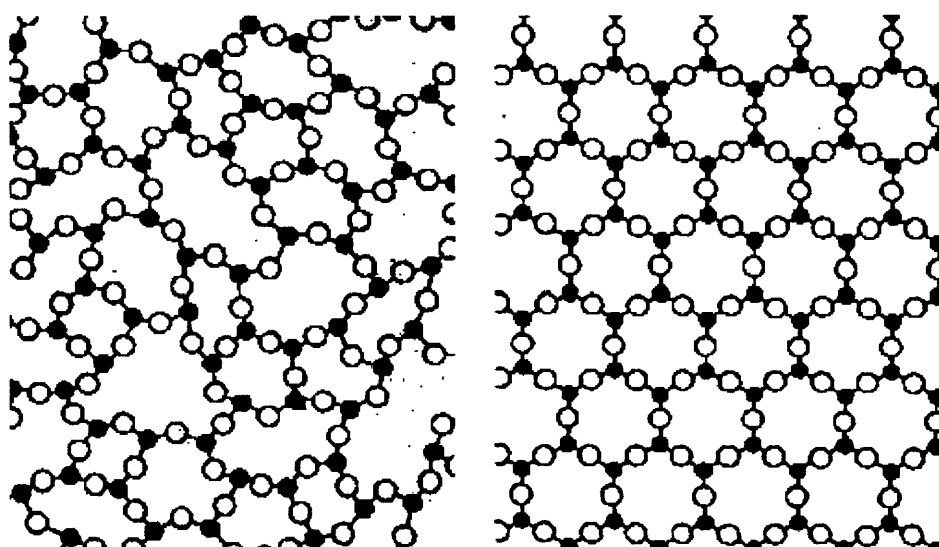


Figure 1.1: Schematic representation of the structure of amorphous (left) and crystalline (right) solids (reproduced from: <http://math.ucr.edu/home/baez/physics/General/Glass/glass.html>).

1.3. Amorphous state

Amorphous materials are characterised by the lack of three-dimensional long-range order in their internal structure (Fig.1.1) [4]. The latter is similar to the liquid structure where the molecules are positioned in a random fashion, although short-range order held, for example, by hydrogen bonding may be encountered in an amorphous solid [4]. As a result, amorphous solids exhibit different properties from their crystalline counterparts. They lack a distinct melting point [4] and exhibit faster dissolution rates [5], enhanced chemical reactivity [6] and higher hygroscopicity [4].

1.4. Advantages and disadvantages of amorphous form from a pharmaceutical perspective

1.4.1. Advantages

The amorphous state provides some advantages over the crystalline state in pharmaceutical settings.

An important advantage of the amorphous state is that it can be an approach for manufacturing poorly water-soluble drugs. This is thanks to its higher apparent solubility compared with the crystalline state. For example, the amorphous state provides a solubility advantage of 1.4 fold for indomethacin, 2 fold for cefalexin and 10 fold for macrolide antibiotics [7]. As a result, amorphous drugs are supposed to show better biopharmaceutical performance [7]. Amorphous materials dissolve faster as they lack the strong intramolecular bonds that hold the crystal lattice. However, the apparent solubility of some materials might exceed the equilibrium solubility and as a result the solubilised molecules can recrystallise in the dissolution medium [7].

Several drugs are available that are formulated in the amorphous state in order to improve their water solubility and hence bioavailability. Examples include formulations for cefditoren pivoxil (Spectracef[®]), rosuvastatin (Crestor[®]) and cefuroxime axetil (Ceftin[®]).

Another advantage of the amorphous state is the improvement of tablet strength. The presence of amorphous lactose in a tablet was shown to result in a better tablet strength [8]. This was attributed to the absorption of moisture by the amorphous regions resulting in lowering the glass transition temperature (T_g) of lactose and hence crystallisation prior to compaction.

Amorphous sugars (eg. trehalose and sucrose) have been demonstrated to stabilise freeze-dried macromolecules (eg. proteins) [9]. There are different theories regarding the mechanism of this stabilisation ability that amorphous sugars acquire. One proposed mechanism is the formation of hydrogen bonds between the macromolecule and the sugar. Hydrogen bonding capacity is optimal when both components are in the amorphous state [10]. It is also believed that trapping the macromolecules within an

amorphous matrix makes them immobilised and protects them from degenerating effects [11].

1.4.2. Disadvantages

The main drawback of using the amorphous state in a pharmaceutical formulation is the inherent instability of the amorphous state and its tendency to crystallise [12]. This can have detrimental effects on the performance of a formulation since the amorphous and crystalline states have different properties. Even a very small amorphous content can lead to dramatic changes as is the case for micronised materials. The mechanical stress applied to powder during the micronisation process to reduce particle size results in the creation of amorphous regions on the surface of particles. These amorphous regions can subsequently crystallise creating bridges between particles and hence particle aggregation which is undesirable, in for example inhaled formulations [13]. Moreover, Mackin et al [14] speculated that the failure of blends manufactured using milled active to conform with blend content uniformity was attributed to the generation of amorphous regions on particle surfaces during the milling process.

Another disadvantage of the amorphous state is its lower chemical stability relative to the crystalline state [12]. For example, amorphous β -lactam antibiotics were chemically less stable than their crystalline counterparts [15]. Similar observations were made for amorphous cefoxitin sodium [16]. Pikal et al [15] reported that an increase in the temperature was accompanied by a decrease in the activation energy for chemical decomposition. As a result, the authors speculated that chemical processes are coupled to molecular mobility and relaxation behaviour. Guo et al [17] examined whether there is a relationship between the chemical instability and physical characteristics of amorphous quinapril hydrochloride. It was found that there was a close correlation

between the temperature dependence of chemical reactivity and temperature dependence of molecular mobility below T_g . On the other hand, as the temperature was raised above T_g chemical degradation rate was noticeably lower than expected from molecular mobility.

High affinity to water can be a further undesired property of the amorphous state. Ahlqvist and Taylor [18] investigated exchange of D_2O vapour with both crystalline and amorphous sugars. They found that all the hydroxyl groups of the amorphous material exchanged their hydrogen with D_2O vapour. This suggested that water molecules have no restricted access to different parts of molecules for amorphous materials. On the other hand, crystalline sugars exchanged their hydrogen with D_2O vapour only at certain molecular sites. These results show why amorphous materials tend to take up more water compared with their crystalline counterparts. Water is a potent plasticiser and it can result in dropping the T_g of the solid to, or below, storage temperature. This can have detrimental effects as the material transforms to the rubbery state (as will be explained later) and molecular mobility is increased resulting in enhancing chemical reactivity and physical transformations.

1.5. Basic concepts of thermodynamics relating to the crystalline and amorphous states

In thermodynamics, the energy transformation that occurs during physical and chemical reaction is studied [19]. The part of the world where the event of interest takes place is referred to as the system, while the part from which observations are made is called the surrounding. There are three types of systems. An open system can exchange matter with the surroundings. A closed system cannot exchange matter with the surroundings

but can exchange energy. Finally, in an isolated system, neither matter nor energy can be exchanged with the surroundings.

There are certain properties that can be used in thermodynamics to describe a system. These include volume (V), pressure (P), temperature (T), internal energy (U), enthalpy (H), entropy (S) and Gibb's free energy (G). The following equations relate these properties:

$$H = U + PV \quad \text{Eq.1.1}$$

$$G = H - TS \quad \text{Eq.1.2}$$

According to the first law of thermodynamics, energy can neither be created nor destroyed; and it can only be transformed from one form to another.

The energy change of a system can be described as follows:

$$\Delta U = q + w \quad \text{Eq.1.3}$$

where:

- ΔU is the change in internal energy
- q is the energy supplied to or lost from the system as heat
- w is the energy supplied to or lost from the system as work

Eq. 1.3 clearly indicates that changes in internal energy (U) result from changes in heat (q) and work (w). At constant volume when no work can be done to, or by, the system, the change in internal energy is equal to the measured heat gain or loss. At constant pressure, however, work can be done to, or by, the system and the measured change in heat is equivalent in this case to the enthalpy change (ΔH) (Eq.1.4)

$$\Delta H = q \text{ at constant } P$$

Eq.1.4

The direction of heat flow depends on the temperature (T) of the system and the surroundings. Heat flows from the object of higher temperature to the object of lower temperature. As heat flows into a system, the motion of its atoms and molecules increases. As a result, the atoms and molecules become more disordered and the system is said to have increased in entropy (S) as entropy is a measure of the degree of disorder.

The second law of thermodynamics states that entropy increases when a spontaneous change occurs in an isolated system. Since processes do not occur in isolation, entropy change, both in the system (ΔS_{sys}), and the surroundings (ΔS_{surr}) should be considered.

The two entropy changes are summed to obtain the total entropy change (ΔS_{total}) as illustrated in the following equation:

$$\Delta S_{\text{total}} = \Delta S_{\text{sys}} + \Delta S_{\text{surr}}$$

Eq.1.5

The second law of thermodynamics becomes crucial when considering processes that result in introducing more order to the system, such as crystallisation. The entropy of a system decreases after crystallisation. However, a significant amount of heat is released from the system to the surroundings during this process. This results in increasing the entropy of the surroundings and hence the change of the total entropy is positive and the process proceeds spontaneously.

1.6. Properties of the amorphous state

1.6.1. The glass transition temperature (T_g)

The glass transition temperature represents a significant descriptor of an amorphous material. It usually occurs at approximately 2/3 to 4/5 of the crystalline melting point

(T_m) measured in Kelvin [20]. It can be defined as the temperature at which a material transforms from a glassy mechanical solid to a rubbery supercooled liquid or vice versa. This transition is accompanied by a change in several of the material's properties (e.g. heat capacity, volume and viscosity). Techniques used to measure the T_g rely on detecting these changes. DSC is the most widely used technique for this purpose and it takes into consideration the kinetic nature of the glass transition [20].

1.6.2. Fragility

As a supercooled liquid is cooled towards the T_g , a dramatic change in viscosity is noted [21]. Viscosity represents a macroscopic measure of a material's resistance to flow. The dependence of viscosity or molecular mobility change on temperature near T_g is used to classify amorphous materials into fragile or strong. Strong liquids show an Arrhenius dependence whereas fragile liquids show non-Arrhenius dependence [21]. A material's behaviour falls in between these two patterns of molecular mobility (or viscosity) dependence on temperature. The Vogel-Tammann-Fulcher equation (Eq.1.18) was proposed to describe this phenomenon [21];

$$\tau = \tau_0 \exp\left(\frac{B}{T - T_\infty}\right) \quad \text{Eq.1.18}$$

where

- τ is the mean molecular relaxation time and could be replaced by viscosity,
- T is the temperature,
- τ_0 is the shortest possible relaxation time,
- T_∞ is the temperature of longest relaxation time,
- B is a material parameter related to its fragility.

1.6.3. Thermodynamic properties

The amorphous state has a higher potential energy relative to the crystalline state [5]. This is attributed to the low packing efficiency and lack of long-range order in the amorphous state. As a result, the amorphous state is thermodynamically unstable and has a potential to revert to the more stable crystalline state.

1.7. Amorphous state formation

Solid material science still suffers from gaps in terms of the elucidation of amorphous structure and mechanism of its formation despite the extensive work conducted in this field. Nevertheless, there is a general consensus that solid amorphous state formation is a kinetic phenomenon as will be explained below [5, 22].

At a given high temperature range, a material exists in the liquid state (a melt) where there is no defined structure holding the molecules together. Upon cooling slowly, the specific volume and enthalpy of the system decrease linearly until a certain temperature, T_m (the melting or the crystallisation temperature) is reached, where the liquid crystallises (Fig.1.2). However, if the cooling rate is very fast the molecules “will not have enough time” to arrange themselves in an ordered manner and organisation to a perfect crystal cannot occur and the liquid state persists, but now it is called a supercooled liquid [5]. The latter is thermodynamically unstable (as it has a higher internal energy than the most stable state of the system below T_m) but it is said to be in a pseudo-equilibrium state since it follows the same response pattern to temperature change as the liquid state [22]. This is thanks to the fast molecular movements that allow it to keep up with the aforementioned changes. If the supercooled liquid maintained this property, it would reach a temperature (known as the Kauzmann

temperature, T_k) at which it would have the same enthalpy as the crystal [22]. However, the molecular mobility in the supercooled liquid decreases gradually as the specific volume decreases (and viscosity increases) and the time needed to accommodate the molecules within the equilibrium volume keeps increasing until it dramatically exceeds the experimental time. At this point, the molecular structure is “frozen” for kinetic reasons and the supercooled liquid is turned into a brittle state known as a glass [21]. This happens at a specific temperature (and pressure) known as the glass transition temperature (T_g) (refer to Fig.1.2).

Figure 1.2: *Enthalpy or specific volume change with temperature for a solid material. T_m is the melting point, T_g is the glass transition temperature, T_a is the annealing temperature and T_k is the Kauzmann temperature. (a) corresponds to structural relaxation, (b) heating during a DSC scan and (c) the enthalpy recovery at T_g (reproduced from Ref [23]).*

This pattern of amorphous state formation is based on quench cooling. There are other methods used to produce the amorphous form. These are, namely, precipitation from

solution, application of mechanical stress and condensation from vapour [4]. These methods, except for mechanical stress, are also based on the kinetic phenomenon in terms of glass formation event [5]. Processes used for each method are summarised in Table 1.1.

Table 1.1: *Methods of manufacturing amorphous pharmaceutical materials (reproduced from Ref[24]).*

From	Method	Examples
Crystal	Disruption/ energy input	Grinding/ milling
		Compression/ decompression
		Reaction
		Dehydration
		Irradiation
Solution	Solvent removal	Freeze-drying
		Spray-drying
		Precipitation
		Polymerisation
		Reaction
Liquid	Cooling/ energy removal	Rapid cooling
		Nucleation suppression
		Polymerisation
		Reaction
Vapour	Cooling/ energy removal	Sublimation
		Reaction

1.8. Relaxation phenomenon of amorphous state

As can be clearly seen in Fig.1.2, the amorphous state has higher enthalpy than the hypothetical equilibrium state (referred to as equilibrium glass) that would have existed if there had been no vitrification (glass formation). What tends to happen is that the very slow molecular mobility retained in the glass below T_g causes energy loss allowing the glass to attain equilibrium energy levels [5]. This phenomenon is what is often referred to as relaxation and is represented by the dashed arrow (a) in Fig.1.2.

It is important to realise that there are different modes of relaxation and the two main ones are known as α and β relaxations. The former is also referred to as structural relaxation since it is concerned with whole molecule movements, whereas β (or Johari-Goldstein relaxation) is a secondary mode of relaxation as it represents intramolecular movements (e.g. independent rotation of polymer side chains) [23].

Assessing the rate at which an amorphous material relaxes is crucial to predict its stability. Relaxation can result in detrimental effects on pharmaceutical formulations in which case it is referred to as “aging” (“unwanted” natural relaxation) [4]. On the other hand, it can be exploited to induce favourable changes in a pharmaceutical component such as improving the mechanical strength by intentional “annealing” [21]. Recent studies have been carried out to correlate the rate of crystallisation [25] and chemical degradation [26] to the rate of relaxation since all these phenomena are somehow controlled by the extent of molecular mobility [23].

1.9. Assessment of relaxation rate

The rate of amorphous relaxation, i.e. the time-dependent changes in glass volume or enthalpy, can be primarily described by a multi-exponential function. This is due to the heterogeneous nature of the amorphous structure which can be regarded as being

composed of many molecular sub-states relaxing exponentially at different rates [27].

Mathematically, this can be represented by the following equation:

$$\phi(t, T) = \sum_i g_i \exp\left(-\frac{t}{\tau_i(T)}\right) \quad \text{Eq.1.6}$$

where $\phi(t, T)$ is the overall decay function at time t and temperature T , and g_i is the weighting factor. The latter essentially represents the probability of a certain molecular sub-state (i) having a defined relaxation time τ_i [23].

This multi-exponential decay function can be described by a simpler empirical equation known as the Kohlrausch-Williams-Watts (KWW) equation:

$$\phi(t, T) = \exp\left[-\left(\frac{t}{\tau(T)}\right)^\beta\right] \quad \text{Eq.1.7}$$

Despite the empirical origin of this “stretched exponential” equation, researchers in the field tried to ascribe some physical meanings to its parameters [23]. τ is considered to represent the mean relaxation time. The distribution of relaxation times of the sub-states around τ is represented by the stretch parameter β . The value of β should vary between 1 and 0 in order to have a physical meaning. Unity indicates that all sub-states are relaxing exponentially at the same rate and as the value of β gets smaller, the distribution of sub-states gets wider [23]. Shamblin et al [28] have shown how these two parameters can be used to obtain crucial information about the shelf-life of an amorphous material.

Different analytical methods can be used to characterise aspects of amorphous relaxation. The KWW equation has been successfully applied to analyse the output data from many of these techniques including thermal methods [28]. Differential scanning calorimetry (DSC) has been the most popular method in this field and more recently the applicability of IMC has been explored [23]. A brief description on how relaxation parameters can be derived from these two techniques using the KWW equation will follow.

An important assumption reproduced when using the KWW equation to describe structural relaxation is that the relaxation time constant τ is time-independent. Simulation studies based on other non-empirical models showed the invalidity of this assumption [23]. As a material relaxes the decrease in its energy and volume as a function of time results also in a time-dependent decline in molecular mobility. This means that the relaxation time is not constant but gets longer as relaxation progresses [23]. In their study, Kawakami and Pikal [23] reported that the value of τ did vary with the annealing period. However, they found that τ and β change with time in opposite directions, i.e. τ increases with time whereas β decreases. It was found then that the value of the relaxation time constant “on the stretched time scale”, τ^β , remains constant throughout the whole lifetime of the relaxation process and it was concluded that this value can be reliably used to compare data. Interestingly, Kawakami and Pikal [23] reported a method by which the “true” values of τ and β can be found.

1.9.1. Enthalpy relaxation measurement with DSC

First of all, by enthalpy relaxation we mean the gradual decline in the enthalpy of the system (resulting in heat release) during structural relaxation in order to achieve equilibrium enthalpy [27]. The difference between the enthalpy of the fresh

unannealed glass and that of the same glass after a certain period of annealing is referred to as relaxation enthalpy ($\Delta_r H$). The isothermal decay in relaxation enthalpy as a function of time (t) can be described by the following equation [23]:

$$\Delta_r H(t) = \Delta_r H(\infty) \cdot \phi(t) \quad \text{Eq.1.8}$$

where $\Delta_r H(t)$ and $\Delta_r H(\infty)$ are relaxation enthalpy at time t and infinity, respectively. $\phi(t)$ is the relaxation decay (Eq.1.6) that can be replaced by the KWW function (Eq.1.7) as was shown earlier.

In a standard DSC method, relaxation enthalpy, $\Delta_r H$, for a material annealed at a particular temperature (below its T_g) for a certain period of time can be measured by heating the sample across its T_g . At or near this temperature the sample recovers the enthalpy it has lost during relaxation. This recovered enthalpy is called recovery enthalpy ($\Delta_{rec} H$) and is assumed to be equal and opposite to $\Delta_r H$ [29]. This recovery event is represented by the dashed line C in Fig.1.2.

The decay (relaxation) function can then be described by the following equation:

$$\phi(t) = 1 - \frac{\Delta_r H(t)}{\Delta_r H(\infty)} \quad \text{Eq.1.9}$$

where $\Delta_r H(t)$ and $\Delta_r H(\infty)$ are relaxation enthalpy at times t and ∞ (infinity), respectively. $\Delta_r H(\infty)$ can be calculated from the T_g , the annealing temperature (T_a) and heat capacity change (ΔC_p) at T_g [23]:

$$\Delta_r H(\infty) = (T_g - T_a) \cdot \Delta C_p \quad \text{Eq.1.10}$$

By conducting several measurements at different time points, $\phi(t)$ can be plotted against time and the resulting plot is then fitted to the KWW equation (Eq.1.7) by nonlinear regression analysis to obtain relaxation time constants τ and β .

In DSC studies, the samples are initially heated across their T_g to standardise their thermal history which offers reliable measurement of $\Delta_r H(t)$. However, a major drawback of this method is its insensitivity to small relaxation enthalpies which is a common issue since relaxation processes tend to be very slow. To get around this issue, samples are usually annealed for long periods, which renders such measurements lengthy and tedious.

1.9.2. Enthalpy relaxation measurement by IMC

When an amorphous material relaxes in an isothermal microcalorimeter, the change in enthalpy relaxation as a function of time (i.e. $d(\Delta_r H)/dt$) is directly recorded. The calorimetric power-time data can then be described as follows [23]:

$$P = \frac{d\Delta_r H}{dt} = \Delta_r H(\infty) \cdot \frac{d\phi(t)}{dt} \quad \text{Eq.1.11}$$

which can take the following final form if $d\phi(t)/dt$ is replaced by the time derivative of the KWW equation:

$$P = \Delta_r H(\infty) \cdot \left(\frac{\beta}{\tau}\right) \cdot \left(\frac{t}{\tau}\right)^{\beta-1} \cdot \exp\left[-\left(\frac{t}{\tau}\right)^\beta\right] \quad \text{Eq.1.12}$$

This equation is then used to fit the calorimetric data by least-squares minimisation in order to derive relaxation parameters [27].

However, one has to be aware of the shortcomings of Eq.1.12. At very short times (i.e. when t approaches 0), a non-physical value of infinity is obtained for P [27]. Another

mathematical expression, known as the modified stretched exponential equation (MSE, Eq.1.13), can then be reproduced in this case [27].

$$\phi(t,T) = \exp \left[- \left(\frac{t}{\tau_0(T)} \right) \left(1 + \frac{t}{\tau_1(T)} \right)^{\beta-1} \right] \quad \text{Eq.1.13}$$

In this equation β keeps the same meaning as in the KWW equation. τ_0 and τ_1 are relaxation time constants. τ_1 can be used to evaluate the time limit of the KWW equation, i.e. the time before which the KWW equation is not applicable as will be explained below:

- When $t \ll \tau_1$, Eq.1.13 becomes:

$$\phi(t,T) = \exp \left(- \frac{t}{\tau_0(T)} \right) \quad \text{Eq.1.14}$$

The time derivative of this (non-stretched) exponential equation is finite, and hence applicable to fit calorimetric data [27].

- At longer times, when $t \gg \tau_1$, the MSE expression in fact becomes mathematically equivalent to the KWW equation, and it can be written as:

$$\phi(t,T) = \exp \left[- \left(\frac{t}{\tau_D(T)} \right)^{\beta} \right] \quad \text{Eq.1.15}$$

where τ_D is a time constant that can be considered equivalent to the τ (time constant) expressed in the KWW equation. τ_D can be obtained from both τ_0 and τ_1 and β as follows:

$$\tau_D = \left(\tau_0 \tau_1^{\beta-1} \right)^{1/\beta} \quad \text{Eq.1.16}$$

When the MSE model is used to describe isothermal microcalorimetric data, the time derivative should be employed for data fitting:

$$P = \frac{\Delta_r H_\infty}{\tau_0} \cdot \left(1 + \frac{\beta t}{\tau_1}\right) \cdot \left(1 + \frac{t}{\tau_1}\right)^{\beta-2} \cdot \exp\left[-\left(\frac{t}{\tau_0(T)}\right) \left(1 + \frac{t}{\tau_1(T)}\right)^{\beta-1}\right] \quad \text{Eq.1.17}$$

The high sensitivity of IMC offers the advantage of monitoring and assessing relaxation processes at low storage temperatures. Unlike DSC, IMC also provides extensive data points, which enhances the accuracy of the fitting process.

An important issue that can be encountered with IMC, but not with DSC, is controlling the thermal history of samples. This effect is greater as relaxation increases. This dictates very careful sample handling in order to obtain reproducible data [23].

1.10. Polyamorphism

Polyamorphism refers to the idea of the existence of more than one amorphous form of the same material. The real meaning of the phenomenon implies that one polyamorph can revert to another through a first order transition [20]. This phenomenon has not been shown to exist for organic materials [5]. However, the term polyamorphism has been used inappropriately to refer to amorphous states obtained via different preparation routes or of different thermal histories [20]. These states are still related through relaxation phenomenon and not separated with a first order transformation and hence are not real polyamorphs [20].

1.11. Water interaction with the amorphous state

The amorphous state is known to show greater affinity to water than the crystalline counterpart [30]. Ahlqvist and Taylor [18] have shown that water molecules have no

fixed interaction sites with the solid molecules. Unlike the crystalline materials which mainly adsorb water, amorphous materials absorb water and the amount of sorbed water is dependent on the total mass of the material [30]. Sorption is a term which encompasses both the adsorption (interaction on the surface) and absorption (interaction with the bulk) phenomena [31]. It is speculated that the disordered nature of the amorphous state allows it to dissolve water molecules within its bulk [30]. As a result, if a small amount of amorphous material is present in a predominantly crystalline matrix, water will be localised preferentially in the amorphous regions which will have greater water content than the total crystalline matrix. This can lead to detrimental effects on product performance since water is a potent plasticiser and can induce crystallisation of the amorphous regions or enhance chemical reactivity [30].

1.12. Water as a plasticiser

A plasticiser is an additive which results in lowering the T_g of a material, whereas an additive that results in increasing the T_g of material is referred to as an antiplasticiser [32].

Water is known to be a potent plasticiser for amorphous materials [32]. The water content of an amorphous pharmaceutical product should therefore be controlled since amorphous materials tend to absorb water vapour readily. The plasticising effect of water can be generally described by the Gordon-Taylor model (Eq.1.19) [32].

$$T_{gmix} = \frac{w_1 T_{g1} + K w_2 T_{g2}}{w_1 + K w_2} \quad \text{Eq.1.19}$$

where:

- T_{gmix} is the T_g of the water-solid mixture
- T_{g1} is the T_g of component 1 (water)
- T_{g2} is the T_g of the component 2 (solid)
- w_1 is the weight fraction of component 1 (water)
- w_2 is the weight fraction of component 2 (solid)
- K is a constant measured from the free volume of component 1 and component 2

The Gordon-Taylor equation describes the relationship between the T_g of a mixed amorphous system and its composition. This model is based on the assumption that there is a perfect additivity of the free volumes of the two components and the absence of specific interactions between the two components. An amorphous solid containing water can be considered as a mixed amorphous system. Fig. 1.4 represent a schematic illustration of the effect of water content on the T_g of the wet solid, which is represented by the solid line that joins the T_g of the solid with the T_g of water. Water has a low T_g (135K) and as its concentration increases within the solid, the more it depresses the T_g of the wet solid material [30]. An important consequence of this is the depression of the T_g to temperatures near, or below, the processing or storage temperature. In this case the material will transform from the glassy (solid) state to the rubbery state leading to changes in the physical properties of the material [30]. Moreover, the presence of water within an amorphous matrix can greatly increase molecular mobility to the extent that spontaneous crystallisation is induced [33]. This has been the basis for the use of

gravimetric and perfusion calorimetric techniques to measure the amorphous content in predominantly crystalline powders [34, 35].

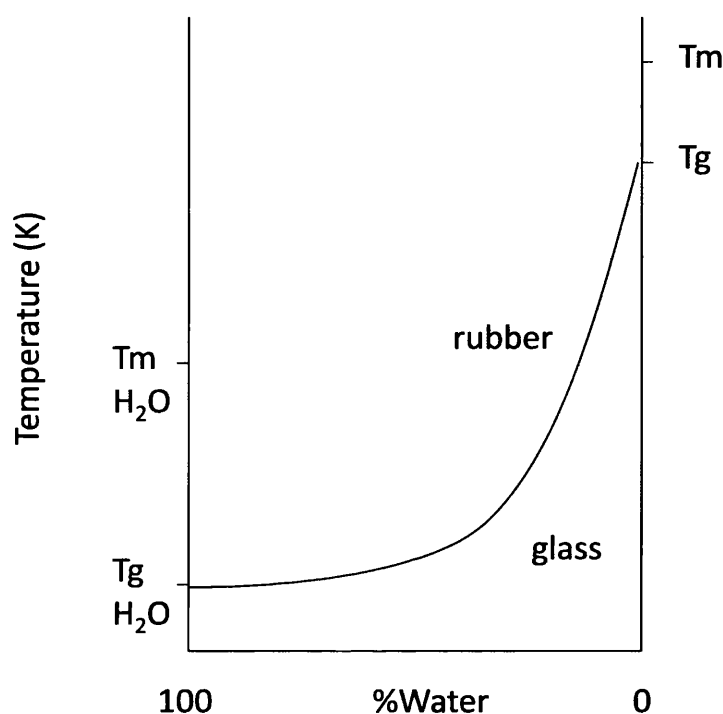


Figure 1.3: Schematic illustration of the effect of water on the T_g of an amorphous material (reproduced from Ref [30]).

1.13. Crystallisation from the amorphous state

As mentioned earlier, the amorphous state is thermodynamically unstable and has high molecular mobility. As a result, an amorphous material is prone to spontaneous crystallisation to attain the thermodynamically stable (crystalline) state [12]. A good understanding of the crystallisation phenomenon is important since this process needs to be promoted (in the case of unintentionally introduced amorphisation during

processing) or inhibited (in the case of intentional production of amorphous state) in a controlled manner. This phenomenon still represents a subject for ongoing research since different factors contribute to it. Crystallisation from the amorphous state, like crystallisation from the melt, is the consequence of two independent phenomena, nucleation and crystal growth [4, 12].

Nucleation is the first step in the crystallisation process and it involves the formation of stable molecular assemblies known as nuclei from which crystals can grow [2]. In primary nucleation, nuclei are formed in the bulk (homogeneous nucleation) or they form around a foreign body present in the system (heterogeneous nucleation) [36]. Secondary nucleation takes place after primary nucleation and it involves the formation of nuclei from existing crystals [2]. An interface is formed between the amorphous (or liquid) region and the stable nuclei. Crystal growth then takes place by transporting the material to this interface and as the molecule is integrated into the crystal heat of crystallisation is taken away [36]. Nucleation and crystal growth are two separate phenomena and each is described by certain independent models. However, difficulties in characterising each process independently has resulted in most studies considering the effect of both processes [12].

The overall crystallisation process is usually described using solid-state mathematical models. Some of these models were developed based on certain mechanistic assumptions, whereas other models are empirical and only provide mathematical descriptions of solid-state reactions without mechanistic information [37]. The choice of a model that best describes a solid-state reaction should be supported by complementary techniques such as spectroscopy and x-ray powder diffraction [37].

The rate of a solid-state reaction (da/dt) can be described by the following equation:

$$\frac{d\alpha}{dt} = Ae^{-\left(\frac{E_a}{RT}\right)}f(\alpha) \quad \text{Eq.1.20}$$

where A is the pre-exponential factor, E_a is the activation energy, T is absolute temperature, R is the gas constant, $f(\alpha)$ is the reaction model and α is the conversion fraction [37].

At isothermal conditions, $Ae^{(E_a/RT)}$ is constant and it will be replaced by the constant k and Eq.1.20 becomes [38]:

$$\frac{d\alpha}{dt} = kf(\alpha) \quad \text{Eq.1.21}$$

There are two different ways by which solid-state reaction models are classified. The first one depends on the graphical shape of their isothermal curves ($d\alpha/dt$ versus α); four different shapes can be observed: acceleratory, deceleratory, constant and sigmoidal (Fig.1.5) [37]. The second classification method is based on the mechanistic assumptions made to construct the model. There are four main types of mechanistic models. These are nucleation models, geometrical contraction models, diffusion models and reaction-order models. The mathematical expressions for these models are summarised in Table 1.2.

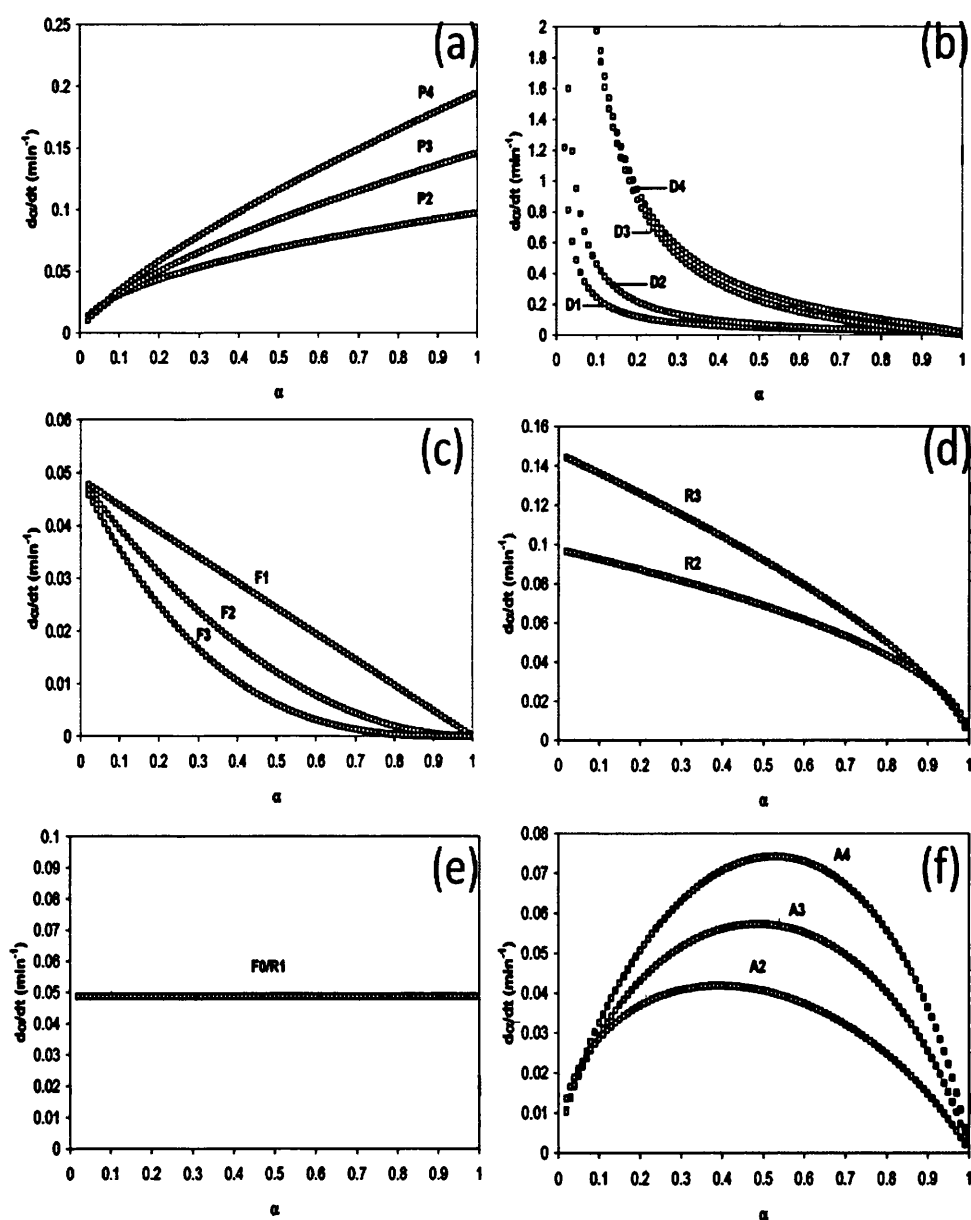


Figure 1.4: Isothermal da/dt as a function of time for solid-state reactions: data simulated with a rate constant of 0.049 min^{-1} (a) acceleratory; (b-d) deceleratory; (e) constant; (f) sigmoidal (reproduced from Ref[37]).

Table 1.2: Summary of solid-state reaction models (reproduced from Ref [37]).

model	$f(\alpha)$
Nucleation models	
power law (P2)	$2\alpha^{1/2}$
power law (P3)	$3\alpha^{2/3}$
power law (P4)	$4\alpha^{3/4}$
Avrami-Erofeyev (A2)	$2(1 - \alpha)[- \ln(1 - \alpha)]^{1/2}$
Avrami-Erofeyev (A3)	$3(1 - \alpha)[- \ln(1 - \alpha)]^{2/3}$
Avrami-Erofeyev (A4)	$4(1 - \alpha)[- \ln(1 - \alpha)]^{3/4}$
Prout-Tompkins (B1)	$\alpha(1 - \alpha)$
geometrical contraction models	
contracting area (R2)	$2(1 - \alpha)^{1/2}$
contracting volume (R3)	$3(1 - \alpha)^{2/3}$
diffusion models	
1-D diffusion (D1)	$1/(2\alpha)$
2-D diffusion (D2)	$-[1/\ln(1 - \alpha)]$
3-D diffusion-Jander (D3)	$[3(1 - \alpha)^{2/3}]/[2(1 - (1 - \alpha)^{1/3})]$
Ginstling-Brounshtein (D4)	$3/[2((1 - \alpha)^{1/3} - 1)]$
reaction-order models	
zero-order (F0/R1)	1
first-order (F1)	$(1 - \alpha)$
second-order (F2)	$(1 - \alpha)^2$
third-order (F3)	$(1 - \alpha)^3$

1.14. Factors affecting crystallisation from the amorphous state

Crystallisation from the amorphous state is a complex phenomenon and different factors play a role in determining the onset and rate of crystallisation and types of polymorphs that emerge as a result of the process. Bhugra and Pikal [12] carried out a survey of the different studies that examined this subject; the authors identified certain factors that control crystallisation from the amorphous state as summarised below:

1.14.1. Thermodynamic factors

The thermodynamic driving force for crystallisation is described by Eq.1.22 [12]:

$$\Delta\mu(T) = \int_T^{T_m} \left[\frac{\partial \Delta\mu(T)}{\partial T} \right] dT = - \int_T^{T_m} \Delta S(T) dT \quad \text{Eq.1.22}$$

where:

- $\Delta\mu$ is the difference in the chemical potential between the crystalline and amorphous phase
- ΔS is the difference in the molar entropies between the crystalline and amorphous (supercooled) phase
- T is the temperature
- T_m is the melting temperature

Eq.1.22 suggests that the free energy change between the crystalline and amorphous (supercooled) phases is a significant parameter in controlling the crystallisation process [12]. Studies regarding the effect of configurational entropy on crystallisation came to contradictory conclusions. Zhou et al [39] found that amorphous materials of lower configurational entropy showed a greater tendency to crystallise since their molecules are in a better position to re-pack. On the other hand, in their study on four different hexitols Siniti et al [40] found that compounds that have lower heat of melting (hence lower entropy) formed more stable glasses.

Carpentier et al [41] identified that the interfacial energy, which reflects molecular conformations, is an important thermodynamic factor in determining the crystallisation tendency of four different pentitols.

1.14.2. Effect of additives

The addition of an excipient to the amorphous matrix can influence the different factors that determine the crystallisation process. Excipients can affect the stability of an amorphous matrix through either physical or chemical interactions with the API [12]. Physical interactions include plasticisation or antiplasticisation effect where the excipient impacts upon the T_g of the system and hence its molecular mobility [12]. The excipient may also act as a diluent or accumulate at the crystal-glass interface. Chemical interactions are mainly represented in the formation of hydrogen bonds between the excipient and the API and hence affecting the intermolecular interactions between the API molecules that can be important in initiating nucleation [12].

1.14.3. Kinetic factors (molecular mobility)

Several research studies have focused on determining the correlation between molecular mobility of the amorphous pharmaceuticals and crystallisation. It was demonstrated that some pharmaceuticals show partial coupling between structural (or α) relaxation and crystallisation rate, whereas other amorphous drugs showed complete coupling [12, 42]. For example, in a study carried out by Masuda et al [43] the molecular mobility of amorphous indomethacin and salicin was assessed using ¹³C NMR spectroscopy; it was found that salicin had multiphasic and a shorter relaxation time compared with indomethacin. This was speculated to be the reason for greater tendency of salicin to crystallise.

β -relaxation is also speculated to correlate with crystallisation, particularly with nucleation since β -mobility is a measure of local and fast molecular motions and nucleation requires molecules in the proper orientation, which β -mobility can provide [12]. This was demonstrated experimentally for a drug denoted as SSR by correlating both modes of relaxation (α and β) to crystallisation kinetics above T_g [44]. β -relaxation was found to provide a better correlation.

1.14.4. Effect of sample preparation method

The four different routes to prepare amorphous materials (quench cooling, condensation from the vapour state, precipitation from solution and mechanical disruption of the crystal lattice) result in exposing the glass to different thermal histories and different levels of mechanical stress [12]. Thermal history affects molecular mobility, whereas mechanical stress can result in the creation of nucleation sites. As a result, glasses of the same material prepared by different methods will have different crystallisation profiles [12].

1.15. Aims

The amorphous state has become part of pharmaceutical research as it can offer some advantages to product performance. A significant part of the research in this field has focused on the stability of this solid state. Relaxation and crystallisation represent the main manifestations of amorphous state instability. These two phenomena have been explored using different analytical techniques including thermal techniques. IMC is a thermal technique that has several advantages that can be exploited to assess the stability of amorphous pharmaceuticals. IMC has better sensitivity than the standard DSC technique. For example, a typical isothermal heat conduction microcalorimeter

such as the TAM (Thermal Activity Monitor, TA Instruments) is 10 000 fold more sensitive than a standard DSC [45]. IMC can be used to directly monitor any chemical or physical changes through continuous capturing of heat change during these processes. This is because heat change is a universal phenomenon that accompanies all chemical and physical processes (with very few exceptions) [22]. The technique does not provide any molecular information directly but this can be deduced by fitting the calorimetric output to mathematical models that describe the process. This requires prior knowledge about the process being monitored. However, as multiple processes occur simultaneously the calorimetric output will reflect the total heat change without distinguishing between the different processes. This renders calorimetric data analysis problematic. This thesis focuses on exploring some aspects of amorphous state stability using mainly IMC.

Structural relaxation is widely assessed through enthalpy relaxation using thermal techniques, namely DSC and IMC. There are, however, contradicting results in the literature regarding the enthalpy relaxation studies with DSC and IMC as will be explained in Chapter 3. The first section of Chapter 3 attempts to address this issue via carrying comparative enthalpy relaxation studies with both techniques using amorphous indomethacin as a model system.

Most enthalpy relaxation studies have focused on single-phase systems. However, amorphous pharmaceutical formulations may consist of more than one amorphous phase. The second section of Chapter 3 discusses the feasibility of using IMC to assess the relaxation of two-phase amorphous systems.

Physical properties, which determine physical stability, are dependent on different factors such as the preparation method and thermal history. Some pharmaceutical materials exist in more than one isomeric form. Whether such minor chemical differences can affect the physical properties in the amorphous state was investigated in Chapter 4. Amorphous lactose, which has two anomeric forms, was used as a model pharmaceutical material.

Crystallisation from the amorphous state is another major stability concern for pharmaceutical formulators. A good understanding of the crystallisation phenomenon is therefore required to better control and predict the behaviour of the amorphous form.

Crystallisation from the amorphous state can be described by solid-state reaction models including the universal Sestak-Berggren equation which is described in Chapter 5. The use of IMC to analyse solid-state reactions has been restricted as the parameters of the Sestak-Berggren equation are not usually integral and hence cannot be manipulated to describe calorimetric output directly [22]. Chapter 5 discusses a new calculation approach to analyse calorimetric data for a crystallising drug. The crystallisation of amorphous indomethacin below T_g was used as a model system.

The calculation method described in Chapter 5 is only valid when the amorphous material crystallises to one polymorph. If more than one polymorph emerges, a different analysis approach should be adopted. This will be discussed in Chapter 6. This Chapter also explored the effect of preparation method on the crystallisation profile of amorphous indomethacin above its T_g .

In summary, the overall aims of this thesis are to;

- compare enthalpy relaxation profiles for a hydrophobic drug using IMC and DSC.
- explore the feasibility of using IMC to assess enthalpy relaxation for two-phase amorphous systems.
- explore the effect of the anomeric composition of amorphous lactose on some aspects of its physical properties.
- develop a calculation method to determine the reaction parameters for solid-state reactions using IMC.
- assessment of complex crystallisation processes with IMC
- explore the effect of the preparation method on the crystallisation process of amorphous indomethacin above T_g using IMC.

2) Chapter 2: Materials and Methods

2.1 Materials

All materials were used as received unless otherwise stated.

Table 2.1: List of materials used with supplier and grade.

Material	Supplier	Purity/ Grade
Sucrose	Sigma, UK	HPLC grade, $\geq 99.5\%$
Anhydrous Lactose	Sigma, UK	Ph Eur grade
α -lactose monohydrate	Merck Sharp and Dohme, UK	-
Indomethacin	Molekula, UK	100.2%
Talc	VWR International, UK	Extra Pure
Indium	Sigma, UK	99.999%
Acetone	Fisher Scientific, UK	$\square 99\%$

2.2. Methods

2.2.1. Preparation of amorphous lactose and sucrose using spray-drying

2.2.1.1.Introduction

Spray drying is a technique widely used to dry and form pharmaceutical particles. By controlling the spray drying conditions, one can optimise particle properties such as bulk density, moisture content and morphology [46].

In a spray drying process, a feed solution is introduced to an atomiser to form spray droplets. These are then introduced to a drying chamber where they come into contact with hot air. The drying process is monitored via controlling the temperature and the airflow. As the dried particles leave the drying chamber, they become separated from the drying gas using a cyclone to collect the main powder fraction. Very small particles are collected using a filter bag [46]. A schematic for the main parts of an open-mode spray dryer like the one used for this work is illustrated in Fig.2.1.

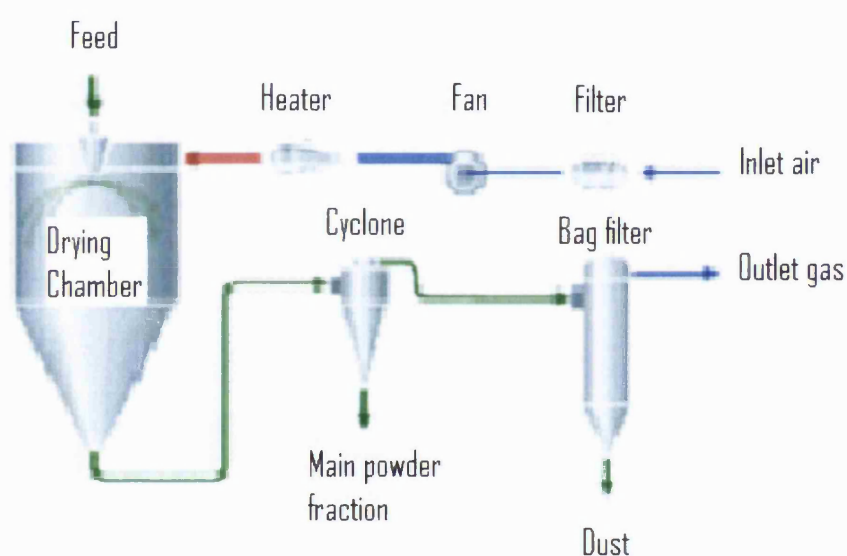


Figure 2.1: Schematic for an open-mode spray dryer (adapted from [46]).

2.2.1.2. Experimental

Preparation of amorphous sucrose:

A 12% w/w sucrose solution was prepared by dissolving the sugar in distilled water : acetone (3 : 2) solvent system. The solution was then spray-dried using an SD Niro (GEA Niro, Denmark) spray-dryer, employing the following spray-drying parameters:

- inlet temperature: 90°C,
- outlet temperature: 56 °C,
- chamber gas flow: 30 kg/h,
- atomising gas flow: 2.5 kg/h.

Preparation of amorphous lactose:

Lactose was dissolved in water and the resulting suspension was heated to 60°C and stirred to allow complete dissolution. After cooling the solution, a defined volume of acetone was added to the solution so that a solvent system of water: acetone (3:2) was obtained. The solution was then spray-dried using the same parameters used for sucrose as described above.

Spray-dried samples were collected from the collection bottle and cyclone then stored at -20°C until further use.

2.2.2. Preparation of amorphous lactose with ball milling

2.2.2.1. Introduction

Mechanical activation of a crystalline mass is one of the methods used to produce the amorphous state [4]. This could be achieved using ball milling. The ball mill used in this work was a planetary ball mill (Fritsch pulverisette 5). In this type of ball mill pots are installed on a rotating disc (Fig.2.2). The milling process is based on rotating the disc and the pots separately and simultaneously at a high speed [47]. Large ball impact energy is then created due to the strong and violent movement of the balls in the pots. This created energy results in fracturing the powder crystalline particles along natural fault lines leading to particle size reduction [48]. When these natural fault lines are

exhausted, the imparted mechanical energy results in creation of surface dislocations and eventually the amorphisation of the material [48].

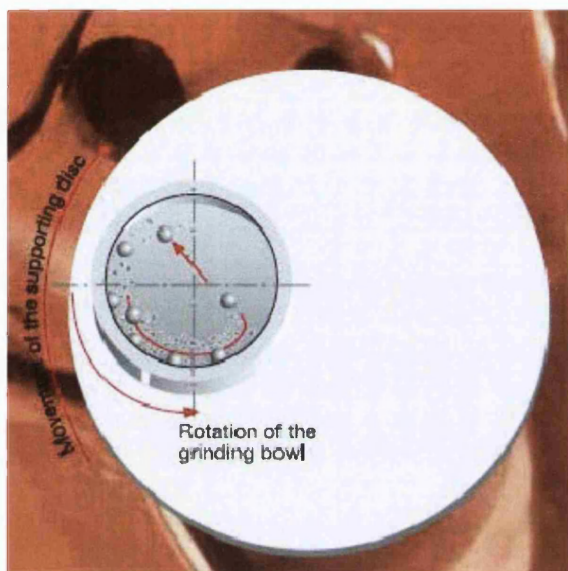


Figure 2.2: Principle of a planetary ball mill (reproduced from manual of Pulverisette 5, Fritsch).

2.2.2.2. Experimental

Ball milling was performed using a Fritsch pulverisette 5 planetary mill. 2.5 g of crystalline lactose was loaded in a 250mL ZrO_2 jar with 44 balls ($\Phi = 15\text{mm}$). Amorphous β -lactose was prepared using crystalline anhydrous β -lactose. Amorphous α -lactose was prepared using thermally dehydrated α -lactose monohydrate. Thermal dehydration was carried out at 150°C for 30 min. Crystalline lactose was loaded in the jar which was then flushed with dry nitrogen gas and sealed with parafilm M inside the glove bag (at $\leq 5\%$ RH) in order to minimise hydration of powder during the milling process. Milling was carried out at 300rpm for 8 hours. Milled samples were then

removed from the jar in the glove bag (at $\leq 5\%$ RH) and passed through a $125\mu\text{m}$ sieve then stored at -20°C until further use.

2.2.3. Isothermal microcalorimetry

2.2.3.1. Introduction

Calorimetry refers to measurement of heat change during a process. Mostly all processes that occur in nature result in a proportional change in heat. This, in theory, has made calorimetric measurements applicable to any kind of chemical or physical reaction [22].

Isothermal calorimeters, as opposed to temperature scanning calorimeters, operate at a *constant* temperature [49]. These allow the monitoring of drug/formulation behaviour for a certain period of time at a certain temperature. The latter can be ambient temperature thanks to the development of highly sensitive calorimeters (known as microcalorimeters), which can detect thermal changes down to $0.1\mu\text{W}$. The measurement of heat output (q in Joules, J) allows the derivation of thermodynamic data like enthalpy changes and Gibbs energies. Kinetic information can also be obtained as all isothermal calorimeters measure heat change as a function of time, known as heat flow (dq/dt in Js^{-1} or Watts, W) [50].

Isothermal microcalorimeters can be divided into three main types based on the measurement method:

- *Power compensation calorimeters:* in these calorimeters the heat change that results from a process is compensated for by introducing electrical energy either to remove heat (in the case of exothermic output) or to add heat (for an endothermic output). This approach both ensures isothermal conditions in the calorimetric vessel

and allows the measurement of process power output since the latter is equal and opposite to the electrical power supplied [49].

○ *Adiabatic calorimeters:* in the ideal scenario with these calorimeters, the calorimetric vessel is thermally isolated from the surroundings. Any change in its temperature will therefore result from changes occurring in the sample. The power output is the product of temperature change and the heat capacity of the vessel plus the sample. However, a more practical approach is to use semi-adiabatic calorimeters and any heat exchange with the surroundings is usually accounted for [50].

○ *Heat conduction calorimeters:* these are the most commonly used of the three types [49] and this type was used for all the isothermal calorimetric measurements in all the studies described in this thesis.

2.2.3.2. Operating principle of heat conduction microcalorimetry

In a heat conduction calorimeter, the sample vessel is surrounded by a heat sink (usually a metal block). As a reaction takes place within the sample vessel, the heat absorbed (or evolved) results in temperature change within the vessel. A temperature gradient is then created between the vessel and the heat sink leading to heat transfer between the two media [22]. This heat transfer is detected by an array of thermocouples (a thermopile) positioned between the vessel and the heat sink. Thermocouples are characterised by their ability to generate an electrical voltage (U) when a temperature gradient exists between their endings. This voltage is proportional to the temperature gradient created [49]. The output power (P) recorded, which is also determined by the temperature gradient, can therefore be defined as:

$$P = \frac{dq}{dt} = \varepsilon U \quad \text{Eq.2.1}$$

where ε is a proportionality constant that can be identified by electrical calibration [22].

The time integral of Eq.2.1 gives the heat output (q) from the calorimeter (Eq.2.2).

$$q = \varepsilon \int U dt \quad \text{Eq.2.2}$$

With most heat conduction microcalorimeters, the twin (or differential) design is adopted. In this design the calorimeter consists of two identical vessels: one for reaction measurements (sample vessel) and the other contains an inert material which should match the sample in heat capacity, heat conductance and weight [49]. The thermopiles on the sides of the two vessels are placed in opposition. This ensures the cancellation (or minimisation) of any environmental noise affecting both vessels so that only the thermal output from the reaction is recorded [51].

From this brief description of the operating principle of isothermal heat conduction microcalorimetry, it appears that this highly sensitive technique is in fact fairly simple and unlike many other techniques there is no need for sample pre-treatment for analysis i.e. there is no loss of the sample's physical or chemical characteristics prior to measurement. Sample analysis at controlled conditions (e.g. relative humidity and light intensity) can now be conducted thanks to recent developments in microcalorimeter design [22]. The non-specificity of the calorimetric measurements has attracted researchers from different fields in the recent era to characterise their systems by looking at their thermal behaviour at isothermal conditions. Most of these studies, however, remained qualitative rather than quantitative. The reason for this leads to pointing out the main limitation of IMC, which is the universal nature of heat [50]! In a typical pharmaceutical formulation, for instance, the drug and the excipients can be degrading both chemically and physically. There is also the potential for the different components to interact. All these events collectively contribute to the heat flow

recorded in the microcalorimeter. Getting quantitative information from such a signal represents, in effect, a real challenge. Recent efforts in this field have focused on introducing different methods in an attempt to address this issue.

2.2.3.3. Quantitative analysis of calorimetric data

The main methods used to derive quantitative information from calorimetric data, briefly, are:

- *Empirical fitting:* this approach relies on finding an empirical equation that can simply fit the data without describing the actual process. The main information that such analysis can offer is how far a process has proceeded [52].
- *Kinetic modelling:* in many cases, the mechanism of the process is known and can be described by a mathematical model. This model can be manipulated to obtain an equation that can fit the calorimetric data for the process in question. The reaction parameters can be obtained by importing the data into a mathematical software which can conduct an iterative procedure to find the best fit. The application of this method was demonstrated to be successful for the analysis of relatively simple and well-defined processes [52, 53].
- *Direct calculation:* this method also requires prior knowledge about the reaction mechanism. Different calculations derived from both the calorimetric equation that describes the data and the heat flow curve are conducted to determine accurately the reaction parameters. This was first introduced by Beezer et al [54] to analyse solution phase reactions and later work was carried out to investigate its applicability to solid-state reactions [55].
- *Chemometrics:* this was recently introduced in response to the fact that all the previous methods fail when a certain degree of complexity is introduced to the data.

Preliminary work [56] using simulated data has shown that principal component analysis (PCA) can be used to identify the different events occurring simultaneously in a complex system and which all contribute to the calorimetric signal.

2.2.3.4. Experimental

A 2277 Thermal Activity Monitor (TAM, TA Instruments) was used for all isothermal microcalorimetric measurements at different temperatures as specified in the following relevant chapters.

Both the sample and reference ampoules were loaded into the TAM twin channels and were first kept at the equilibrium position for 30 minutes. At this position the ampoules were not in contact with the thermocouples but were well placed within the thermostatted water bath, which allowed the sample and reference ampoules to reach the desired experimental temperature. Afterwards, both ampoules were lowered slowly to the measuring position where they were in full contact with the thermocouples and heat flow data recording could be initiated. Power-time data generated in the TAM were recorded via the dedicated software package Digitam 4.1. A minimum of three measurements for each system were carried out.

Before starting the actual experiment, the TAM was first electrically calibrated. Both the sample and reference channels were loaded with a predefined amount of the reference material, which was talc in all the experiments. After adjusting the baseline to zero, an electrical current of certain magnitude was passed through heater resistors placed below the ampoules. This generated a well-defined heat flow and the full scale level was adjusted according to the magnitude of this heat flow.

2.2.4. Calorimetric data analysis

Power-time data corresponding to the first two hours were discarded from each data set to ensure all data used for analysis were free from disturbances that result from lowering the ampoules. The time axis was adjusted by adding the time period (30 minutes) during which the sample was held in the equilibration position. By doing this, it was assumed that the monitored process started when the sample was put in the TAM. Data fitting to relevant models was performed using the iterative non-linear curve fitting tool in Origin 7.0, Microcal Software Inc.

2.2.5 Differential scanning calorimetry (DSC)

2.2.5.1. Introduction:

Out of all the thermal techniques, DSC is the most widely used method to analyse pharmaceutical materials. Generally, the material is heated or cooled over a certain temperature range. As the material undergoes a thermal event, a change in temperature or energy is recorded. A wide range of thermal events can be detected with DSC including melting, crystallisation, glass transition and chemical degradation [57]. The technique is characterised by its simplicity and rapidity. Moreover, it requires a small size and provides a wide temperature range (-120 to 600⁰C) for sample characterisation.

DSC instrumentation can be divided into two types. In the first type, known as heat flux DSC (Fig.2.3), the sample crucible and the empty reference crucible are both placed in the same furnace (denoted as A in Fig.2.3). The crucibles are in a close contact with two thermocouples (denoted as B in Fig.2.3) connected in opposite directions. A temperature difference between the two crucibles results in the development of a voltage from the thermocouple pair.

Heat flow from the furnace to each crucible is described by the following equation:

$$\frac{dQ}{dt} = \frac{\Delta T}{R} \quad \text{Eq.2.3}$$

where Q is heat, t is time, ΔT is temperature difference between the furnace and the crucible and R is the thermal resistance of the heat path between the furnace and the crucible [57].

Differences in temperature between the sample crucible and reference crucible result in differences in heat flow and this reflects changes in the sample properties.

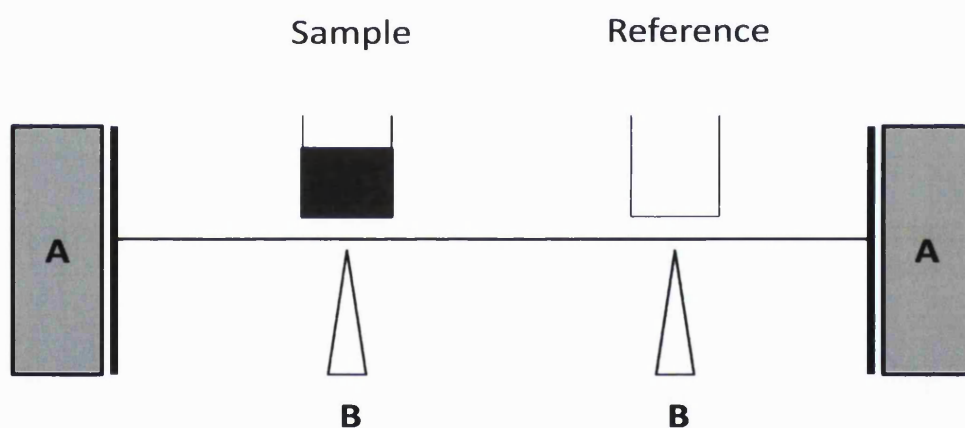


Figure 2.3: A schematic diagram of a heat flux DSC. A = furnace, B = thermocouple (reproduced from Ref [57]).

The other instrumentation DSC type is referred to as power compensation DSC and is represented schematically in Fig.2.4. In this type the sample and reference crucibles (denoted as B in Fig.2.4) are heated by two separate furnaces (denoted as A in Fig.2.4). The furnaces are programmed to keep the two crucibles at the same temperature. As the sample goes through a thermal event, a difference in power supply from the furnaces to

the crucibles is recorded. This power difference then reflects changes in samples properties [57].

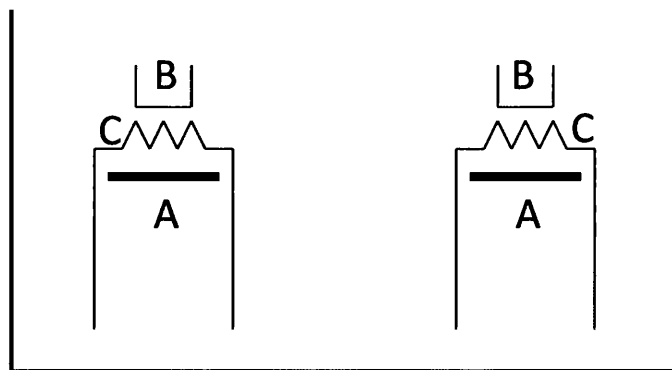


Figure 2.4: A schematic diagram for power compensation DSC. A = furnaces, B = sample and reference crucibles, C = sample and reference platinum resistance thermometers (reproduced from Ref [57]).

When the temperature programme used to heat or cool the sample is linear as shown in Fig.2.5, the technique is referred to as conventional DSC.

2.2.5.2. Experimental

A Pyris 1 DSC (PerkinElmer Instruments, Beaconsfield, UK) connected to a cooling unit (Intracooler IIP, PerkinElmer Instruments) was used for conventional DSC measurements. The DSC cell was purged with dry nitrogen at a flow rate of 20cm³/min. Temperature and enthalpy calibration was performed using Indium standard. The specific heating programme used will be described in the experimental sections of results chapters.

2.2.6. Modulated temperature DSC (MTDSC)

2.2.6.1. Introduction

Modulated temperature DSC was introduced in the early 1990's. It is characterised by the use of a sinusoidal or modulated heating programme instead of the linear heating or cooling ramp used in conventional DSC [57] as illustrated in Fig.2.5. The temperature profile in the two types of DSC is illustrated in Fig.5. MTDSC allows deconvolution of total heat flow to two separate components. The first component is heat flow arising from contribution of sample heat capacity (C_p) and is referred to as *reversing* heat flow. The second component (*non-reversing* signal) results from any other kinetic event a sample undergoes [57].

Three different elements characterise the temperature profile in a MTDSC as described in following equation (Eq.2.4) [58]:

$$T = T_0 + at + A \sin (2\pi t/p) \quad \text{Eq.2.4}$$

where T is temperature, T_0 is starting temperature, a is underlying heating rate, t is time and p is the period of oscillation.

MTDSC offers some benefits over conventional DSC. For example, it allows accurate measurement of heat capacity, separation of overlapping events such as glass transition and accompanying relaxation endotherm. However, the technique also has some disadvantages such as the use of slow heating rates (typically $2^\circ\text{C}/\text{min}$) and the need to optimise different parameters to obtain reliable data [57]. For examples, it should be ensured that there are at least six modulations through the event of interest in order to be able to deconvolute the signal.

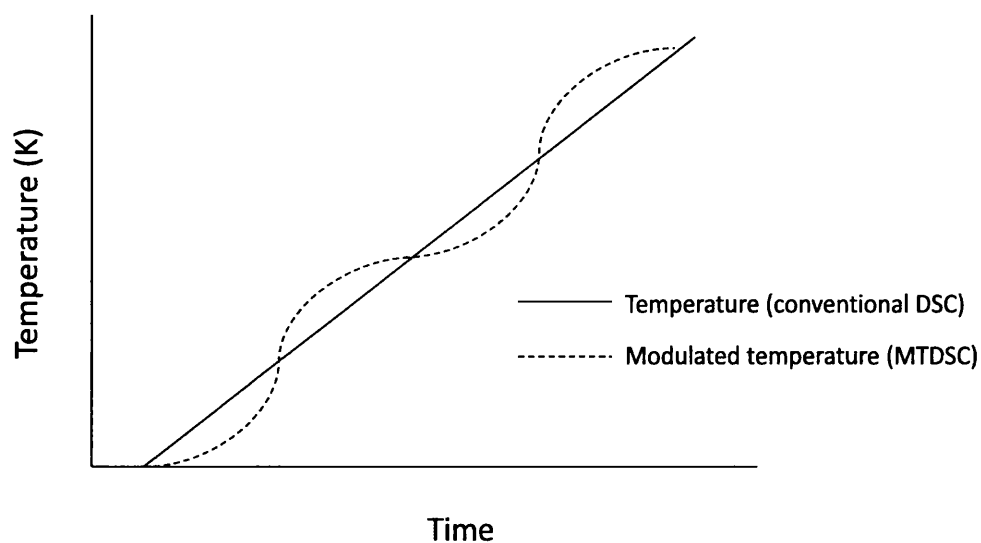


Figure 2.5: Illustration of temperature as a function of time for conventional DSC and modulated temperature DSC (reproduced from Ref [57]).

2.2.6.2. Experimental

Modulated DSC (Q2000, TA Instruments, New Castle, DE) with a refrigerated cooling accessory (RCS) was used to measure glass transition temperature (T_g), heat capacity change (ΔC_p) and apparent relaxation enthalpy ($\Delta_r H$) for amorphous indomethacin. The modulation parameters were optimised as will be described in Chapter 3. The DSC cell was purged with 50 cm³/min dry nitrogen. The DSC cell was calibrated for temperature and enthalpy using Indium standard ($T_m = 156.61^\circ\text{C}$) and for heat capacity using Sapphire Standard. For the relaxation study, indomethacin samples were loaded in non-hermetically sealed pans (TA Instruments) inside the glove bag ($\leq 5\% \text{ RH}$) then immediately placed in the DSC cell at 25°C . The temperature programme was initially optimised as described in Chapter 3 then based on the optimisation results it was decided to use a heating rate of $2^\circ\text{C}/\text{min}$, amplitude of 0.5°C and frequency of 60s for the relaxation studies.

2.2.7. X-ray powder diffraction (XRPD)

2.2.7.1. Introduction

XRPD is widely used to distinguish substances of different internal structure. In principle, the powdered material scatters the applied x-rays. The pattern of the scattered x-rays, known as the diffraction pattern, is unique to the internal physical structure. Bragg's law is used in order to interpret X-ray diffraction as follows:

$$n\lambda = 2d \sin\theta \quad \text{Eq.2.5}$$

where n is an integer, λ is the wavelength of the x-rays, d is the interplanar spacing generating the diffraction and θ is the diffraction angle [2]. A schematic diagram for an X-ray powder diffractometer is shown in Fig.2.6.

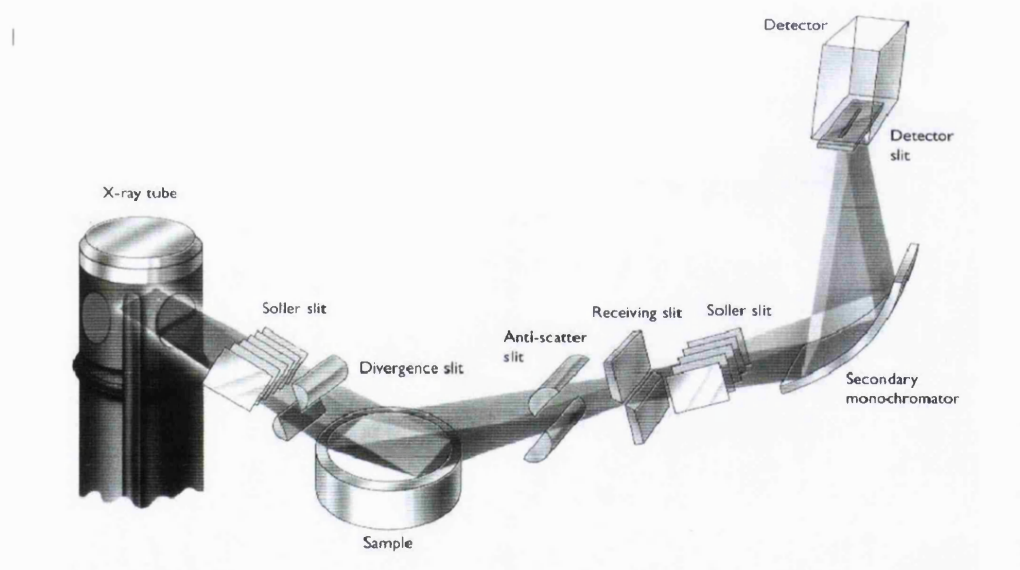


Figure 2.6: Schematic diagram for an X-ray powder diffractometer (reproduced from PANalytical manual)

2.2.7.2. Experimental

An X-ray diffractometer (Philip PW3710, Holland) was used to carry out XRPD experiments using CuK α radiation with 45 kV voltage and 30 mA current. The powder sample was loaded and flattened on a copper plate then placed in the XRPD detection chamber.

For the characterisation of amorphicity, samples were scanned from 5° to 35° at a scanning speed of 0.50°/min.

For crystallisation kinetics of indomethacin, samples were scanned from 5° to 35° at a scanning speed of 0.25°/min.

2.2.8. Dynamic vapour sorption (DVS)

2.2.8.1. Introduction

In a dynamic vapour sorption instrument, the two pans of a microbalance are contained in two sealed chambers, the sample chamber and the reference chamber. An electronic mass flow controller is connected to each chamber and it allows the control of relative humidity (RH) by mixing dry gas (eg. nitrogen) with moisture-saturated gas in proportions according to the desired experimental RH [59]. A schematic diagram for a DVS instrument is shown in Fig.2.7.

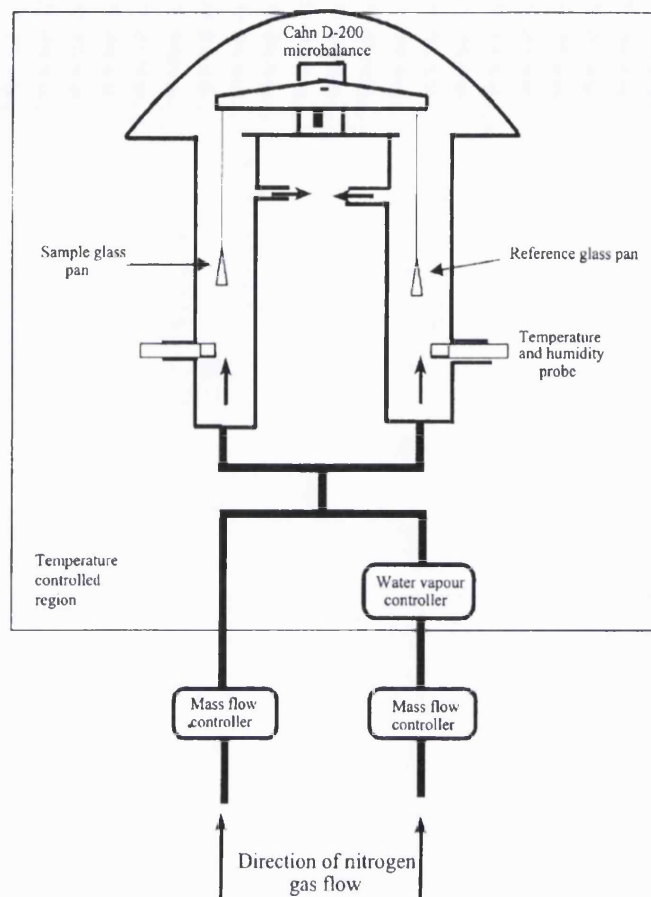


Figure 2.7: Schematic diagram for a DVS instrument (reproduced from Ref [60]).

2.2.8.2. Experimental

A humidity-controlled microbalance (DVS, Surface Measurement Systems, UK) was used to determine water sorption isotherms for ball-milled lactose samples at 25⁰C. The powder sample (about 20mg) was loaded in a quartz DVS flat bottom sample pan then placed in the humidity-controlled chamber. The sample was kept at 0% RH for 800min. Samples were considered to be totally dry when the signal became constant. The RH was then increased to the desired experimental RH for 2000min. The %RH range used was from 5% to 60% in 5% increments. The gas flow in the DVS was set to 200cm³/min.

2.2.9. Other methods

2.2.9.1. Thermal gravimetric analysis (TGA)

Moisture content of samples was measured using a TGA (Perkin Elmer Instruments, Beaconsfield, UK). 10-20 mg of sample was loaded in the measuring pan and scanned from 30-200°C at 20°C/min.

2.2.9.2. Polarised light microscopy

A Nikon light microscope (Macrohot-FXA) was used to examine indomethacin samples. Polarisation was achieved by using polarising filters. TAM ampoules containing indomethacin were placed directly on top of the microscope stage for examination. x4-x10 magnification range was used.

2.2.9.3. High performance liquid chromatography (HPLC)

An HPLC instrument (Agilent Technologies, 1200 Series, USA) was used to verify the purity of quench cooled indomethacin samples. The following method was used (as adapted from the United States Pharmacopeia)

Mobile phase: solutions of 0.01M monobasic sodium phosphate and 0.01M dibasic sodium phosphate in acetonitrile and water (approximately 1:1 v/v) were prepared.

Standard preparation: an accurately weighed quantity of indomethacin was dissolved in the mobile phase to obtain a solution having a known concentration of about 0.1mg/ml.

Assay preparation: 100mg of indomethacin was accurately weighed and transferred to a 100ml volumetric flask. Mobile phase was then used to dissolve the powder and dilute to volume with mixing. 10ml of this solution was transferred to a 100ml volumetric flask and diluted with mobile phase. The detector was set at 254-nm. The flow rate was about 1ml/min.

2.2.9.4. Nuclear magnetic resonance (NMR)

NMR was used to determine the anomeric composition of lactose samples. 10mg of lactose was dissolved in 1ml of deuterated dimethyl sulfoxide (DMSO). This solvent was used as it greatly reduces the rate of mutarotation [61]. Lactose solutions were analysed with NMR spectroscopy (^1H NMR). NMR spectra were obtained using a Bruker Advance 500MHz NMR spectrometer equipped with broadband and triple resonance (^1H , ^{13}C and ^{15}N) inverse probes.

α -lactose shows a doublet at 6.3, whereas β -lactose shows a doublet at 6.6. The anomeric composition was then identified from the ratio of integrated peaks at 6.3 and 6.6 ppm downfield to TMS reference that are due to α -lactose and β -lactose respectively [62].

***3) Chapter 3: Isothermal
microcalorimetry as a tool to study
enthalpy relaxation of pharmaceuticals.***

3.1. Introduction

Investigation of structural relaxation has been considered a significant aspect of stability studies of amorphous pharmaceuticals. A relaxing system undergoes continuous structural changes that can affect its physical properties and hence its pharmaceutical performance [4]. Relaxation dynamics are also considered as a direct reflection of molecular mobility which can be coupled to other phenomena (eg. chemical stability and crystallisation) [27, 63].

Relaxation phenomenon can be studied using different techniques depending on which physical property is being investigated [23]. DSC is one of the most widely used techniques and it is employed in essence to study enthalpy relaxation [23, 27]. In recent years isothermal microcalorimetry (IMC) has been used for the same purpose [27]. Briefly, enthalpy relaxation results from the fact that the amorphous system is thermodynamically out of equilibrium and hence energy is lost in the form of heat in order to attain the equilibrium state. As explained previously in Chapter1 (Introduction) IMC can measure this heat loss directly whereas DSC measures the energy recovered by a relaxed system as it is heated across its T_g [23]. This difference in investigation principles between the two techniques has presented an incentive to investigate whether DSC and IMC are measuring the same property. The studies carried out for this purpose are not numerous and reveal some contradictory results. In a study by Liu et al [27] DSC and IMC provided reasonably similar enthalpy relaxation profiles for amorphous sucrose. In a different study by Bhugra et al [64] the enthalpy relaxation for two different hydrophobic drugs, indomethacin and ketoconazole, was assessed with IMC and DSC. In this case, the results obtained by the two techniques were significantly different. This was attributed to the possibility that IMC is recording additional modes of molecular motion which the less sensitive DSC cannot capture.

This caused a problem in deciding which data should be coupled to relaxation above T_g obtained by dielectric spectroscopy [64]. Therefore, further research is needed to investigate the origin of this discrepancy between DSC and IMC relaxation results. The first section of this chapter aims at exploring some aspects of this research using amorphous quench cooled indomethacin as a model pharmaceutical material.

IMC being a sensitive and simple experimental technique has only been used, to the best of our knowledge, to study enthalpy relaxation of one-component amorphous systems. These include either pure amorphous APIs and excipients [23, 27, 65-67] or amorphous solid solutions (in which the API is molecularly dispersed within an inert matrix) [68-72]. A pharmaceutical formulation, however, can consist of more than one amorphous component (for instance, if an amorphous excipient is added to a formulation already containing an amorphous API). Two-component amorphous dispersions (or solid suspensions) are another good example. The second section of this chapter explores the feasibility of using IMC to quantify the relaxation of two-component amorphous systems using the model fitting approach.

Isothermal microcalorimetric data (represented as power-time data) resulting from enthalpy relaxation of a one-component amorphous system are usually fitted to a model that describes this process. The most commonly used equations for this particular purpose are the time-derivatives of the Kohlrausch-Williams-Watts (KWW) equation (Eq.1.12) and the modified stretched exponential equation (MSE, Eq.1.17) [23, 27]

In the KWW equation, structural relaxation is characterised by the relaxation time, τ , and the stretch power, β [27]. The MSE equation is a modified version of the KWW equation and has been employed for the analysis of microcalorimetric enthalpy relaxation data in order to overcome the inability of the KWW time-derivative to

describe such data as time approaches zero [27]. β holds the same meaning in the MSE equation as in the KWW equation, whereas the equivalent parameter to τ , known as τ_D , is calculated from β and time constants τ_0 and τ_1 from Eq.1.16 described in Chapter 1.

When two co-existing amorphous components relax at different rates in an isothermal microcalorimeter, the resulting total heat flow should be the linear sum of the power-time data resulting from the two components as they relax separately under the same conditions. The calorimetric data for a two-component amorphous system can be then described by the sum of two relaxation models i.e. $KWW_1 + KWW_2$ (2-KWW, Eq.3.1) or $MSE_1 + MSE_2$ (2-MSE, Eq.3.2) **(note that in this study all the equations are in the time differential form).**

$$P = m_i \cdot \Delta_r H_{\infty i} \cdot \left(\frac{\beta_i}{\tau_i} \right) \cdot \left(\frac{t}{\tau_i} \right)^{\beta_i - 1} \cdot \exp \left[\left(\frac{t}{\tau_i} \right)^{\beta_i} \right] \\ + m_{ii} \cdot \Delta_r H_{\infty ii} \cdot \left(\frac{\beta_{ii}}{\tau_{ii}} \right) \cdot \left(\frac{t}{\tau_{ii}} \right)^{\beta_{ii} - 1} \cdot \exp \left[\left(\frac{t}{\tau_{ii}} \right)^{\beta_{ii}} \right] \quad \text{Eq.3.1}$$

$$P = m_i \cdot \frac{\Delta_r H_{\infty i}}{\tau_{0i}} \cdot \left(1 + \frac{\beta_i t}{\tau_{1i}} \right) \cdot \left(1 + \frac{t}{\tau_{1i}} \right)^{\beta_i - 2} \cdot \exp \left[- \left(\frac{t}{\tau_{0i}} \right) \cdot \left(1 + \frac{t}{\tau_{1i}} \right)^{\beta_i - 1} \right] \\ + m_{ii} \cdot \frac{\Delta_r H_{\infty ii}}{\tau_{0ii}} \cdot \left(1 + \frac{\beta_{ii} t}{\tau_{1ii}} \right) \cdot \left(1 + \frac{t}{\tau_{1ii}} \right)^{\beta_{ii} - 2} \cdot \exp \left[- \left(\frac{t}{\tau_{0ii}} \right) \cdot \left(1 + \frac{t}{\tau_{1ii}} \right)^{\beta_{ii} - 1} \right] \quad \text{Eq.3.2}$$

where the subscripts i and ii correspond to the two relaxing components of the system.

It is clear that these two models are quite complex and contain many unknown variables. This can impose a great burden on the fitting process since this is usually carried out iteratively. As a result, the best starting point is to test the ability of these

models to recover the correct relaxation parameters for pre-characterised two-component systems. This was achieved initially using simulated calorimetric data. Positive results encouraged us to proceed with real model systems; co-blended amorphous lactose, amorphous sucrose and amorphous indomethacin.

3.2. Aims & Objectives

3.2.1. Section I: the general aim of this section is to compare the relaxation profile of amorphous indomethacin determined by IMC with that determined by DSC.

Objectives:

- Determination of the effect of the preparation method of amorphous indomethacin on its T_g.
- Optimisation of the modulated temperature-DSC parameters to be used to characterise the enthalpy relaxation of amorphous indomethacin at 25⁰C.
- Characterisation of the enthalpy relaxation profile of amorphous indomethacin with IMC and DSC.

3.2.2. Section II: this section aims at determining the feasibility of quantifying the relaxation behaviour of two-component amorphous systems using isothermal microcalorimetry.

Objectives:

- Assess the ability to recover the correct relaxation parameters for simulated calorimetric data for two-component systems using model fitting approach and explore the effect of varying the difference between the relaxation times of the two phases on the sensitivity of the model used.

- Characterise the relaxation profile of model amorphous pharmaceutical materials (sucrose, lactose and indomethacin) with IMC using the KWW and MSE functions.
- Monitor enthalpy relaxation of physical mixtures of the characterised materials in the isothermal microcalorimeter and assess the ability of the 2-KWW and 2-MSE models to recover the expected relaxation parameters for the two phases.

3.3. Experimental

3.3.1. Materials and methods

3.3.1.1. Section I

3.3.1.1.1. Preparation of amorphous indomethacin

In order to investigate the effect of the preparation method on the thermal history of amorphous indomethacin, the latter was prepared using three different methods:

1. Crystalline indomethacin ($\approx 3\text{mg}$) was loaded in a hermetic aluminium pan. The sample was heated in the DSC to 15°C above its melting point (175°C) then cooled to sub-ambient temperature (-30°C) at 20 or $100^{\circ}\text{C}/\text{min}$ and eventually heated to 25°C (at $20^{\circ}\text{C}/\text{min}$) to be annealed inside the DSC for 24h. This sample will be referred to as DSC in-situ sample.
2. Crystalline indomethacin ($\approx 3\text{mg}$) was loaded in a hermetic aluminium pan. The sample was then melted on a hot plate set at 175°C for 20s then quench cooled with liquid nitrogen. The pan was then annealed at 25°C inside the DSC for 24h. This sample will be referred to as DSC ex-situ sample.

3. Crystalline indomethacin (20mg) was loaded into a 3ml glass ampoule. The ampoule was then sealed and melted in an oven at 175°C for 5min. The melted drug was then quench cooled with liquid nitrogen and the ampoule was then loaded in a TAM channel at 25°C and left there for 24h. This sample will be referred to as TAM sample.

After 24h of annealing, all samples were heated across their T_g in the DSC at 20°C/min.

All drug loading and sealing of DSC pans and Thermal Activity Monitor (TAM) ampoules (TA Instruments Ltd.) was carried out in a glove bag flushed with nitrogen to maintain the RH below 5%. All samples were prepared at least in duplicate. Samples prepared on hot plate and in TAM ampoules were analysed with HPLC as described in section 2.2.9.3 to assess their chemical stability after quench cooling.

DSC and TAM studies were carried out using the same batch of amorphous indomethacin. This was prepared by melting crystalline indomethacin on hot plate using aluminium foil boats then quench cooling with liquid nitrogen. After being dried in a desiccator for 1h, the formed glass was ground gently with a mortar and pestle then dried in a desiccator for 1h then stored at -80°C until further use.

3.3.1.2 Section II

3.3.1.2.1. Data simulation:

Microcalorimetric data for enthalpy relaxation were simulated using Mathcad software (Mathsoft Inc). Data for single systems were generated using the time derivative for the KWW model. All data sets for single-component systems were produced using the same values for $\Delta_f H$ (1J/g) and β (0.8) and only τ values were varied between 10⁵s and 10⁸s.

Data sets for two-component systems were produced by summing two data sets for single –component systems generated as described above. A range of two-component system data sets was generated in which the difference between the relaxation time constants for the two phases varied in an increased manner.

3.3.1.2.2. Preparation of binary amorphous systems:

Two different binary (two-component) amorphous systems were prepared. The first one consisted of amorphous sucrose and amorphous lactose. The second one was made of melt-cooled indomethacin and oven-dried spray-dried sucrose.

- Sucrose-lactose binary system:

Amorphous samples used for this system were prepared with spray drying as was described in section 2.2.1.2.

The amorphicity of spray-dried sucrose and spray-dried lactose samples was confirmed with X-ray powder diffraction (XRPD). Gravimetric analysis revealed that spray-dried sucrose and lactose samples had 1.7 (\pm 0.1) % and 2.5 (\pm 0.1) % moisture content, respectively. Spray-dried samples were sieved and stored at -20°C until further use for calorimetric measurements.

Sucrose-lactose binary systems were prepared by directly loading 300 mg of each sugar in standard glass ampoule for the Thermal Activity Monitor (TAM, TA Instruments Ltd) system (3 mL volume). Some level of mixing was achieved with the aid of a small spatula.

- Sucrose-indomethacin system:

Amorphous sucrose used for sucrose-indomethacin system was spray dried as described in section 2.2.1.2. then vacuum dried at 72⁰C and 1000 mBar for two hours. The dried sample was confirmed to remain amorphous with XRPD analysis and was found to contain 0.7 (± 0.1) % moisture.

Amorphous indomethacin was prepared by melt-cooling. Crystalline indomethacin, pre-weighed and sealed in air-tight glass ampoules, was melted in an oven at 175 ⁰C for 5 min. The molten material was then spread around the inner walls of the ampoule and immediately cooled under tap water. This method was proved with XRPD analysis to result in the production amorphous indomethacin. The advantage of adopting this preparation method was that the sample was not exposed to any mechanical stress (usually exerted by liquid nitrogen in quench cooled samples) that can affect sample behaviour [73]. Amorphous indomethacin samples were analysed gravimetrically and were found to contain less than 0.2% moisture.

The sucrose-indomethacin system was prepared by directly adding amorphous sucrose (500mg) to TAM glass ampoules (3 ml volume) which already contained amorphous indomethacin (200mg). Mixing the two components was not possible because amorphous indomethacin formed a thin layer around the ampoule and any attempt to scratch the solid could introduce some mechanical stress which was originally intentionally avoided.

3.3.1.2.3. Data analysis:

Simulated data analysis

Each simulated data set for two-component systems was imported into Origin 7.0 (Microcal Software Inc., USA) and fitted to the 2-KWW equation (Eq.3.1). The fitting was conducted by least-squares regression carried out by iteration. This method requires entering initial estimations for all the unknown parameters. The same input values were entered for all systems as summarised in Table 3.1. Values for m_i and m_{ii} were fixed to 1(g) as these would be known in real experimental settings.

Table 3.1: *Estimated values for relaxation parameters used for iteration process to fit simulated data to the 2-KWW model.*

	Component 1	Component 2
$\Delta_r H(\infty)$ (J/g)	7	12
B	0.4	0.7
τ (s)	7×10^5	2×10^5

Microcalorimetric data analysis

Power-time data for single-component components were fitted to the KWW (Eq.1.12) and MSE (Eq.1.17) equations to obtain “true” relaxation parameters. Power-time data for two-component amorphous systems were fitted to 2-KWW (Eq.3.1) and 2-MSE (Eq.3.2) models. The mean values of relaxation parameters for individual components were used for the iteration process.

3.4. Results & Discussion

3.4.1 Section I: *Comparison of enthalpy relaxation studies of one-component amorphous systems by IMC and DSC.*

3.4.1.1. Effect of preparation method on thermal history

When comparing the results from different techniques for some material property, one has to ensure that the same material is being used. This is particularly important when investigating enthalpy relaxation of amorphous materials since the relaxation profile is greatly dependent on the thermal history of the material, which is in turn partly determined by the preparation method [27]. Although in this study both samples were prepared by quench cooling, the use of different heating and cooling settings can affect the properties of the resulting glass. This is demonstrated by the simple annealing study of quench cooled indomethacin. Fig.3.1 shows the DSC scan of the three annealed samples prepared as described in the experimental section (DSC in-situ, DSC ex-situ, TAM sample). It is clear that preparing the sample inside or outside the DSC did not affect the thermal history of the material (solid and dash-dotted lines). This suggests that a cooling rate of 20⁰C/min employed to produce the DSC in-situ sample resulted in the same glass as cooling with liquid nitrogen. This was confirmed by increasing the cooling rate in the DSC to 100⁰C/min, which resulted in the formation of a glass behaving the same as that formed by cooling at 20⁰C/min (Fig.3.2). Quantitatively, in-situ DSC samples had a slightly higher T_g ($52.43 \pm 0.52^{\circ}\text{C}$) than ex-situ DSC sample ($51.42 \pm 0.14^{\circ}\text{C}$). When comparing the samples prepared in the DSC pan with that prepared in the TAM ampoule, it can be seen that the TAM sample had a lower T_g ($50.59 \pm 0.31^{\circ}\text{C}$) and a broader glass transition (Fig.3.1).

Percent recovery from HPLC analysis was 100.96 ± 0.57 % for samples prepared on the hot plate (equivalent to samples prepared in DSC pan) and 98.33 ± 0.10 % for TAM

samples. This indicates that TAM samples underwent some chemical degradation, whereas DSC samples did not. The presence of degradation products might have acted as plasticisers and resulted in lowering and broadening the T_g of the TAM samples.

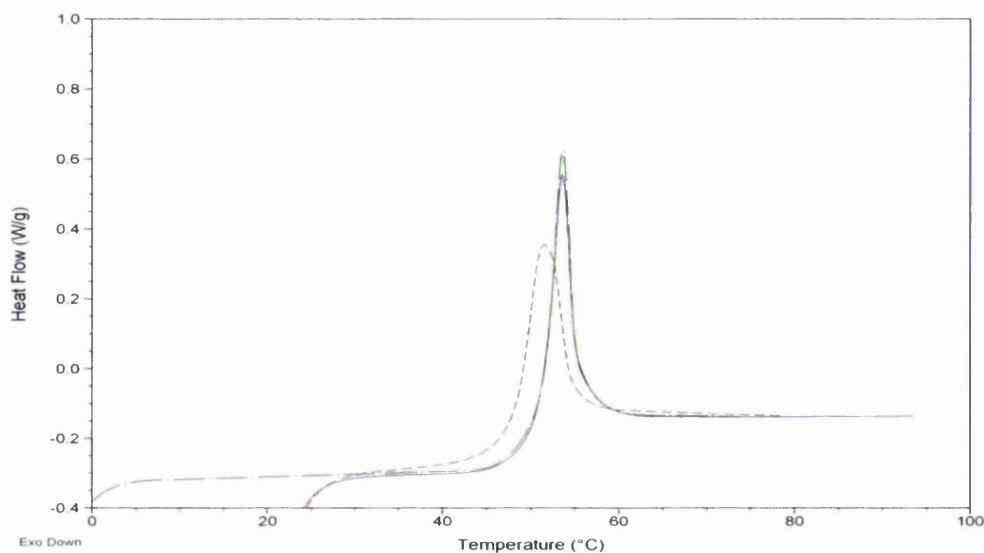


Figure 3.1: DSC scans for annealed DSC in-situ (solid line), DSC ex-situ (dash-dotted line) and TAM samples (dashed line).

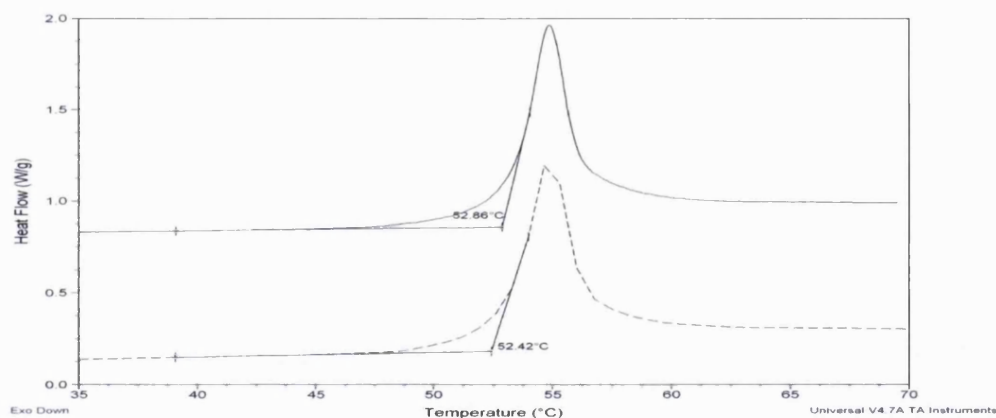


Figure 3.2: DSC scans for DSC in-situ samples: one cooled at 20°C/min (solid line) and the other at 100°C/min (dashed line).

The main advantage of preparing amorphous samples inside the measuring container (DSC pans or TAM ampoules) is that it minimises the mechanical stress that can result in the creation of nuclei which precedes crystallisation [73]. However, based on the

results discussed above it appears that the quench cooling settings affect the properties and thermal history of the resulting glass. Therefore, if data from DSC and TAM for a relaxing glass were to be compared, the ideal scenario would be to use the same batch of amorphous material.

3.4.1.2. Enthalpy relaxation with IMC

Fig.3.3 shows typical power-time data for relaxing amorphous indomethacin in an isothermal microcalorimeter. Only data for up to 27h are shown. As the system relaxes over time, the power signal decays until it reaches 0 μW , when the system has totally relaxed.

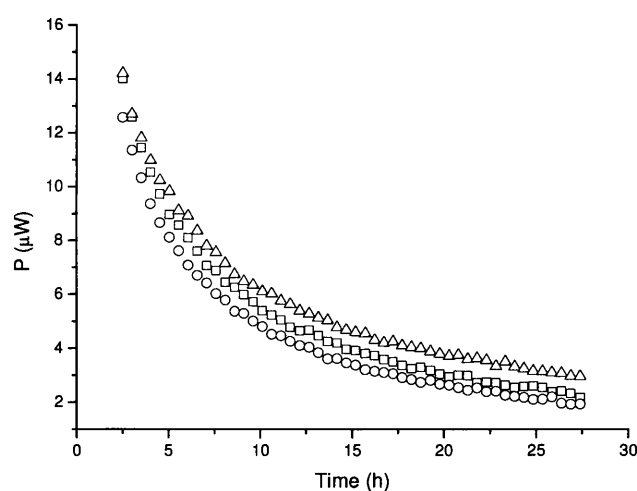


Figure 3.3: Power-time data for three different samples of the same batch of amorphous indomethacin.

All data sets for 24h relaxation period were well fitted by both KWW and MSE equations. Relaxation parameters are summarised in Table 3.2. As can be concluded from Fig.3.3 and Table 3.2 (from RSD), there is some scatter in the data. This was

expected since IMC is a very sensitive technique and slight variations in the thermal history can be captured and will be reflected in the fitting process.

Both MSE and KWW equations provided equivalent relaxation parameters (t-test for $\Delta_r H(\infty)$: $p = 0.630$, t-test for β : $p = 0.186$, t-test for τ^β : $p = 0.606$), although results obtained by KWW equation were less variable. It is worth noting that when comparing relaxation time constants, one should compare the combined time constant τ^β since it is a more robust parameter than the independent parameters τ and β which are more sensitive to experimental errors [27]. This can be confirmed from the lower value of RSD for τ^β compared with that for τ .

Table 3.2: Relaxation parameters obtained by fitting IMC data for amorphous indomethacin at 25°C to MSE and KWW equations. SD and RSD refer to standard deviation and relative standard deviation.

	τ (h)	β	τ^β	$\Delta_r H(\infty)$ (J/g)
	MSE			
Mean	51.76	0.529	7.57	3.53
SD	36.52	0.039	2.25	1.04
RSD (%)	70.57	7.437	29.77	29.46
	KWW			
Mean	27.88	0.569	6.67	3.19
SD	9.28	0.018	1.63	0.45
RSD (%)	33.29	3.301	24.47	14.28

3.4.1.3. Enthalpy relaxation by DSC

DSC was used in the modulated mode as this mode facilitates the separation of heat flow due to enthalpy recovery from that due to heat capacity change at glass transition [74].

3.4.1.2.1. Optimisation of modulation parameters

In order to ensure that the modulation parameters will not introduce any artefacts in the measured glass properties, different modulation parameters were employed to measure the T_g ; the change in heat capacity at glass transition (ΔC_p) and apparent recovery enthalpy (without annealing) using amorphous indomethacin prepared in-situ. All heating rates and frequency combinations employed allowed at least six modulations over the glass transition (data not shown). Results are summarised in Table 3.3. It appeared that the modulation parameters used provided similar results and were equivalent with literature values. ΔC_p was reported to be $0.46 \text{ J/g} \cdot ^\circ\text{C}$ in Ref [64]. The T_g was not compared to literature values as this parameter is dependent on the heating rate. A heating rate of 2°C/min , amplitude of 0.5°C and frequency of 60s were then chosen to carry out our enthalpy relaxation study with modulated temperature DSC.

Table 3.3: Effect of modulation parameters on glass properties of amorphous indomethacin.

Modulation Parameters (heating rate, amplitude, frequency)	$T_{g \text{ onset}}(^{\circ}\text{C})$	$\Delta C_p (\text{J/g} \cdot ^{\circ}\text{C})$	$\Delta_r H (\text{J/g})$
1°C/min , 1C, 100s	40.71	0.455	2.33
1°C/min , 0.5C, 60s	41.69	0.475	3.15
2°C/min , 1C, 60s	41.84	0.459	2.62
2°C/min , 0.5C, 60s	42.59	0.440	2.45

3.4.1.2.2. Estimation of $\Delta_r H(t)$

Apparent $\Delta_r H(t)$ was calculated by integrating the non-reversing heat flow signal for a sample annealed for time t . This $\Delta_r H(t)$ is described as apparent as it consists of several contributing factors. The first factor is known as the “frequency effect” [23, 27]. This is an artefact that results from difference in T_g values obtained from the total and reversing signals. The T_g obtained from the reversing signal represents the sample response to the oscillating heating programme and not to the underlying (linear) heating programme. This results in a slightly higher T_g from the reversing signal. Consequently, upon subtracting the reversing signal from the total signal an apparent enthalpy contribution to the non-reversing signal is obtained [74]. Another contributing factor is relaxation during sample preparation for DSC measurement. This can be significant since our samples were prepared externally, and hence relaxation during sample preparation and handling should be accounted for. The final contributing factor is relaxation during DSC heating from the annealing temperature (25°C) to a temperature above the T_g . This factor is particularly pertinent with MTDSC since slow heating rates are required for this technique to ensure that there is adequate number of oscillations across the glass transition [74]. The best strategy to account for all these factors in the calculations was to subtract the apparent recovery enthalpy for unannealed samples, $\Delta_r H(0)$ from subsequently measured apparent recovery enthalpy for annealed samples, $\Delta_r H(t)$ [23].

3.4.1.2.3. Estimation of $\Delta_r H(\infty)$

$\Delta_r H(\infty)$ is usually estimated based on the following equation (Eq.1.10) as described earlier in section 1.8.1: $\Delta_r H(\infty) = \Delta C_p (T_g - T_a)$

ΔC_p was taken as the mean value for heat capacity change at T_g for all samples. A figure of 0.41 J/g was found. T_a is the annealing temperature and was kept at 25°C . The

calculated value for $\Delta_r H(\infty)$ needs to be normalised like the calculated $\Delta_r H(t)$ by subtracting the apparent recovery enthalpy for unannealed samples, $\Delta_r H(0)$, from the calculated $\Delta_r H(\infty)$ based on Eq.1.10. However, it should be remembered that $\Delta_r H(0)$ also has contribution from “frequency effect”. This contribution should not be accounted for in $\Delta_r H(\infty)$. Apparent ΔH due to frequency effect only was measured from the cooling cycle and was found to be 1.72 ± 0.23 J/g.

It remains to determine the value of T_g that should be used in the calculation. The glass transition is a broad transition and can be represented either by the onset of the inflection (T_g onset) or the temperature at which the heat capacity change is half the total value (T_g mid). Kawakami et al [23] suggested that if the annealing temperature is 30°C below T_g , using either T_g (onset) or T_g (mid) will not have a significant impact on the calculated $\Delta_r H(\infty)$. In our case, T_g (onset) and T_g (mid) were determined to be $42.63 \pm 0.37^\circ\text{C}$ and $43.89 \pm 0.21^\circ\text{C}$, respectively. Given that T_a was 25°C , when the normalised $\Delta_r H(\infty)$ was calculated using T_g (onset) a value of 4.53 J/g was recorded. This value was 0.51 J/g lower than the value calculated using T_g (mid). Both values were used to calculate the relaxation decay function and the results are discussed in the section below. Another possible value of T_g can be used, this is the T_g at zero heating rate. T_g is dependent on the heating rate used and hence it would be reasonable to use a value for T_g which is not affected by the heating rate. This was determined by measuring the T_g as a function of heating rate and extrapolation to zero heating rate as it is illustrated in Fig.3.4. T_g at zero heating rate, $T_g(0)$, was found to be 41.22°C and the calculated $\Delta_r H(\infty)$ based on this figure was 3.95 J/g.

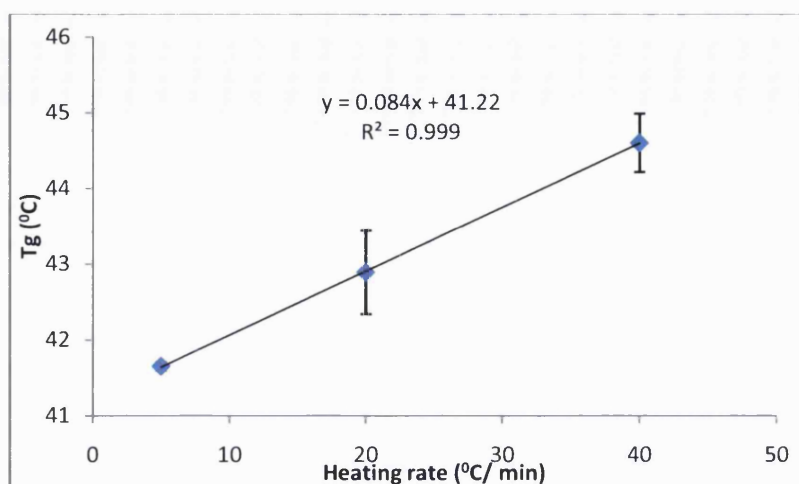


Figure 3.4: Glass transition temperature (T_g) as a function of heating rate. Line represents linear fit to the data.

3.4.1.2.4. Relaxation parameters from DSC data

The decay function was determined as from Eq.3.3 derived from Eq.1.8 described in Chapter 1.

$$\phi(t) = 1 - \frac{\Delta_r H(t)}{\Delta_r H(\infty)} \quad \text{Eq.3.3}$$

Three different relaxation functions were determined for indomethacin at 25°C using three different values for T_g : $T_g(\text{onset})$, $T_g(\text{mid})$ and $T_g(0)$. Data were then fitted to the KWW equation to obtain relaxation parameters τ and β . Data and the resulting fit lines are illustrated in Fig.3.5. For the three different cases, a reasonable fit was obtained with the KWW model; the resulting relaxation parameters along with the T_g and calculated $\Delta_r H(\infty)$ used to determine the relaxation functions are summarised in Table 3.4.

As was suggested by Kawakami and Pikal [23], using $T_g(\text{onset})$ or $T_g(\text{mid})$ did not result in a significant change in the determined relaxation profile (Table 3.4). When $T_g(0)$ was used, slightly different relaxation parameters were obtained. When relaxation

profiles determined using DSC (Table 3.4) were compared with those obtained using IMC (Table 3.2), it can be concluded that the DSC results obtained with $T_g(0)$ agreed very closely with IMC results (paired t-test: $p = 0.248$), although results obtained with $T_g(\text{onset})$ and $T_g(\text{mid})$ still reasonably agreed with IMC results (paired t-test: $T_g(\text{onset}): p = 0.156$, $T_g(\text{mid}): p = 0.225$). This includes both time constants (τ and β) and $\Delta_r H(\infty)$. This conclusion is not consistent with what was reported by Bhugra et al [64] as they showed that values for τ^β determined with DSC are three times higher than that determined with IMC for amorphous indomethacin (see Table 3.5).

Table 3.4: T_g , $\Delta_r H(\infty)$ (J/g) and relaxation parameters obtained for indomethacin at 25°C using DSC.

$T_g(^{\circ}\text{C})$	$\Delta_r H(\infty)$ (J/g)	τ (h)	β	τ^β
$T_g(\text{onset}) = 42.63$	4.53	36.02	0.655	10.47
$T_g(\text{mid}) = 43.89$	5.04	46.01	0.639	11.55
$T_g(0) = 41.22$	3.95	33.76	0.579	7.69

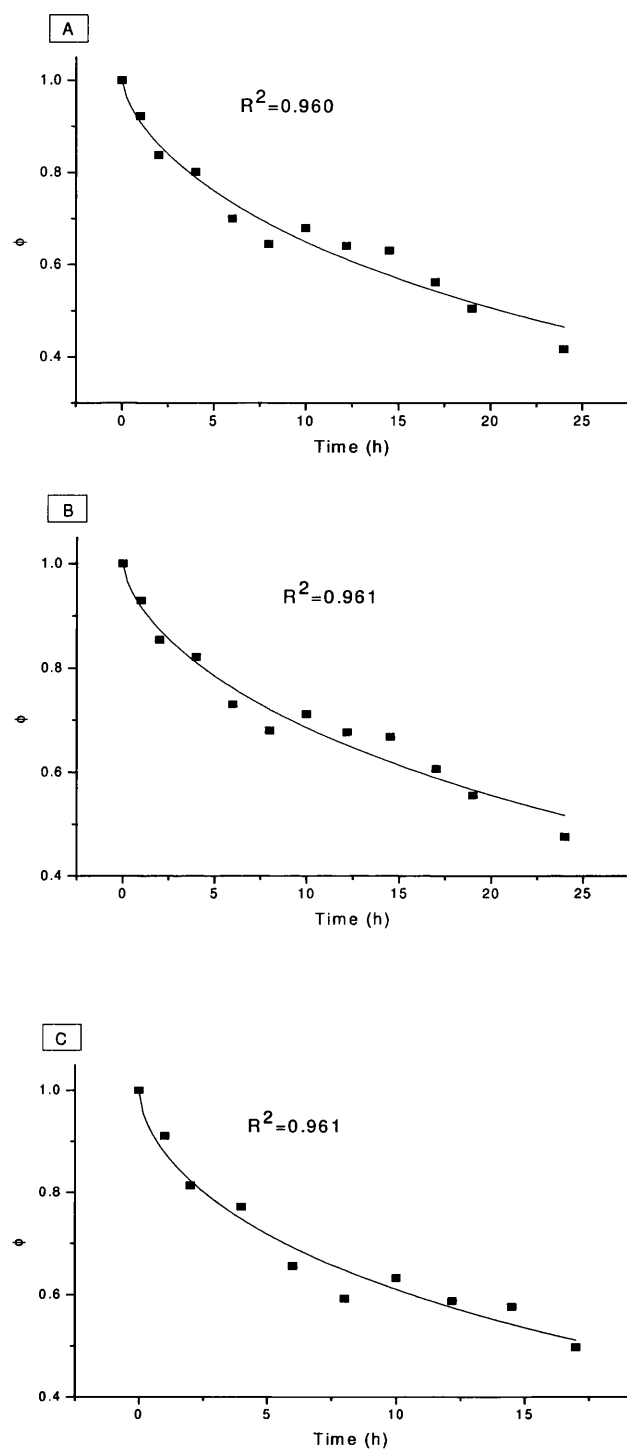


Figure 3.5: The relaxation functions Φ and their fit to the KWW equation for indomethacin at 25°C determined using A) T_g (onset), B) T_g (mid) and C) T_g (0). Solid lines represent best fit to the KWW equation.

Table 3.5: Comparison between calorimetric relaxation times obtained from isothermal microcalorimetry and modulated DSC (in hours) along with enthalpic relaxation and recovery obtained at two temperatures for indomethacin for the study reported by Bhugra et al (adapted from Ref [64]).

	Isothermal microcalorimetry MSE		Modulated DSC KWW	
Temperature (°C)	Enthalpy Relaxed (J/g)	Relaxation Time, τ^β (h $^\beta$)	Enthalpy Relaxed (J/g)	Relaxation Time, τ^β (h $^\beta$)
25 (16h)	3.1 \pm 0.1	3.4 \pm 0.3	2.6 \pm 0.1	12.0 \pm 0.9
30 (16h)	3.5 \pm 0.2	1.5 \pm 0.5	2.9 \pm 0.1	4.4 \pm 0.4

The time in parenthesis is the longest time point for the experiment in modulated DSC and also the time point for comparison between the enthalpic relaxation and recovery. Data are means of three replicates.

As mentioned previously, Bhugra et al [64] used samples prepared in the measuring container for both DSC and IMC assuming that a material of the same physical properties was being studied. Our results demonstrate that the difference between DSC and IMC results in Bhugra et al's work is very likely to be attributed to differences in the physical properties of the material rather than differences in the nature of the property being measured by the two techniques. This is also confirmed by a study carried out by Liu et al [27] in which DSC and TAM provided similar results for the relaxation of amorphous sucrose. In this study sucrose samples used for DSC and IMC measurements were prepared externally in the same way i.e. a material of the same thermal history was used.

3.4.2. Section II: Quantitative assessment of enthalpy relaxation of two-component amorphous systems with IMC.

3.4.2.1. Simulated data

Simulated power-time data for two-component amorphous systems were fitted to a 2-KWW model and the resulting fit values are summarised in Table 3.6. Values of relaxation time constants used to construct each data set are also shown in Table 3.6. All data were well fitted by the model as seen from the very small values of χ^2 and by visual observation of the fit lines (data not shown). The fit values agreed reasonably with the true values when the two relaxation time constants of the two phases were of the same order of magnitude. The fit values started to deviate from the true values as the difference between the two time constants increased. As this difference increased to three orders of magnitude, non-physical values for $\Delta_r H(\infty)$ and β were obtained for one component, whereas the true values for the component with smaller τ value were fully recovered. Fig.3.6 illustrates simulated power-time data for 2-component amorphous systems. It illustrates that as the difference between the two time constants of the constituting phases increased, one component dominated the ‘overall’ signal. As a result, the fitting model lost the resolution to detect the contribution from the minor component.

Table 3.6: Fit values for relaxation parameters obtained by fitting simulated data to 2-KWW model.

	$\tau_1 = 2 \times \tau_2 = 2\text{E}+05\text{s}^a$		$\tau_1 = 10 \times \tau_2 = 1\text{E}+06\text{s}^a$		$\tau_1 = 100 \times \tau_2 = 1\text{E}+07\text{s}^a$		$\tau_1 = 1000 \times \tau_2 = 1\text{E}+08\text{s}^a$	
	Comp. ^b 1	Comp.2	Comp.1	Comp.2	Comp.1	Comp.2	Comp.1	Comp.2
$\Delta_r H(\infty)$	0.63	1.30	0.84	1.12	0.36	1.01	-0.90	1.00
β	0.82	0.79	0.96	0.79	1.01	0.79	-0.10	0.79
τ (s)	2.6E+05	1.0E+05	1.1E+06	1.0E+05	2.2E+06	1.0E+05	3.4E+09	1.00E+05

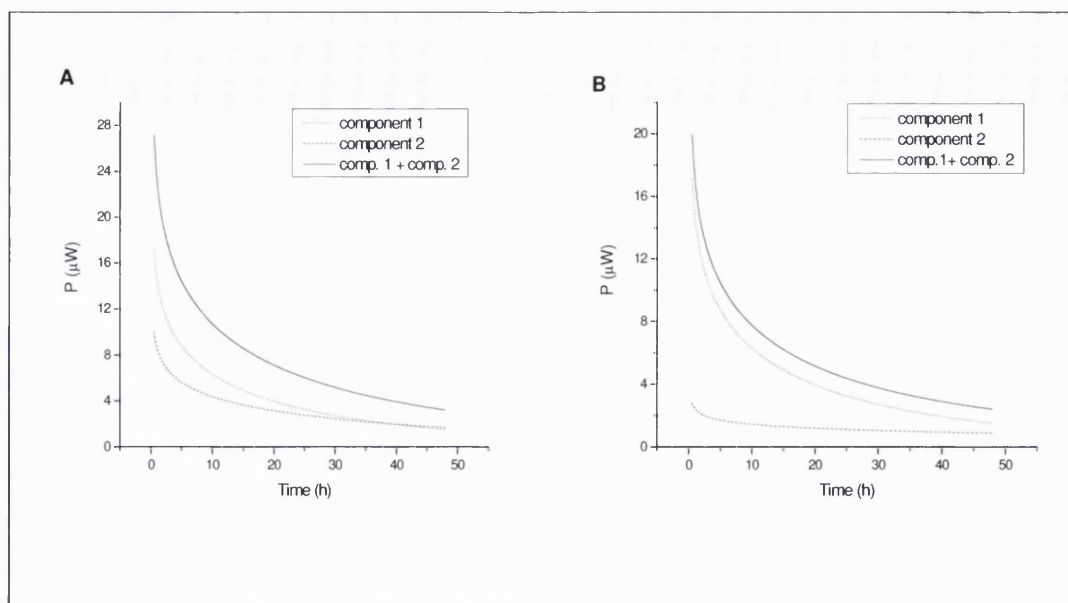


Figure 3.6: Simulated calorimetric data for relaxation of a 2-component system produced by summing data for two single-component systems having time constants A) of the same order of magnitude and B) different by one order of magnitude.

3.4.2.2. Experimental calorimetric data

3.4.2.2.1. Amorphous sucrose-lactose binary system

Amorphous sucrose and lactose batches used to prepare the binary system were annealed separately in the TAM to characterise their relaxation rates. Typical power-time traces for the two sugars are shown in Fig.3.7. Both the KWW and MSE models resulted in a good fit for the resulting power-time data as can be seen from the fit lines in Fig.3.7. The fit values for relaxation parameters are summarised in Table 3.7. In Table 3.7, τ and β are combined in one parameter, τ^β , since this parameter is supposed to give a better representation of the relaxation rate [27] and can be used as a more comprehensive tool to compare the relaxation behaviour of different materials [23].

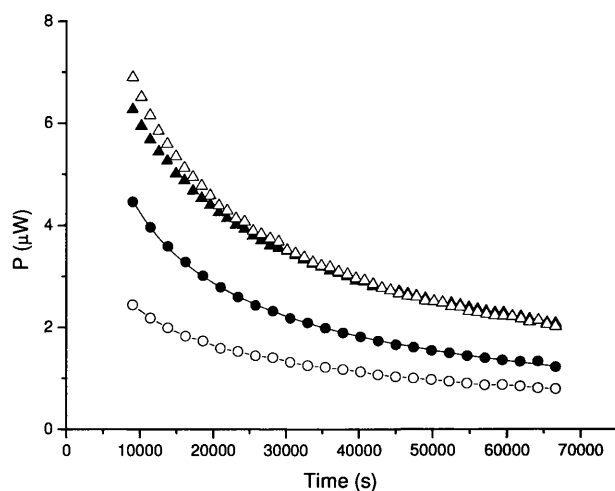


Figure 3.7: Power-time traces resulting from relaxation of sucrose (●), lactose (○), experimental sucrose-lactose binary system (▲) and theoretical sucrose-lactose binary system (△). Solid line for sucrose and lactose data represents fit to KWW equation.

Table 3.7: Relaxation parameters for individual sucrose and lactose samples obtained by fitting power-time data to KWW and MSE equations. (Standard deviation values in parentheses, $n = 3$).

	KWW				MSE			
	τ (h)	β	τ^β	ΔH_∞ (J/g)	τ_D (h)	β	τ_D^β	ΔH_∞ (J/g)
Sucrose	25.03 (2.37)	0.63 (0.01)	7.77 (0.46)	1.13 (0.05)	41.70 (7.20)	0.56 (0.02)	8.30 (0.65)	1.29 (0.10)
Lactose	36.08 (3.24)	0.67 (0.01)	11.22 (0.76)	0.74 (0.31)	45.93 (19.70)	0.66 (0.04)	11.98 (1.42)	0.79 (0.13)

Fig.3.7 also shows the power-time data resulting from the relaxation of the binary mixture of amorphous sucrose and lactose (denoted as experimental binary system). The expected heat flow trace of the binary mixture is also depicted in the same figure (referred to as theoretical binary system). The latter was obtained by summing the

power-time data for sucrose and for lactose as they relaxed individually in the TAM. It can be seen that the trace for summed data does not totally superimpose on the experimental trace.

The experimental power-time data for the sucrose-lactose binary mixtures were fitted to the double form of KWW and MSE equations (i.e. 2-KWW and 2-MSE). As mentioned earlier, the iteration process requires the provision of preliminary estimates of the parameters. In this case, the mean relaxation parameters identified earlier for individual components (summarised in Table 3.7) were employed for this purpose. The resulting fit values are summarised in Table 3.8.

Table 3.8: Fit values for relaxation parameters returned by 2-KWW and 2-MSE models for binary sucrose-lactose samples. Standard deviation values in parentheses, $n = 3$.

	KWW				MSE			
	τ (h)	β	τ^β	ΔH_∞ (J/g)	τ_0 (h)	β	τ_0^β	ΔH_∞ (J/g)
Comp. 1	20.27 (2.70)	0.683 (0.020)	7.79 (0.34)	1.22 (0.02)	37.82 (20.28)	0.717 (0.166)	13.48 (7.87)	0.98 (0.23)
Comp. 2	116.67 (43.33)	0.907 (0.163)	106.97 (96.12)	1.11 (0.23)	130.97 (26.59)	0.517 (0.131)	14.53 (10.20)	1.59 (0.22)

The data in Table 3.8 were derived from three independent measurements. The choice of component 1 and component 2 to calculate the mean parameters was based on the values of τ , i.e. the component with larger τ value was considered as component 1 and the one with the smaller τ value was taken as component 2.

By comparing the relaxation parameters for sucrose and lactose (as demonstrated in Table 3.7) with the fit values summarised in Table 3.8, it can be seen that the KWW

model reasonably recovered the expected relaxation parameters for sucrose (component 1), whereas the fit values for the second component, besides their great variability, clearly differed from those of lactose.

The fit values obtained from the MSE equation seemed to be more variable and the parameters for the two components did not match any of those for sucrose or lactose.

3.4.2.2.2. Sucrose-Indomethacin binary system

Power-time data for the individual components (sucrose and indomethacin) and for experimental and theoretical binary sucrose-indomethacin systems are shown in Fig.3.8. Similar to the sucrose-lactose system, the trace for the theoretical sucrose-indomethacin system does not superimpose on that for the experimental system.

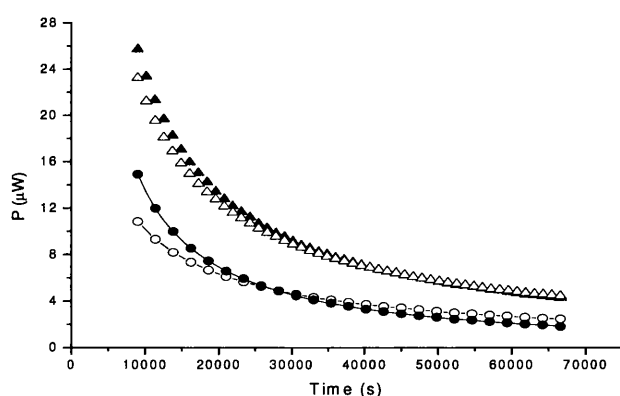


Figure 3.8: Power-time traces resulting from relaxation of sucrose (\circ), indomethacin (\bullet), experimental sucrose-indomethacin binary system (Δ) and theoretical sucrose-indomethacin binary system (\blacktriangle). Solid line for sucrose and lactose data represents fit to KWW equation.

The relaxation behaviour of the constituting materials of this system was characterised as they relaxed individually in the TAM. The mean relaxation parameters obtained by

fitting the power-time data for each material to the KWW and MSE models are listed in Table 3.9.

Table 3.9: Relaxation parameters for individual sucrose and indomethacin samples obtained by fitting power-time data to KWW and MSE equations. Standard deviation values in parentheses, $n = 3$.

	KWW				MSE			
	τ (h)	β	τ^β	ΔH_∞ (J/g)	τ_0 (h)	β	τ_0^β	ΔH_∞ (J/g)
Sucrose	35.91 (3.07)	0.483 (0.011)	5.64 (0.18)	1.92 (0.14)	43.48 (1.98)	0.506 (0.003)	6.74 (0.22)	1.81 (0.08)
Indomethacin	5.31 (1.16)	0.352 (0.023)	1.80 (0.21)	5.40 (0.55)	7.89 (0.92)	0.422 (0.016)	2.40 (0.20)	4.14 (0.26)

Both the KWW and MSE models fitted the data for the two materials very well as can be seen from the fit lines in Fig.3.8.

Isothermal microcalorimetric data for the experimental binary system were then fitted to 2-KWW and 2-MSE equations using the identified mean relaxation parameters for each material to carry out the iteration process. Results are illustrated in Table 3.10.

Unlike the sucrose-lactose binary system, the MSE model reasonably recovered the expected values of τ^β and ΔH_∞ for both components (compare Table 3.9) and with tight variability.

On the other hand, a similar outcome was obtained with the KWW model, which only recovered the expected relaxation time constant τ^β for one component (indomethacin, referred to as component 2 in Table 3.10) but not for the other component (sucrose). Only values for ΔH_∞ were reasonably recovered for both components.

Table 3.10: Fit values for relaxation parameters returned by 2-KWW and 2-MSE models for binary sucrose-indomethacin samples. Standard deviation values in parentheses, $n = 3$.

	KWW				MSE			
	τ (h)	β	τ^β	ΔH_∞ (J/g)	τ_0 (h)	β	τ_0^β	ΔH_∞ (J/g)
Comp. 1	111.86 (30.60)	0.529 (0.126)	14.85 (11.64)	2.10 (0.13)	90.83 (6.68)	0.436 (0.032)	7.16 (0.80)	2.09 (0.10)
Comp. 2	9.48 (3.73)	0.426 (0.026)	2.53 (0.31)	5.34 (0.16)	25.50 (9.28)	0.354 (0.026)	3.11 (0.49)	45.23 (0.26)

3.4.2.3. General discussion

3.4.2.3.1. Reliability of the 2-KWW model based on simulated data

The use of isothermal microcalorimetry in the pharmaceutical field has been compromised by the lack of robust methods for quantitative analysis. The model fitting approach is one of the methods employed to overcome this problem. There are two main requirements for this method to be successful. First, there should exist prior knowledge about the processes being recorded by the calorimeter. Second, these processes should be describable by a model which can be manipulated to fit microcalorimetric data. The fitting process is usually carried out iteratively; as the complexity of the model increases, which is the case with the 2-KWW and 2-MSE models, the more time-consuming the fitting process becomes and the more likely it is that the model will reasonably describe the data. The reliability of at least one of these two models (which was the 2-KWW) was evaluated on simulated data for which the real values for all the parameters are known. Simulated data are also free from any random noise that can affect the fitting process.

Based on the results in Table 3.6., the 2-KWW model appeared to be able to recover reasonably the correct parameters for both components as long as the relaxation time constants differed by less than three orders of magnitude. This in effect reflects the influence of the ratio between the two components in terms of contributing to the total signal. This becomes clear when the data are plotted as shown for illustration in Fig.3.6, which shows how this ratio increases in favour of the component with lower relaxation time constant until this latter predominates and the 2-KWW model fails to “see” the minor component. These results demonstrated proof of concept and gave confidence in carrying the study using real calorimetric data.

3.4.2.3.2. Factors affecting model resolution with experimental data

In both the binary amorphous systems used in this study, the two components contributed significantly to the total calorimetric system (Figs.3.8 and 3.7). By mere visual examination of the experimental and expected power-time traces for both binary systems, it can be seen that the experimental heat flow for the mixture is not simply the linear summation of the heat flow of each component. The only source of possible artefacts that was suspected was differences in sample weight between individual and binary systems. The expected data were constructed by summing data for the two components as they relaxed individually in the TAM. The weight of each component was the same as that used for the mixture. During the TAM measurements, the mixture therefore had higher weight than the individual components and this could have affected the way the data is conveyed by the calorimeter. The effect of sample weight changes was examined by a simple experiment in which the summed data for relaxation of two amorphous indomethacin samples each weighing 200mg were compared to the data for relaxation of an indomethacin sample weighing 400mg. As figure 3.9 shows, the experimental power-time trace superimposed the expected data. This confirms that the

observed difference between the experimental and expected data for the binary systems was not caused by sample weight differences.

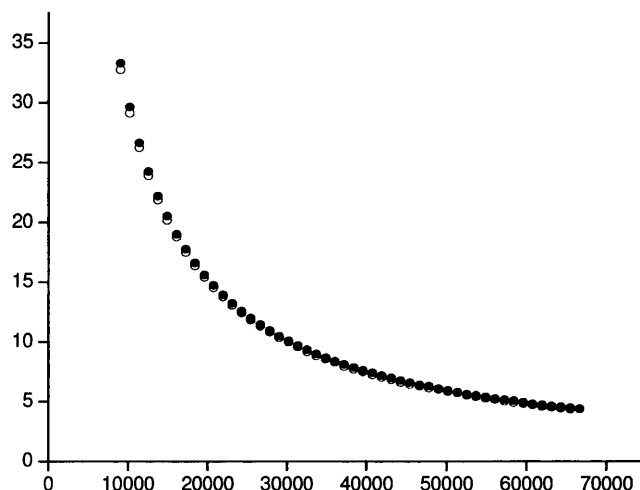


Figure 3.9: Calorimetric signal for relaxation of indomethacin. Closed circle (●) represent experimental signal of 400mg indomethacin sample, whereas open circles (○) represent summation of two 200mg experimental data.

When the experimental data were analysed quantitatively, the two binary systems behaved differently based on which model was employed to fit the data. For both systems, the 2-KWW model recovered the expected τ^{β} value for the component with lower τ^{β} value (see Tables 3.8 and 3.10). Simulating the data based on the fit values obtained for each measurement provides a better comprehension of the results. The fit values for a representative sucrose–lactose binary sample were used for this purpose; the plots are depicted in Fig.3.10 along with the average experimental traces for the two sugars as they relaxed individually. It is clear that the component with higher τ^{β} , which contributes less to the total signal (i.e. lactose), suffers from severe deviation from the expected behaviour. Similar observations were recorded with the sucrose-indomethacin system (data not shown).

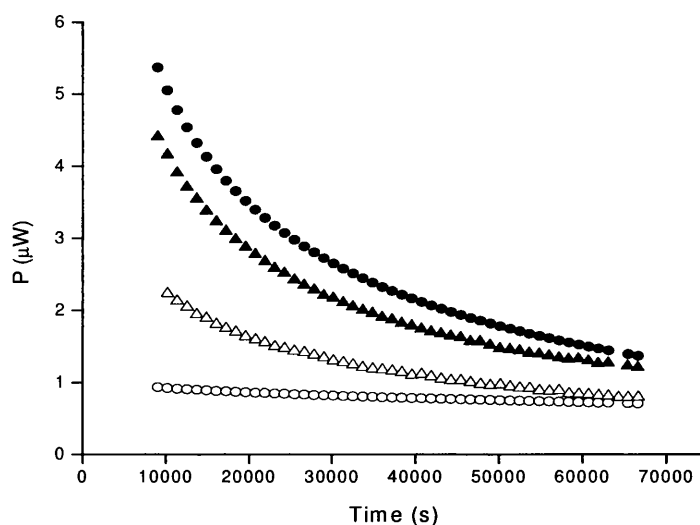


Figure 3.10: Deconvoluted calorimetric signal for a representative sucrose-lactose system as obtained from 2-KWW fit (●: component 1, ○: component 2) as compared to experimental calorimetric signal for relaxation of individual sucrose (▲) and lactose (Δ) samples.

When the same analysis was carried out on the results obtained with the 2-MSE model (Tables 3.8 and 3.10), the traces obtained for the sucrose-lactose system were scattered and no correlation could be observed between the simulated and experimental traces (data not shown). On the other hand, the simulated traces for the sucrose-indomethacin system were in very good agreement with expected (experimental) traces (Fig.3.11).

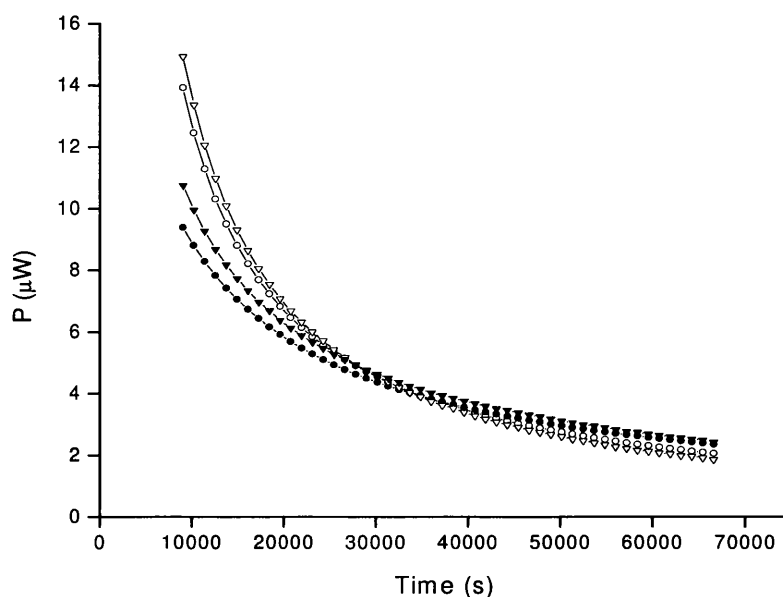


Figure 3.11: Deconvoluted calorimetric signal for a representative sucrose-indomethacin system as obtained from 2-MSE fit (-●-: component 1, -○-: component 2) as compared to calorimetric signal for relaxation of individual sucrose (-▲-) and indomethacin (-Δ-) samples.

When summed data for sucrose and lactose were fitted to the 2-MSE model, the extent of correct relaxation parameters recovery was greatly dependent on how closely the iteration parameters related to the correct ones. This implies that the failure of the 2-MSE model to recover the expected parameters for real sucrose-lactose systems is most likely resulting from the two components (or one of them) not behaving as expected for different possible reasons. The first possibility can simply arise from variability in relaxation behaviour between different samples from the same batch. The variability in τ^β value within individual sucrose and lactose batches used to construct the binary system is clearly greater than those for sucrose and indomethacin batches constituting the sucrose-indomethacin system (see Tables 3.7 and 3.9). Another source for change of behaviour in the sucrose-lactose system can be attributed to possible interaction between the two constituting sugars. The most potential type of interaction between

sucrose and lactose, which both had at least 1.5% moisture content, is moisture redistribution within the solid mixture. When materials are mixed together in a closed container, the total moisture content is likely to redistribute between the different components via the vapour phase [30, 75]. Water is a potent plasticizer for amorphous materials [32] and changing the moisture content can greatly affect the molecular mobility and hence the structural relaxation [27]. Any water exchange between the two sugars can also result in the creation of heat output, which can affect the fitting process. In the sucrose-indomethacin system such interaction is very unlikely since both components were in a practically dry state as indomethacin contained less than 0.2% of moisture and sucrose was in the collapsed state, in which moisture is usually trapped firmly. Any of these two different factors can explain why the MSE model reasonably returned the expected outcome for the sucrose-indomethacin system but not for the sucrose-lactose system.

When comparing the outcomes obtained from the two different models (2-KWW model versus 2-MSE model) based on the previous discussion, the 2-MSE model seems to be superior to the 2-KWW model. This is based on the outcome for the sucrose-indomethacin system since none of the two models offered satisfactory results for the sucrose-lactose system. A similar observation was made by Liu et al [27] regarding the difference between the two models but in the single form; and it was speculated that the superiority of the MSE equation might stem from the fact that it contains more parameters that appear to be less interdependent. This makes the 2-MSE model less sensitive to the inherent noise in the data unlike the 2-KWW model, which explains the contradiction between the outcome from the latter model with simulated and real calorimetric data. This was confirmed by the fact that the 2-KWW model was found to recover the correct parameters for simulated sucrose-lactose relaxation data. Inherent

noise in microcalorimetric data has been reported previously to affect the analysis using iterative least squares regression [76].

3.5. Summary

Enthalpy relaxation studies are often carried out to determine the stability of amorphous materials. IMC has been adopted as a sensitive and simple method to study relaxation. In the first section of this work, relaxation studies with DSC and IMC for a model pharmaceutical drug, indomethacin, were compared to investigate the origin of the contradictory evidence present in the literature. It was shown that the preparation method (either in the DSC pan or in TAM ampoule) affects the physical properties of the resulting glass. It was therefore decided that a fair and accurate comparison between the two techniques requires the use of the same material batch. It was found that with DSC measurements the value of T_g used to calculate $\Delta_r H(\infty)$ affects the relaxation function; T_g at zero heating rate provided relaxation parameters in agreement with that obtained with IMC. It should be stressed that care should be taken when normalising the calculated $\Delta_r H(\infty)$ and $\Delta_r H(t)$. This work has demonstrated that disagreement between DSC and IMC data for relaxation might arise from comparing materials of different thermal histories and not accounting for relaxation enthalpy that occurs during preparation when calculating $\Delta_r H(\infty)$. It was therefore concluded that DSC and IMC measure the same physical property.

Most enthalpy relaxation studies were restricted to one-component amorphous systems. In the second section of this work the feasibility of using isothermal microcalorimetry to assess the relaxation of two-component amorphous systems was explored using the model fitting approach. It was found using simulated data that the 2-KWW model has the resolution to deconvolute the total signal into its constituting components. This resolution was, however, weakened when the signal from one component dominated the

total calorimetric signal. Inherent noise in real calorimetric data was another factor that led to compromising the resolution of the 2-KWW equation. The 2-MSE model, on the other hand, was found to be less sensitive to the effect of noise and successfully recovered the expected relaxation parameters for the individual components of an amorphous sucrose-indomethacin system. The failure of the 2-MSE model to recover the expected relaxation parameters of the constituting components of an amorphous sucrose-lactose system could be considered as a sign of change in the behaviour of the components. This shows that isothermal microcalorimetric data can be used to detect the effect of co-existence of two amorphous pharmaceuticals on their relaxation behaviour given that the individual components are well characterised.

***4) Chapter 4: Effect of the anomeric form
on the physical stability of amorphous
lactose.***

4.1. Introduction

Lactose is a widely used pharmaceutical excipient both in the crystalline and amorphous states and is most commonly used in the (partially) amorphous state [77]. Crystalline lactose exists in different crystal forms including α -monohydrate, anhydrous α and β , and several α/β compounds. This diversity in lactose crystalline form is exerted by differences in its chemical form [78]. This excipient exists in two anomeric forms α or β which show a chemical difference at the conformation of the anomeric C₁ carbon of the glucopyranose ring [78] as illustrated in Fig.4.1. One anomer can convert to the other in a phenomenon called mutarotation.

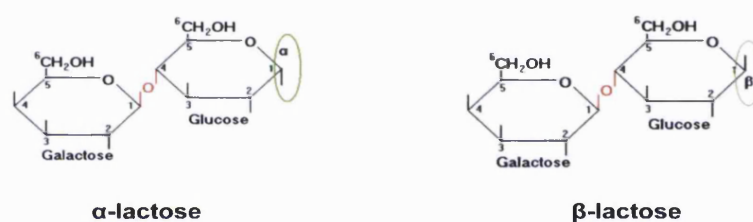


Figure 4.1: Chemical structure of α and β lactose anomers.

Amorphous lactose can exist as a mixture of both anomers as is the case with spray-dried lactose for example. The ratio of the two anomers can vary according to the processing conditions such as the spray-drying feed temperature [79] or milling conditions [62, 80]. The effect of the anomeric composition of amorphous lactose on physical properties such as moisture-induced crystallisation has been studied using isothermal microcalorimetry [79]. However, there have been no studies in the literature that have investigated whether the anomeric form of lactose can affect its vitreous properties. Investigation of the effect of isomeric conformation on the physical properties was carried out on some pharmaceutical isomers [41, 81, 82]. For example,

Diogo et al [81] found that 2-biphenylmethanol has good vitrification properties whereas its isomer, 4-biphenylmethanol has a strong tendency to crystallise upon cooling from the melt. Carpentier et al [41] investigated the glass properties of four different pentitol isomers and their work revealed that all the four isomers vitrified upon quench cooling. It was found that the isomers can be classified into two groups in terms of their glass properties including the T_g , ΔC_p and fragility index. It was presumed that although these isomers have the same molecular mass, molecular conformational differences have led to these variations in their dynamic behaviour. On the other hand, this conclusion was contradicted by Diogo's study [82] which investigated the properties of the same pentitols and found that all these isomers share the same dynamic behaviour based on results from primary and secondary relaxation studies.

These studies represent a good platform for the first aim of the study reported in this chapter which focuses on determining whether the two anomers α -lactose and β -lactose have similar dynamic properties when present in the amorphous form based on structural relaxation and T_g width studies.

The other aim of this study is to compare the interaction of the two anomers in the amorphous state with moisture. Such comparison is very important since water is a potent plasticizer [32] and can greatly affect the stability of amorphous sugars in pharmaceutical settings by lowering the T_g to, or below, storage temperatures, hence inducing crystallisation. Equilibrium moisture sorption isotherms and moisture-induced crystallisation have been investigated for amorphous spray-dried and freeze-dried lactose using dynamic vapour sorption [59]. This work will focus on determining whether the starting crystalline material in the milling process will have an impact on the nature of moisture interaction with the resulting amorphous sample.

4.2. Aims and objectives

As stated above, the main aim of this study is to determine the effect of the anomeric form of lactose on its dynamic behaviour and its interaction with moisture. This will be achieved through the following objectives:

- Preparation of predominantly α or β amorphous lactose.
- Determine structural relaxation profiles for amorphous α -lactose and β -lactose with isothermal microcalorimetry.
- Determine the T_g width of amorphous α -lactose and β -lactose with DSC.
- Construction of equilibrium water sorption isotherms for amorphous α -lactose and β -lactose with DVS.

4.3. Experimental

4.3.1. Preparation of amorphous lactose

Amorphous α -lactose was prepared by ball milling thermally dehydrated crystalline α -lactose monohydrate. Dehydration of α -lactose monohydrate was carried out by leaving the sample at 150⁰C for 30 min. No sample browning (a sign of sample degradation) was observed. TGA analysis proved all the crystal water was removed. Amorphous β -lactose was prepared by ball-milling anhydrous β -lactose. Ball milling conditions employed were as described in section 2.2.2.2. Ball milled samples were then passed through a 125 μ m sieve. Ball milled samples were handled inside a glove bag ($\leq 5\%$ RH) to prevent moisture absorption.

4.3.2. Characterisation of lactose samples

- XRPD was used to verify the amorphocity of the ball-milled lactose samples. Traces for scanning angle (2θ) from 5° to 35° were obtained at a scanning speed of $0.5^\circ/\text{min}$.
- ^1H NMR was used to determine the anomeric composition of crystalline and amorphous lactose samples as described in section 2.2.9.4.
- TGA was used to determine the water content of ball-milled samples. Samples ($\approx 15\text{mg}$) were heated from 30°C to 200°C at $20^\circ\text{C}/\text{min}$. Water content was taken as the percentage of weight loss.

4.3.3. Structural relaxation with IMC

Milled samples (200 mg) were loaded in 3 ml glass ampoules and crimped whilst in a glove bag ($\leq 5\% \text{ RH}$). Samples were then annealed in TAM at 25°C for 24h . The resulting power time data were then fitted to the KWW equation (Eq.1.12) to obtain relaxation parameters. At least three different batches were prepared for each anomer and from each batch three different samples were analysed.

4.3.4. T_g width measurement with DSC

Samples ($\approx 10 \text{ mg}$) were loaded in non-hermetically sealed aluminium DSC pans. Samples were then heated above their T_g to 145°C to remove moisture and standardise their thermal history, cooled below T_g to 80°C and then heated again above T_g to 250°C .

Lactose is known to mutarotate during DSC scans. The effect of heating rate on the extent of mutarotation was investigated to choose the optimal heating rate which provides reasonable mutarotation and stable baseline. Samples were removed from the DSC pan after being heated using the temperature programme described above at

different heating rates (10, 25, 30, 50, 100 and 200 °C/min) and then analysed for their anomeric composition with ^1H NMR.

4.3.5. Dynamic Vapour Sorption

Water sorption isotherms for ball milled samples were generated using a dynamic vapour sorption apparatus (SMS, UK). Samples ($\approx 20\text{mg}$) were first dried at 0% RH for 800 min then exposed to a certain %RH for 2000min. The %RH values used ranged from 5% to 60% in 5% increments.

4.3.6. Statistical analysis

The ANOVA test was used to verify reproducibility of data between different batches of the same anomer. An unpaired two-sampled Student t test was used to compare results for the two anomers. p values smaller than 0.05 were taken as significant.

4.4. Results and discussion

4.4.1. Characterisation of ball milled samples

4.4.1.1. Amorphocity

The ball-milling conditions used resulted in “X-ray” amorphous samples. This was confirmed by the X-ray diffractograms for ball-milled α -lactose and β -lactose. Both diffractograms showed a broad hump characteristic of amorphous materials as is illustrated in Fig.4.2. Therefore, in the subsequent text ball-milled lactose will be referred to as amorphous lactose.

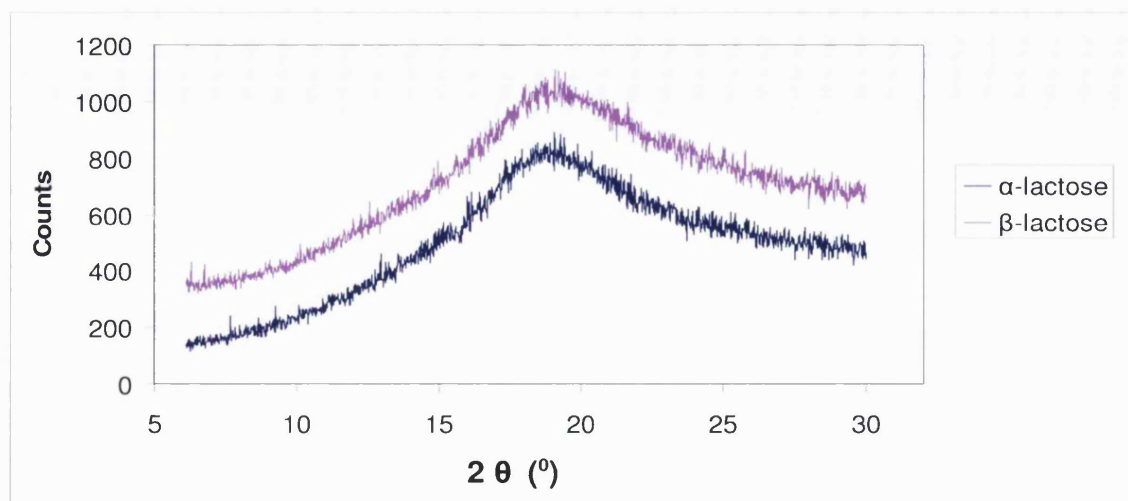


Figure 4.2: X-ray diffractogram for ball milled α -lactose and β -lactose.

4.4.1.2. Anomeric composition

The anomeric compositions for ball-milled (amorphous) lactose samples are summarised in Table 4.1. The data revealed that ball milled samples contained one of the two anomers in a major percentage ($\geq 70\%$). Milling is suggested as the only method that can result in the preparation of amorphous lactose of predominant anomeric composition [78]. All other methods (i.e. spray-drying, freeze-drying and quench cooling) result in significant mutarotation. Mutarotation during milling was also reported in the literature but to a lesser extent compared to the other methods [80]. In their study, Willart and co-workers [62] presumed that mutarotation during the milling process is most likely caused by the presence of residual moisture.

Table 4.1: Anomeric composition of lactose samples after ball-milling. $n = 4$ for each anomer.

	α %	β %
Crystalline α -lactose monohydrate	86.5 (\pm 3.0)	13.5 (\pm 3)
Anhydrous β -lactose	27.2 (\pm 5.6)	72.8 (\pm 5.6)

These results indicated that the ball milled samples satisfied the requirements to carry our study as the samples were “X-ray” amorphous and were present in a predominant anomeric form.

4.4.2. Structural relaxation with IMC

Fig.4.3 shows representative power-time data for amorphous α -lactose and β -lactose as they relaxed in the TAM. As the two anomers relaxed in the TAM, the heat flow output decayed gradually. Power-time data for 17h relaxation period were fitted to the KWW equation (Eq.1.12) to obtain relaxation parameters for each anomer. The KWW equation provided a good fit for all data and results are summarised in Table 4.2. The first observation from Table 4.2 is the variability of the data. However, statistical analysis using ANOVA test revealed that the relaxation parameters for different batches of the same anomer are the same ($p \geq 0.05$). This gave confidence in comparing data between the two anomers. Interestingly, the two anomers had the same excess relaxation enthalpy $\Delta_r H(\infty)$ (t-test, $p = 0.79$). This is the total excess enthalpy a glass loses to attain an equilibrium state when it is annealed below its T_g . The fact that the two anomers had the same $\Delta_r H(\infty)$ suggests that they need to get rid of the same amount of energy to reach the equilibrium state. However, the two anomers had statistically different τ and β values. β -lactose had a lower combined time constant τ^β than α -lactose

which indicates that β -lactose relaxes faster. This was proved when the fraction relaxed after 24h, $\Phi(24h)$, was calculated based on the KWW equation. It appeared that a higher fraction of β -lactose has relaxed than α -lactose (Table 4.2). However, TGA analysis revealed that α -lactose contained a statistically higher amount of water ($[2.06 \pm 0.63] \%$, $n = 15$) than β -lactose ($[1.61 \pm 0.23] \%$, $n = 11$), (t-test: $p \leq 0.05$). Water is a potent plasticizer for amorphous materials [32] and higher water content is usually associated with higher molecular mobility and hence lower relaxation time constant (τ^β) [27]. This difference in water content could have made interpretation of relaxation data problematic. However, it appeared that the anomer (β) which had lower water content also had, paradoxically, a lower τ^β value (Table 4.2). This lack of correlation between water content and the value of τ^β emphasises the conclusion that β -lactose had a higher molecular mobility than α -lactose.

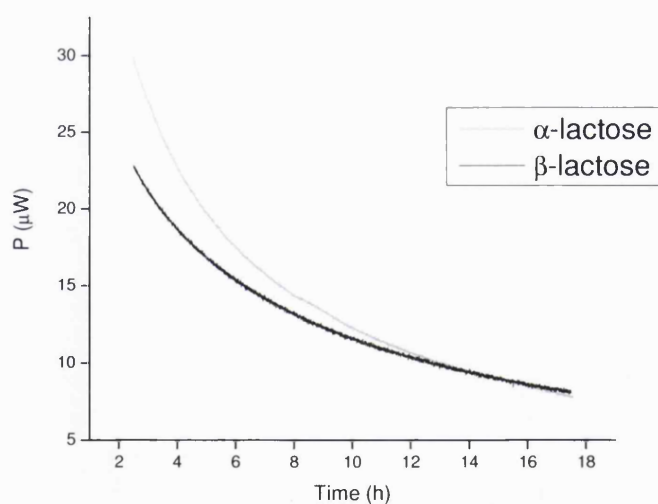


Figure 4.3: Representative power-time data for relaxing amorphous α -lactose and β -lactose.

Table 4.2: Relaxation parameters for amorphous α -lactose and β -lactose as obtained by fitting power-time data to KWW equation. Standard deviation is shown between parentheses.

	α -lactose ^a	β -lactose ^b
$\Delta_r H(\infty)$ (J/g)	3.1 (1.1)	3.2 (1.4)
β	0.64 (0.04)	0.54 (0.08)
τ (h)	68.9 (51.5)	37.0 (18.7)
τ^β (h ^{β})	13.5 (3.7)	6.7 (1.5)
Φ (24h)	0.45 (0.10)	0.57 (0.09)

^a n = 15, ^b n = 11.

4.4.3. T_g width study

The aim of this study was to use a simple method to compare the fragility of the anomers. Fragility is an important property of a glass. It is a measure of molecular mobility dependence on temperature changes in the glass transition region. Generally, if the viscosity, η , of a supercooled liquid shows an Arrhenius-like relationship with temperature the material is referred to as a “strong” glass. Deviation from the Arrhenius behaviour is a sign of the fragile nature of a glass [83]. Fragility is usually represented by the fragility index “m” which is calculated using the following equation [84]:

$$m = \Delta H / (2.203 R T_g) \quad \text{Eq.4.1}$$

where ΔH is the activation energy for molecular motions at T_g and R is the gas constant.

The fragility of a material can be assessed using different methods. The simplest

method depends on the measurement of glass transition width. Theoretically, when a glass is being formed it possesses a distribution of molecular motions. Hence the glass transition occurs across a temperature range. The width of this range depends on the fragility of the material. A “fragile” glass former will exhibit a quicker change in molecular mobility as compared to a “strong” glass former and as a result the former will have a narrower T_g width [83].

Fragility determination from the T_g width relies on the calculation of the activation energy ΔH using the following formula:

$$\begin{aligned}\Delta H &= C R / [(1/T_g^{onset}) - (1/T_g^{end})] \\ &= C R T_g^{onset} T_g^{end} / \Delta T_g\end{aligned}\quad \text{Eq.4.2}$$

where C is a constant, T_g^{onset} and T_g^{end} represent the onset and end of glass transition and ΔT_g is the width of glass transition. Eq.4.2 was developed empirically based on analysis of several inorganic “strong” glass formers [83, 84]. Hancock and co-workers [84] carried an investigation to test the validity of this equation to determine the fragility of typical pharmaceutical materials including lactose. The authors reported results for a DSC scanning rate of 10^0C/min and they developed a revised version of Eq.4.2 for small molecule pharmaceutical glasses (Eq.4.3).

$$\Delta H = 87 + 1.12R / [(1/T_g^{onset}) - (1/T_g^{offset})] \quad \text{Eq.4.3}$$

Based on this discussion, the ideal heating rate to measure the T_g width of amorphous α -lactose and β -lactose is 10^0C/min since there is a formula available to calculate ΔH from Ref [84]. However, when the extent of mutarotation as a function of heating rate was measured using the β anomer, it appeared that at 10^0C/min more than 45% of the sample is in the α form (Fig.4.4) i.e. only 55% remains in the β form. DSC might not be sufficiently sensitive to pick up a difference in T_g width for α -lactose and β -lactose at

10⁰C/min since the remaining difference range between the two anomers samples is only 10%. The effect of heating rate on the extent of mutarotation was therefore investigated in order to determine if mutarotation can be minimised at higher heating rates. As can be seen from Fig.4.4, as the heating rate was increased from 10⁰C/min to 50⁰C/min the extent of mutarotation decreased as it was indicated by the decrease of $\alpha\%$. Interestingly, a linear relationship was observed between heating rate and $\alpha\%$ up to 50⁰C/min ($R^2 = 0.999$) (Fig.4.4). However, heating rates higher than 50⁰C/min did not result in a noticeable minimisation of mutarotation. Lefort et al [78] have argued that the mutarotation kinetics of lactose are closely related to its molecular mobility in the glassy state. Based on this, when slow heating rates are used the molecules have enough time to reside at temperatures where molecular mobility is high (i.e. temperatures around the T_g). As the heating rate increases the molecules spend less time at these temperatures and hence mutarotate less. However, beyond a certain heating rate the extent of mutarotation becomes relatively constant and does not decrease with increased heating rates. This implies that the mutarotation phenomenon is *also* governed by thermodynamic factors which are not affected by the speed of heating. This explains the trend seen in Fig.4.4.

However, the use of a heating rate higher than 30⁰C/min resulted in perturbation of the baseline rendering accurate measurement of T_g width unacheivable (Fig 4.5). Samples heated at 30⁰C/min were found to contain about 41% α form. This means that the difference range between the two amorphous forms of lactose is about 19%. Moreover, a stable baseline could be obtained at this heating rate. It was therefore feasible to measure the T_g width at this heating rate and restrict our comparison to T_g width without measuring the fragility index since no formula has been developed for this heating rate.

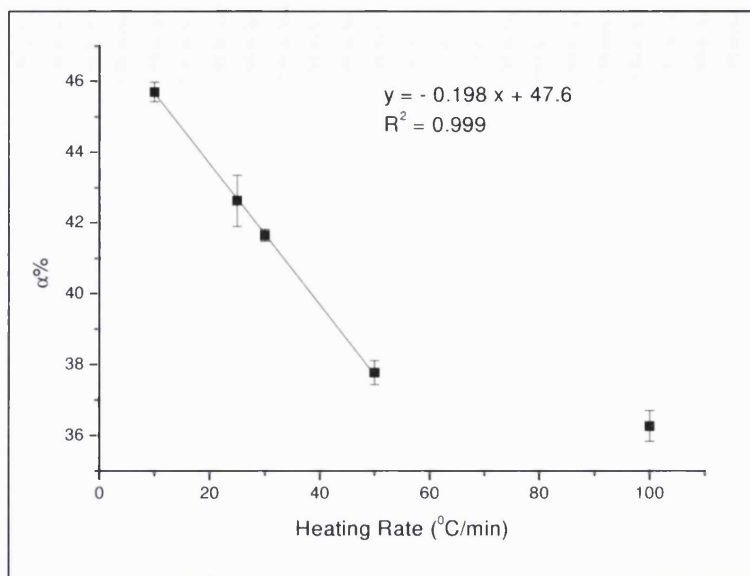


Figure 4.4: Percentage of α anomer in ball-milled β -lactose as it is heated in the DSC at different heating rates. Solid line and equation represent linear fit.

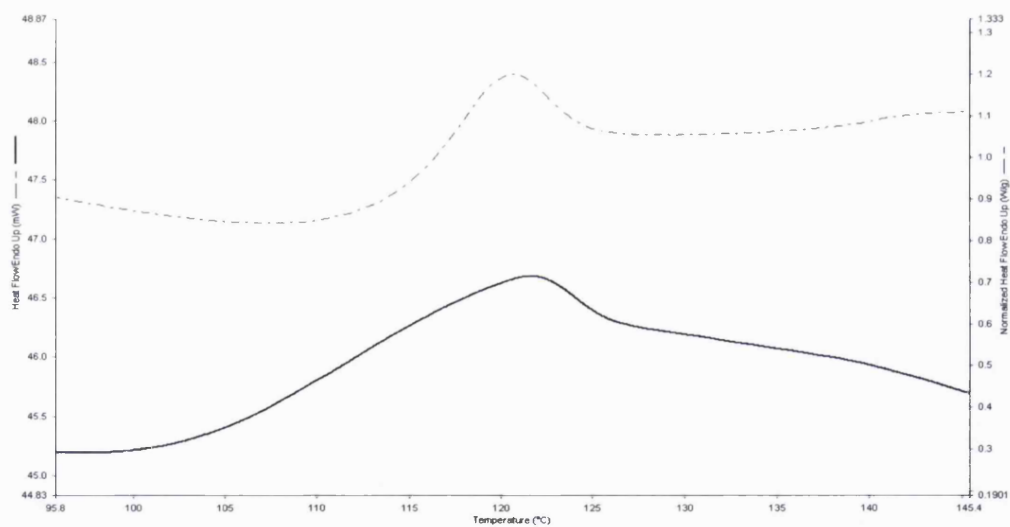


Figure 4.5: Glass transition for amorphous β -lactose measured at $30^{\circ}\text{C}/\text{min}$ (dashed line) and $50^{\circ}\text{C}/\text{min}$ (solid line).

The T_g width (ΔT_g) for amorphous α -lactose and β -lactose was obtained by measuring the difference between T_g^{onset} and T_g^{end} . These latter were determined according to the Moynihan method [85, 86] as illustrated in Fig.4.6.

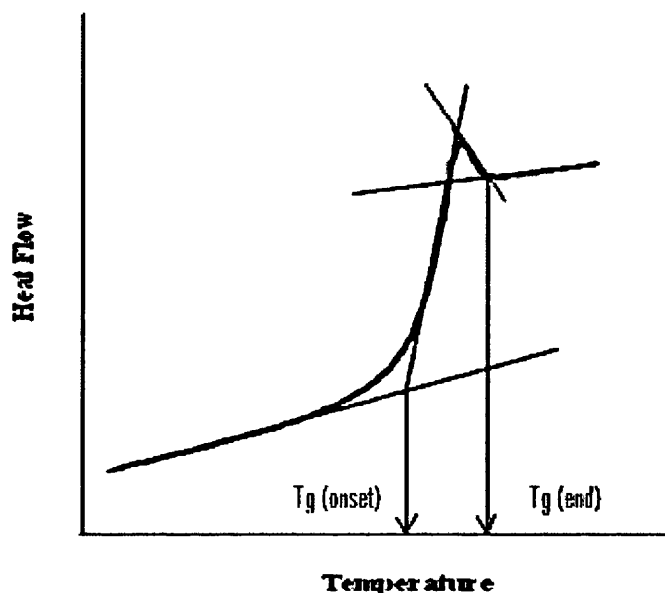


Figure 4.6: Clarification of the method used to determine T_g^{onset} and T_g^{end} to measure ΔT_g .

T_g width measurements for amorphous α -lactose and β -lactose are summarised in Table 4.3. Student t-test analysis revealed that ΔT_g 's for the two anomers are analogous. This finding can be interpreted in two ways. One possible scenario is the incapacity of the DSC to pick up the difference between the two anomers because of significant mutarotation. Alternatively, the results suggest that the anomeric form of lactose does not effectively influence its fragility. In this case, the T_g width study results might seem inconsistent with those of the structural relaxation study in which the two anomers were found to have different relaxation profiles. However, it is worth noting that the two studies investigated two different glass properties. The T_g width is a measure of the

glass fragility which represents the dependence of molecular mobility on temperature, whereas structural relaxation study measures the rate at which the glass relaxes to attain the equilibrium state. However, significant mutarotation during DSC run seem to be a more likely reason for this discrepancy.

Table 4.3: Glass transition temperature width (ΔT_g) for amorphous α -lactose and β -lactose as measured by DSC at $30^\circ\text{C}/\text{min}$.

	α -lactose ^a	β -lactose ^b
ΔT_g ($^\circ\text{C}/\text{min}$)	10.0 (± 0.9)	10.5 (± 0.6)

^a n = 15 (from two different batches).

^b n = 21 (from three different batches).

4.4.4. Other thermal characteristics of amorphous lactose anomers

After determining the T_g width of ball-milled lactose samples, further heating was carried out above the T_g . All samples (both α and β anomers) re-crystallised upon heating then melting endotherms were observed. α -lactose showed two distinctive melting peaks whereas β -lactose showed only one melting peak. Table 4.4 summarises the temperatures at which these events occurred together with the measured T_g and ΔC_p for both anomers.

Table 4.4: Thermal characteristics (T_g , ΔC_p , T_c : crystallisation temperature, T_m : melting temperature) of amorphous α -lactose and β -lactose based on DSC scans at $30^\circ\text{C}/\text{min}$.

	$T_{g(\text{mid})}$ ($^\circ\text{C}$)	ΔC_p (J/g. $^\circ\text{C}$)	T_c ($^\circ\text{C}$)	T_{m1} ($^\circ\text{C}$)	T_{m2} ($^\circ\text{C}$)
α -lactose ^a	115.7 (± 1.01)	0.41 (± 0.04)	167.49 (± 2.76)	208.08 (± 0.38)	223.31 (± 0.98)
β -lactose ^b	114.80 (± 1.03)	0.38 (± 0.03)	166.42 (± 1.55)	235.03 (± 0.71)	-

^a n = 6

^b n = 11

Analysis of Table 4.4 reveals that the two anomers have comparable thermal characteristics and the only difference lies in the number and type of polymorphs that re-crystallised from the amorphous state (Fig.4.7). Amorphous α -lactose crystallised to two different polymorphs. the first polymorph which melted at 208°C is likely to be crystalline α -lactose monohydrate, whereas the second polymorph ($T_m = 223^{\circ}\text{C}$) can be a complex mixture of α - and β - lactose anhydrous as was proposed elsewhere [87]. Amorphous β -lactose crystallised to anhydrous β - lactose ($T_m = 235^{\circ}\text{C}$) as its melting point compares to the melting point that has been reported in the literature (232°C) [87] for reference anhydrous β - lactose . It is interesting that α -lactose crystallised to a complex mixture of α - and β - lactose anhydrous, whereas β -lactose did not. It has been reported that α -lactose mutarotates to β -lactose upon heating [88] and this can explain the presence of the β anomer in recrystallised milled α -lactose.

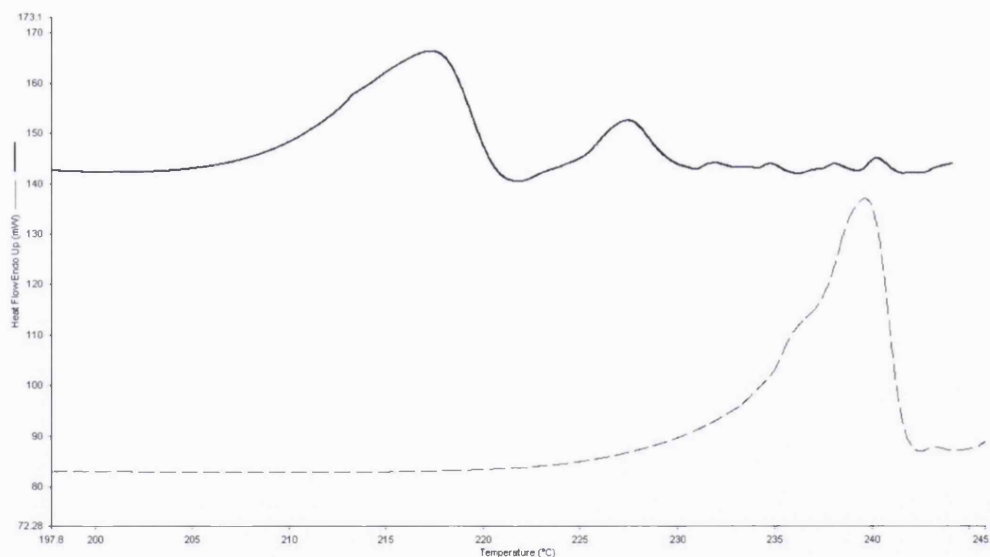


Figure 4.7: Melting endotherms for recrystallised amorphous α -lactose (solid line) and recrystallised amorphous β -lactose (dashed line).

4.4.5. Pre- T_g exothermic event

Both anomers showed an unexpected exotherm at temperatures below T_g in addition to the crystallisation exotherm at around 167°C . This exotherm always appeared at temperatures below the dry T_g (115°C) and hence it will be referred to as the pre- T_g exotherm. Fig.4.8 illustrates two DSC scan for two β -lactose samples. The top (red) DSC scan represents a typical DSC scan for an amorphous material where a glass transition (which is not clear in the figure as it is being superimposed by the water evaporation endotherm) is followed by a re-crystallisation exotherm which is in turn followed by a melting endotherm. The bottom (blue) DSC scan represents that for an amorphous β -lactose showing the extra pre- T_g exotherm besides the other events.

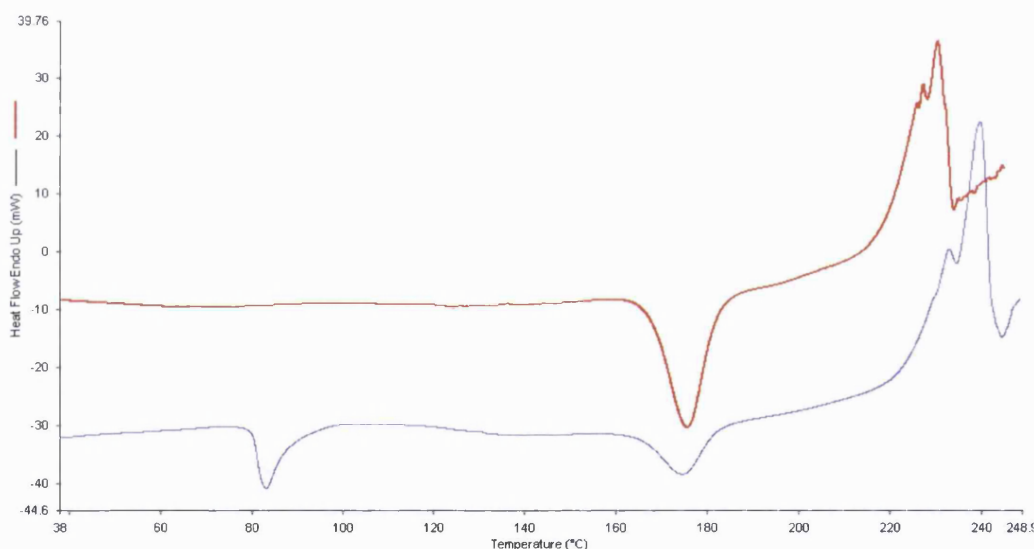


Figure 4.8: DSC scans for amorphous β -lactose samples: top (red) shows a typical thermal events for an amorphous material, bottom (blue) shows an extra pre- T_g exotherm.

The pre- T_g exotherm was erratic both in frequency and magnitude of its occurrence. This has prevented the proper characterisation of this event. However, the presence of this exotherm was accompanied with a decrease in the magnitude of enthalpy of crystallisation and a negative linear correlation was observed between the two events

($R^2 > 0.95$) (Fig. 4.9.A). Moreover, when samples that showed the pre- T_g exotherm were heated across the T_g , there was a drop in the value of ΔC_p although a linear correlation was not noted (Fig.4.9.B). These two observations are indicative of a drop in the amorphocity of the samples as they went through the pre- T_g exotherm, which implies that this event is very likely to be a crystallisation event that occurs at a lower energy level than the usual high temperature re-crystallisation event.

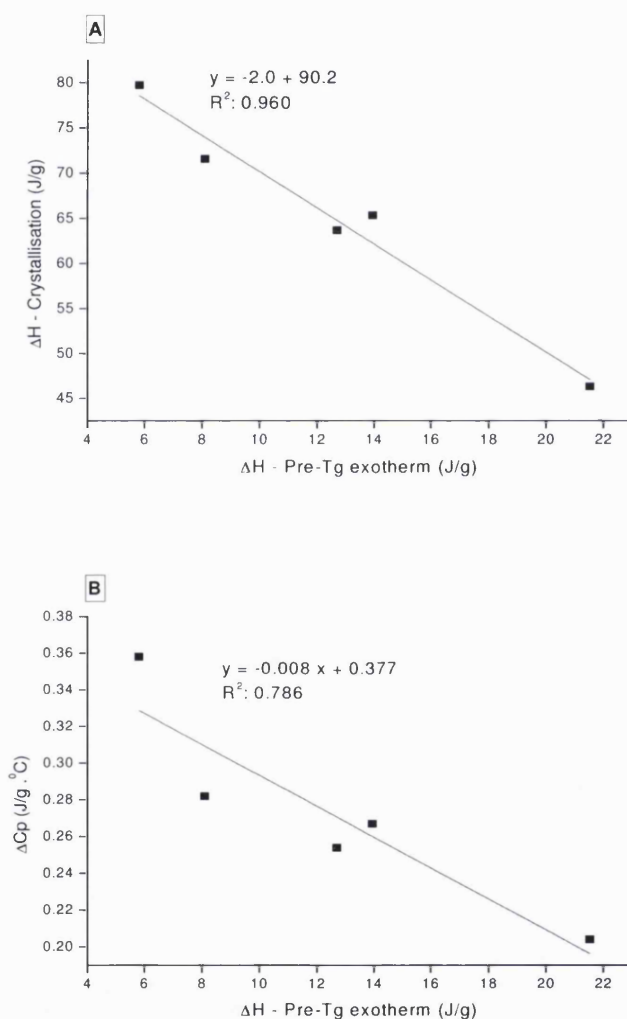


Figure 4.9: Illustration of correlation of pre- T_g exotherm enthalpy with re-crystallisation enthalpy (A) and ΔC_p (B). Lines represent best linear fits.

Another similarity between the two exotherms is the increase in the content of the predominant anomer after the exothermic event as it can be concluded from results in Table 4.5. As shown in Table 4.5, amorphous β -lactose samples that showed no pre- T_g event reproducibly underwent some mutarotation upon crystallisation. The same observation was made after the pre- T_g event but only one example is shown in Table 4.5 since the phenomenon was erratic and the extent of mutarotation was dependent on the enthalpy of the pre- T_g exotherm as can be concluded from Fig.4.10 which shows that there is a trend between the extent of mutarotation (represented in % β) and enthalpy of pre- T_g exotherm. However, statistical testing showed that this trend was not linear ($R^2 < 0.95$). This suggests that there might be a different type of relationship between the two events but most importantly is that the pre- T_g event is accompanied by mutarotation like the crystallisation event.

Table 4.5: Anomeric composition for β -lactose before and after exothermic events (re-crystallisation at 167°C and pre- T_g event).

	Pre-recrystallisation ^a	Post-recrystallisation ^a	Pre(pre- T_g) exotherm	Post(pre- T_g) exotherm
$\beta\%$	53.4 (± 0.1)	67.2 (± 0.5)	75.4	84.0

^a n = 3.

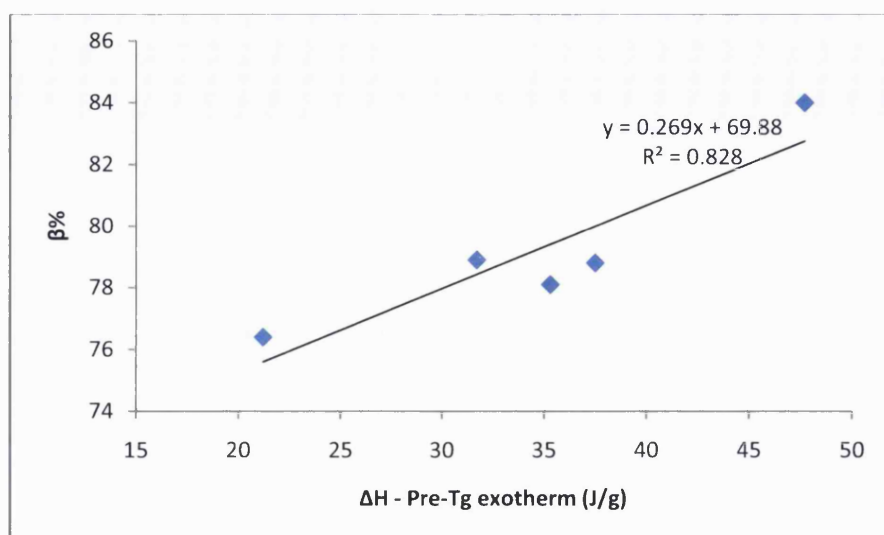


Figure 4.10: Illustration of correlation between pre-T_g exotherm enthalpy and β anomer content (β%).

One possible scenario to explain the emergence of the pre-T_g exotherm is that this exotherm represents the re-crystallisation of a metastable polymorph, whereas in the high temperature exotherm a more stable polymorph is formed. However, in the case of β-lactose samples that was a pre-T_g exotherm there showed an increase in the melting temperature (T_m) but not the emergence of a new polymorph as it can be seen from Fig.4.8. This shift in T_m can be attributed to the increase in the content of the β form after pre-T_g exotherm and hence the formation of a polymorph that is predominantly in the β form. Lactose crystallisation from the amorphous state into different polymorphs has been reported in the literature. Possible evidence via DSC measurements was proposed in a study where freeze-dried lactose containing 4.4% moisture showed a shoulder in the crystallisation exotherm [89]. The shoulder was speculated to be due to the emergence of more than one polymorph. Burnett et al [77] also presented DVS data that suggested the co-occurrence of multiple crystallisation mechanisms for spray-dried lactose at low temperatures and relative humidity. However, to the best of our

knowledge, it has never been reported in the literature that amorphous lactose exhibits two distinctive re-crystallisation exotherms [80, 90].

Another possible interpretation of the pre- T_g exotherm was recently described by Feng and co-workers [91] who investigated the effect of milling on disturbing the order of crystalline griseofulvin. In this study, cryogenically milled crystalline griseofulvin showed an exotherm at a low temperature (58°C) that extended to the T_g (90°C). This event was clearly distinct from the usual recrystallisation that occurred above the T_g (120°C). The authors argued that cryogenic milling resulted in the creation of molecular dislocations referred to as crystal defects. This phenomenon is distinct from amorphisation as the latter results when the long-range order is totally lost. It was hypothesised that defective crystals reside at an intermediate energy level between the crystalline and amorphous states and hence they are thermodynamically unstable and favour reversion to the perfect crystal state. As a result, molecular rearrangement of defective crystals can happen at lower temperatures than that required for recrystallisation from the amorphous state [91]. Defective crystals rearrangement is well investigated with inorganic materials, whereas with pharmaceutical materials it is claimed that Feng et al's work is the first in this field [91]. Our results for milled lactose can be another example of such phenomenon in the pharmaceutical field. The erratic nature of our pre- T_g exotherm can be attributed to the harshness of the ball-milling conditions used which were necessary to produce "X-ray" amorphous lactose samples. This might have resulted in only a small portion of the crystals that underwent local molecular dislocations rather than complete amorphisation.

The implications of the pre- T_g exotherm phenomenon described in our work lie in supporting the crystal defect hypothesis introduced by Feng and co-workers for pharmaceutical materials. This hypothesis represents a further step towards the better

understanding of the effects of the milling process in particular, and mechanical stress in general, on the properties of pharmaceutical products and their performance.

4.4.6. Moisture-solid interactions

Water sorption profiles for amorphous α -lactose and β -lactose were obtained at 25°C. As can be seen from Fig.4.11, which shows a typical net percent change in mass versus time, amorphous lactose loses its residual moisture upon drying at 0% RH. As the %RH is raised, the mass in reference to the dry state increases as water vapour is sorbed by the amorphous sample. The mass then levels off (throughout the 2000 min duration of the experiment) at a certain value depending on the %RH when equilibrium is established between the amorphous sample and the wet environment. This was observed for both lactose anomers up to 25% RH as is illustrated in Fig.4.12 (A and B).

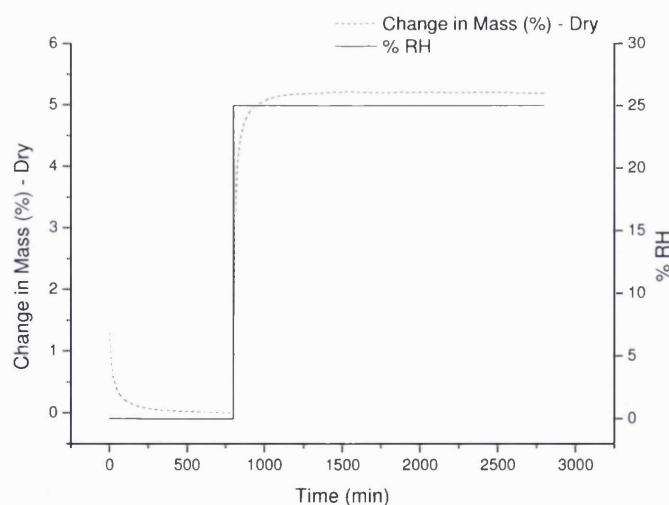


Figure 4.11: Typical water sorption profile for amorphous lactose.

However, between 30% and 50%RH for α -lactose and between 30% and 45% RH for β -lactose, a different behaviour is noticed in which a mass loss is recorded for both

anomers after a short period of established equilibrium as the RH is raised from 0%. This phenomenon is well documented for amorphous sugars, including lactose, and is attributed to water-induced crystallisation [34, 59, 77]. Amorphous materials absorb water vapour [18] which then acts as a plasticiser. If a sufficient amount of water is absorbed, the T_g can be dropped to storage or experimental temperature and the sample transforms to the rubbery state. At this stage the material possesses high molecular mobility and further water absorption results in the induction of crystallisation. This latter event leads to expulsion of previously absorbed water as the crystalline structure has lower water sorption capacity [92].

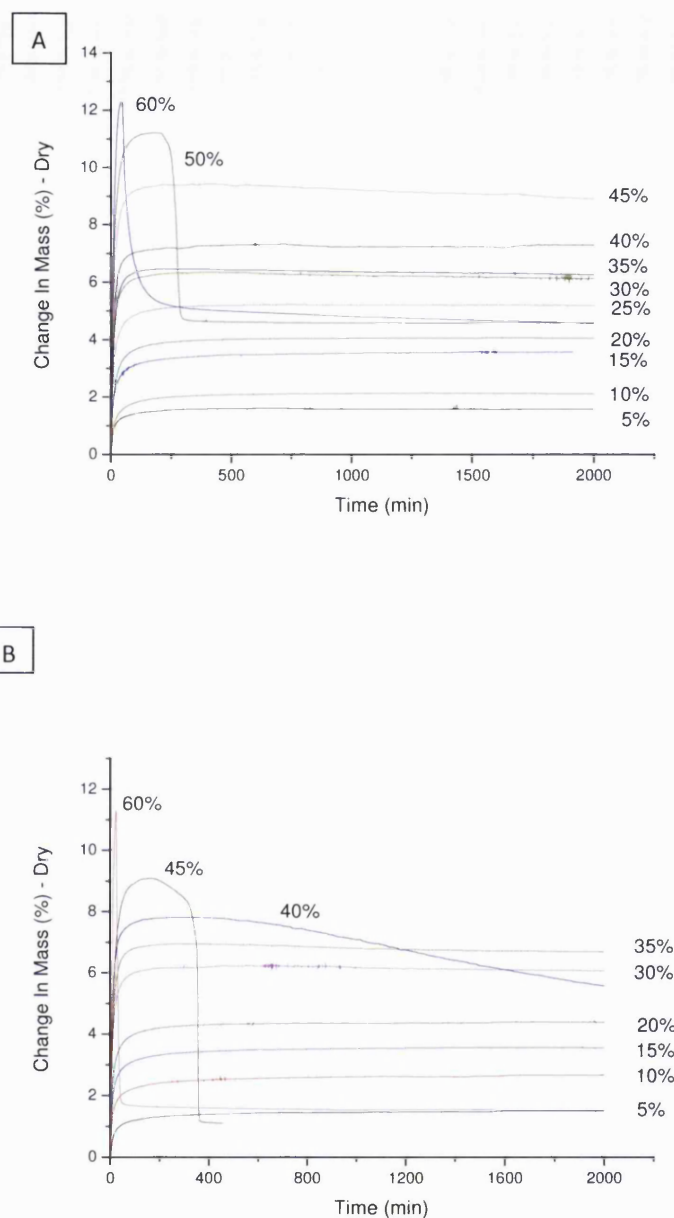


Figure 4.12: Water sorption profiles for amorphous α -lactose (A) and β -lactose (B).

The initiation of water-induced crystallisation from 30% RH has prevented the construction of equilibrium water sorption isotherms throughout the whole experimental %RH range. In such a case, pseudo-equilibrium isotherms can be obtained instead [59]. These represent the water content just before the induction of crystallisation. Fig.4.13

illustrates pseudo-equilibrium isotherms for amorphous α -lactose and β -lactose. It is clear that as the %RH increases the amount of sorbed water increases for both anomers. When paired t-test analysis was applied to the data in Fig.4.13 it appeared that the two anomers absorb a similar amount of water vapour throughout the experimental %RH range ($p >> 0.05$).

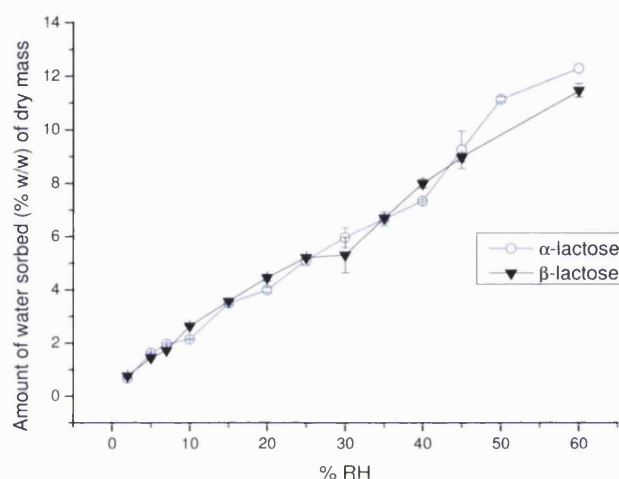


Figure 4.13: Pseudo-equilibrium water sorption isotherms for amorphous α -lactose and β -lactose.

However, there is a noticeable difference between the two anomer's responses above 35% RH. As can be seen from Fig.4.12 (A), at 40% RH α -lactose shows little or no mass loss after attaining equilibrium, whereas β -lactose shows noticeable mass loss (Fig.4.12, B) as an indication of crystallisation. At 45% RH, β -lactose undergoes significant crystallisation after a short period of constant mass gain ($\approx 9\%$) then it retains $0.97 \pm 0.17\%$ of its sorbed water. α -lactose shows a similar response at a higher %RH (50%) after absorbing about 11% w/w of water vapour and then it retains $4.56 \pm 0.03\%$ of it after crystallisation. In both anomers, the retained water after

crystallisation is very likely to be incorporated into the crystalline structure of α -lactose monohydrate. Water constitutes 5% w/w of α -lactose monohydrate. This suggests that 20% of the ball-milled β -lactose converted to α -lactose monohydrate, whereas nearly 90% of ball-milled α -lactose converts to the hydrate form. Interestingly, these percentages of the formed α -lactose monohydrate are in good agreement with the percentages of the “ α ” anomer in the amorphous samples (Table 4.1). This can suggest that the initial anomeric composition is an important factor in determining the types of the crystal forms as was previously proposed in the literature [93].

Both anomers were also exposed to higher %RH (60%). Both anomers showed a rapid mass increase followed by an immediate mass loss when certain amount of water was absorbed. It was noted that α -lactose absorbed an extra 1% of water higher than β -lactose (Fig.4.12). Both anomers retained similar water content as was described above after crystallisation at 50% RH (α -lactose) and 45% RH (β -lactose) indicating that α -lactose crystallises predominantly to the hydrate form whereas β -lactose crystallises to the anhydrous form. Furthermore, the sorption and desorption response was noticeably faster for β -lactose compared to α -lactose. This indicates that the characteristics of this response are dependent on the type of the crystals formed which is in turn dependent on the initial anomeric composition.

Based on the discussion above, it appears that the anomeric composition only affects apparent water-lactose interactions above a certain %RH (40% RH). Ambarkhane et al [94] argued that above 35% RH, amorphous lactose is present in the rubbery state since the amount of absorbed water at this %RH plasticises the T_g to the experimental temperature (25°C) based on calculations using the Gordon-Taylor equation (Eq.1.19) described in Section 1.9 of Chapter 1.

The Gordon-Taylor equation was used to calculate the theoretical amount of sorbed water to drop the T_g of our amorphous lactose samples to 25°C and it was found to be 7.9% when T_g for amorphous lactose was taken as 115°C (387.15 K) as was measured by DSC at 10°C/min and T_g for water and k were taken from the literature as -135°C and 6.56, respectively [94]. For both anomers, this water content corresponds to the amount absorbed at approximately 40%RH (Fig.4.13). This confirms that the anomeric form of amorphous lactose affects its interaction with moisture only when amorphous lactose is present in the rubbery state.

To explore further the effect of anomeric form on water-lactose interaction below T_g (i.e. below 40% RH at 25°C) the calculation of the Henry's Law constant, k_w , from the low vapour pressure region of moisture sorption isotherms was attempted based on the following relationship [95]:

$$P_w = k_w X_w \quad \text{Eq.4.1}$$

where P_w is vapour pressure and X_w is the mole fraction of sorbed water at P_w . k_w values for amorphous α -lactose and β -lactose were then obtained from the slope of P_w versus X_w at low %RH ($\leq 10\%RH$), where infinite dilution of sorbed water into the amorphous solid was assumed. Plots are illustrated in Fig.4.14 and Fig.4.15 for α -lactose and β -lactose respectively. A good linear relationship was observed between the vapour pressure and water mole fraction for β -lactose ($R^2 > 0.95$) but not for α -lactose. This indicates that Henry's law does not hold for amorphous α -lactose. It is presumed that the sorbed water might have triggered some physical changes in the material (e.g. increasing the molecular mobility) resulting in disturbing the solubilisation equilibrium established between amorphous α -lactose and the moisture. These changes are likely to have happened with β -lactose but in a subtle way preventing their observation.

These results have prevented the determination of Henry's law constant that could have enabled the comparison of solid-moisture interactions between the anomers on the chemical level since lower values for Henry's law constant indicate higher polarity [96].

The observation that amorphous α -lactose crystallises at a higher water content compared with β -lactose can be attributed to the fact that α -lactose crystallisation involves the incorporation of water into the crystal lattice, whereas β -lactose crystallises to an anhydrous form. As a result, the formation of α -lactose monohydrate might require higher kinetic energy and hence higher molecular mobility.

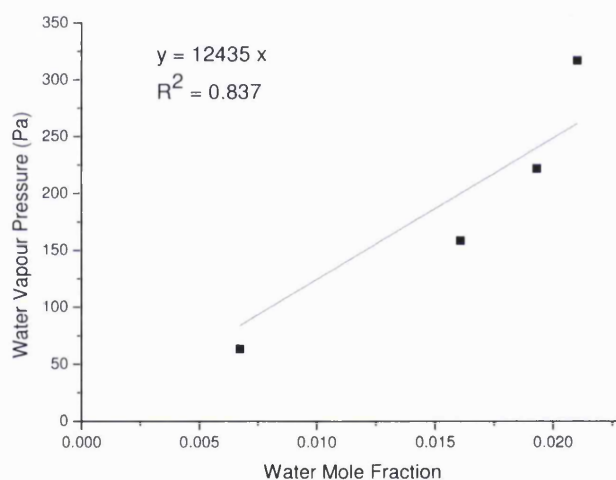


Figure 4.14: Water sorption isotherm for amorphous α -lactose. Line and equation represent linear fit.

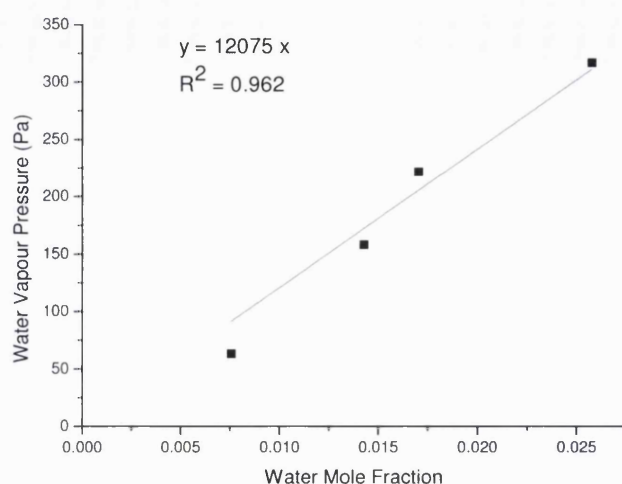


Figure 4.15: Water sorption isotherm for amorphous β -lactose. Line and equation represent linear fit.

4.4.7. Summary

The effect of the anomeric form composition on certain dynamic properties of amorphous ball-milled lactose was investigated. Structural relaxation studies with isothermal microcalorimetry revealed that the two anomers displayed different relaxation profiles although they had the same excess relaxation enthalpies. Amorphous β -lactose was found to relax faster than α -lactose even though the latter had higher water content. This might imply that β -lactose can crystallise earlier than α -lactose if complete coupling between molecular mobility and onset of crystallisation is assumed. However, onset and rate of crystallisation can also be controlled by other factors including thermodynamic and processing factors [12, 63].

Structural relaxation results, however, were not consistent with the results obtained from T_g width study as the two anomers had the same T_g widths. This discrepancy might have originated from the incapability of the DSC measurements to pick up the difference between the two anomers due to significant mutarotation during the DSC

scans. On the other hand, differences in the nature of the molecular mobility being assessed in the two studies might have caused this inconsistency in the results.

An interesting phenomenon was observed with both ball-milled lactose anomers. This was represented in the appearance of an exotherm below the T_g of lactose in addition to the usual high temperature recrystallisation exotherm. Preliminary investigation has revealed that it is more likely to be a crystal defect rearrangement rather than crystallisation from the amorphous state. Further work, nevertheless, is needed to explore this hypothesis which can have significant implications in improving the understanding of the milling process and subsequent product handling.

Water interaction with amorphous lactose anomers was also investigated. The two anomers interacted similarly with water up to 40% RH which was found to be the %RH at which the T_g of lactose is dropped to the experimental temperature. Above the T_g , β -lactose crystallised more readily than α -lactose. Furthermore, the anomeric form played a significant role in determining the type of polymorphs formed. Amorphous α -lactose crystallised predominantly to the hydrate form whereas amorphous β -lactose crystallised to the anhydrous form. These results imply that amorphous ball-milled lactose handling and storage should be tailored according to the starting crystalline form and the anomeric composition of the resulting product.

***5) Chapter 5: Crystallisation Studies with
IMC-Development of a Calculation
Method***

5.1. Introduction

As a significant portion of newly developed drug candidates are lipophilic and hence might suffer from solubility problems, the use of the amorphous solid formulations has been considered as an option for the better bioavailability of such drugs [12]. The amorphous state offers better dissolution properties thanks to its higher free energy compared with the crystalline state [7]. However, this advantage is compromised by the inherent instability of this form, which tends to convert to a more stable crystalline form [4]. Finite amounts of the amorphous form can also be introduced unintentionally during processing. Reversion of this amorphous form to the original crystal form has to be ensured in order to prevent any possible detrimental effects on product performance [4].

A good understanding of the crystallisation phenomenon can therefore help control and predict the behaviour of the amorphous form in either case. Generally speaking, research into crystallisation from the amorphous form can be divided into two aspects. The first aspect concerns the factors that control the onset of crystallisation [12], whereas the second aspect focuses on characterising the crystallisation process once it is initiated. Determination of crystallisation kinetics is a significant part of the second aspect and has been carried out using different techniques including XRPD [93, 97, 98], DSC [97, 99, 100] and polarised light microscopy [101, 102].

Variation of crystallisation mechanisms and types of polymorphs formed with temperature and relative humidity has been reported in the literature [73, 96, 97]. This renders the use of accelerated stability studies at elevated temperatures and relative humidity potentially problematic. Techniques capable of detecting and monitoring crystallisation at pharmaceutically relevant storage temperatures and relative humidity are therefore required. Isothermal microcalorimetry (IMC) has been proposed as a

potential method for this purpose [63, 97, 103]. This technique is highly sensitive to minute heat flow and hence should be ideal to monitor slow crystallisation processes. The limited number of research studies that employed IMC to determine crystallisation kinetics have used the model fitting approach which necessitates the determination of the total heat that evolves from the crystallisation process (denoted as Q) as will be explained later. This has been achieved by allowing the process to proceed to completion [97, 103-106]. However, if the crystallisation rates are very slow this approach becomes unfeasible and the sensitivity advantage of IMC becomes of no practical use. Moreover, the determination of Q might also be a difficult task if the process initiates prior to data recording in the calorimeter during the equilibration period. For example, Schubert et al [107] reported that the calorimeter recorded only 20% of the total heat evolved from the crystallisation of lipid nanoparticles. An alternative method to determine crystallisation kinetics from calorimetric measurements is therefore needed.

Calculation methods have been developed to determine thermodynamic and kinetic parameters for solution phase reactions [22, 108]. O'Neill et al [55] reported the development of a calculation method to determine reaction parameters for solid-state reactions based on the Sestak-Berggren equation. Using simulated data, it was claimed that a fractional extent of reaction of only 0.01 can allow the determination of the target parameters. However, the success of the method was not demonstrated using real calorimetric data and detailed arithmetic of the method was not provided. This leaves a gap in the literature regarding the availability of a direct calculation method for solid state reactions using isothermal microcalorimetric data. This study, therefore, aims at developing such a method and verifying its applicability using both simulated and real calorimetric data. Crystallisation from the amorphous state was taken as an example for

solid-state reactions. This process is usually described by nucleation and growth models, specifically the Avrami models [37]. These and other solid-state models have been claimed to all reduce to a simplified version of the empirical Sestak-Berggren equation (Eq.5.1) (Table 5.1) [38]:

$$f(\alpha) = c \cdot (1 - \alpha)^n \cdot \alpha^m \quad \text{Eq.5.1}$$

where $f(\alpha)$ is a function that describes the reacted fraction (α) dependence, c is an empirical constant, m and n are fitting constants (and do not represent reaction orders).

The theoretical development of the calculation method will therefore be based on this equation.

Table 5.1: “Algebraic expressions for the $f(\alpha)$ functions for the most common mechanisms in solid-state reactions and their corresponding equivalent reduced Sestak-Berggren equations”. Reproduced from Ref [38].

Mechanism	Symbol	$f(\alpha)$	Equivalent reduced Sestak-Berggren Eq.
phase boundary controlled reaction (contracting area, i.e., bidimensional shape)	R2	$(1 - \alpha)^{1/2}$	$(1 - \alpha)^{1/2}$
phase boundary controlled reaction (contracting volume, i.e., tridimensional shape)	R3	$(1 - \alpha)^{2/3}$	$(1 - \alpha)^{2/3}$
unimolecular decay law (instantaneous nucleation and unidimensional growth)	F1	$(1 - \alpha)$	$(1 - \alpha)$
random instant nucleation and two-dimensional growth of nuclei (Avrami-Erofeev)	A2	$2(1 - \alpha)[- \ln(1 - \alpha)]^{1/2}$	$2.079(1 - \alpha)^{0.806} \alpha^{0.515}$
random instant nucleation and three-dimensional growth of nuclei (Avrami-Erofeev)	A3	$3(1 - \alpha)[- \ln(1 - \alpha)]^{2/3}$	$3.192(1 - \alpha)^{0.748} \alpha^{0.693}$
two-dimensional diffusion (bidimensional particle shape)	D2	$1/[- \ln(1 - \alpha)]$	$0.973(1 - \alpha)^{0.425} \alpha^{-1.008}$

5.2. Aims and objectives

Development of a calculation method for the analysis of isothermal calorimetric data for solid-state reactions based on the Sestak-Berggren equation.

Objectives:

- Simulation of calorimetric data for solid-state reaction.
- Development of the arithmetic from the calorimetric form of Sestak-Berggren equation to determine the kinetic parameters.
- Application of the developed calculation method using simulated data.
- Application of the developed calculation method using real calorimetric data for indomethacin crystallisation below T_g .

5.3. Materials and methods

5.3.1. Preparation of amorphous indomethacin

Amorphous indomethacin was prepared by melting crystalline indomethacin in aluminium paper on a hot plate set at 175°C . The melted drug was then quenched with liquid nitrogen then stored in a desiccator over P_2O_5 for 1h. The dried sample was then ground gently using a mortar and pestle then passed through a $90\mu\text{m}$ mesh sieve. The sieved sample was further dried over P_2O_5 for 1h and then stored at -80°C until further use.

5.3.2. Isothermal microcalorimetric measurements

Amorphous indomethacin (300mg) samples were loaded in glass TAM ampoules in the glove bag flashed with nitrogen ($\leq 5\%$ RH) and then sealed with a rubber closure. Ampoules were then placed in the calorimeter in the equilibrium position for 30min then lowered slowly to the measurement position. Measurements were conducted at 25⁰C, 30⁰C and 35⁰C. Each measurement was carried out in duplicate.

5.3.3. Simulation of calorimetric data for solid-state reactions

Simulation of calorimetric data for solid-state reactions requires the determination of the calorimetric form for Eq.5.1. Solid-state reaction rates are usually described in terms of temperature, T , and reaction fraction, α , by the following expression:

$$\frac{d\alpha}{dt} = A \exp\left(\frac{-E}{RT}\right) f(\alpha) \quad \text{Eq.5.2}$$

In the above expression A is the Arrhenius pre-exponential factor, E is the activation energy and R is the gas constant. At isothermal conditions, $A \exp(-E/RT)$ becomes a constant referred to as k and Eq.5.2 becomes:

$$\frac{d\alpha}{dt} = k \cdot f(\alpha) \quad \text{Eq.5.3}$$

Perez-Maqueda et al [38] proposed a general expression, Eq.5.1, derived from the Sestak-Berggren equation, Eq.5.4:

$$f(\alpha) = (1 - \alpha)^n \cdot \alpha^m \cdot (-\ln(1 - \alpha))^p \quad \text{Eq.5.4}$$

for $p = 0$. It should be noted that the Sestak-Berggren equation and its reduced version are empirical and have no physical meaning but they offer the advantage of describing

most solid state reactions as can be seen from Table 5.1 for Eq5.1. Eq.5.3 can now be written as:

$$\frac{d\alpha}{dt} = k \cdot c \cdot (1 - \alpha)^n \cdot \alpha^m \quad \text{Eq.5.5}$$

Since α is the fraction reacted at time t , it can therefore be expressed calorimetrically as:

$$\alpha = \frac{\int_0^t \left(\frac{dq}{dt}\right) dt}{\int_0^\infty \left(\frac{dq}{dt}\right) dt} = \frac{q}{Q} \quad \text{Eq.5.6}$$

And hence:

$$\frac{d\alpha}{dt} = \frac{dq/dt}{Q} \quad \text{Eq.5.7}$$

And:

$$\frac{dq}{dt} = Q \cdot \frac{d\alpha}{dt} \quad \text{Eq.5.8}$$

where q is the heat change to time t and Q is the total heat change upon crystallisation.

Given Eq.5.5, Eq.5.8 can now be written as:

$$\frac{dq}{dt} = P = Q \cdot k \cdot c \cdot (1 - \alpha)^n \cdot \alpha^m \quad \text{Eq.5.9}$$

where P is power. Power-time data can be obtained by simulating data for P versus α and subsequently corresponding time values can be obtained from Eq.5.10:

$$t = q/P \quad \text{Eq.5.10}$$

based on the assumption that

$$P = q/t \quad \text{Eq.5.11}$$

This assumption becomes valid when q values are very small. Time values were then determined using an Excel (Microsoft Office) algorithm. Data were simulated using MathCad[®] (Mathsoft Inc.) software. Four different data sets were constructed using same values for $c.k$ ($5 \times 10^{-6} \text{ s}^{-1}$) and Q (20 J) but different combination values for n and m as summarised in Table 5.2.

Table 5.2: Summary of n and m values used to construct simulated calorimetric data for solid-state reactions.

	n	m
Set 1	0.8	0.5
Set 2	0.5	0.8
Set 3	0.8	0.8
Set 4	0.5	0.5

5.3.4. Theoretical development

A common problem when analysing isothermal microcalorimetric data for crystallisation processes is the loss of initial data during the equilibration period as it is illustrated in Fig.5.1 which represents simulated power-time data for a solid state reaction. The signal started from a non-zero value to demonstrate that the initial part of the data was lost. This prevents the determination of total heat change (Q) required to calculate fraction reacted (α). This in turn prevents the analysis using a model fitting

approach as this requires the determination of α . A calculation method is therefore the most feasible solution.

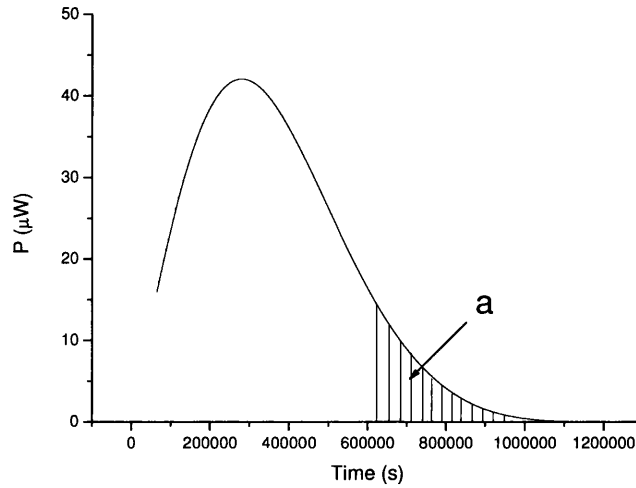


Figure 5.1: Simulated power-time data for crystallisation process. “a” represents the area under the curve used to carry out the calculation as described in Eq.5.13

From Eq.5.6 and Eq.5.9, Eq.5.12 is obtained:

$$\frac{dq}{dt} = P = C \cdot k \cdot Q \cdot \left[1 - \left(\frac{q}{Q}\right)^n\right] \cdot \left(\frac{q}{Q}\right)^m \quad \text{Eq.5.12}$$

When the initial data are lost, the calculations can be done backwards and q can be substituted with the following expression:

$$q = Q - a \quad \text{Eq.5.13}$$

The area a is illustrated in Fig. 5.1.

Given Eq.5.13, Eq.5.12 becomes:

$$\frac{dq}{dt} = P = C.k.Q. \left[1 - \left(\frac{Q-a}{Q}\right)\right]^n \cdot \left(\frac{Q-a}{Q}\right)^m = C.k.Q. \left(\frac{a}{Q}\right)^n \left[1 - \left(\frac{a}{Q}\right)\right]^m$$

Eq.5.14

P_1 and P_2 represent two power data where:

$$P_1 = C.k.Q. \left[1 - \left(\frac{Q-a}{Q}\right)\right]^n \cdot \left(\frac{Q-a}{Q}\right)^m$$

Eq.5.15

and

$$P_2 = C.k.Q. \left[1 - \left(\frac{Q-a_2}{Q}\right)\right]^n \cdot \left(\frac{Q-a_2}{Q}\right)^m$$

Eq.5.16

If

$$a_2 = 2.a$$

Eq.5.17

Eq.5.16 becomes:

$$P_2 = C.k.Q. \left[1 - \left(\frac{Q-2.a}{Q}\right)\right]^n \cdot \left(\frac{Q-2.a}{Q}\right)^m$$

Eq.5.18

Dividing Eq.5.18 by Eq.5.15, R_1 is obtained where:

$$R_1 = \frac{P_2}{P_1} = 2^n \cdot \left(\frac{Q-2.a}{Q-a}\right)^m$$

Eq.5.19

Taking the natural log of Eq.5.19, Eq.5.20 is obtained:

$$\ln R_1 = n \cdot \ln 2 + m \cdot \ln \left(\frac{Q-2.a}{Q-a}\right)$$

Eq.5.20

If another pair of power data, P_1 and P_3 , are selected so that $a_3=3.a$ and the same steps used to obtain $\ln R_1$, $\ln R_2$ is obtained (Eq.5.21):

$$\ln R_2 = n \cdot \ln 3 + m \cdot \ln \left(\frac{Q-3.a}{Q-a} \right) \quad \text{Eq.5.21}$$

Subtracting Eq.5.21 from Eq. Eq.5.20 gives:

$$\ln R_1 - \ln R_2 = n \cdot \ln \left(\frac{2}{3} \right) + m \cdot \ln \left(\frac{Q-2.a}{Q-3.a} \right) \quad \text{Eq.5.22}$$

By taking two other pairs of power data, (P_1, P_4) and (P_1, P_6) so that $(a_4 = 4.a)$ and $(a_6 = 6.a)$ and $(R_3 = P_4/P_1)$ and $(R_4 = P_6/P_1)$, Eq.5.23 is obtained:

$$\ln R_3 - \ln R_4 = n \cdot \ln \left(\frac{2}{3} \right) + m \cdot \ln \left(\frac{Q-4.a}{Q-6.a} \right) \quad \text{Eq.5.23}$$

Subtracting Eq.5.23 from Eq.5.22 gives:

$$(\ln R_2 - \ln R_1) - (\ln R_3 - \ln R_4) = m \cdot \left[\ln \left(\frac{Q-2.a}{Q-3.a} \right) - \ln \left(\frac{Q-4.a}{Q-6.a} \right) \right] \quad \text{Eq.5.24}$$

m can now be obtained by rearranging Eq.5.24:

$$m = \frac{(\ln R_2 - \ln R_1) - (\ln R_3 - \ln R_4)}{\left[\ln \left(\frac{Q-2.a}{Q-3.a} \right) - \ln \left(\frac{Q-4.a}{Q-6.a} \right) \right]} \quad \text{Eq.5.25}$$

Now, n can be obtained from Eq.5.21:

$$n = \frac{\ln R_2 - m \cdot \ln \left(\frac{Q-3.a}{Q-a} \right)}{\ln 3} = \frac{\ln R_2 - \frac{(\ln R_2 - \ln R_1) - (\ln R_3 - \ln R_4)}{\left[\ln \left(\frac{Q-2.a}{Q-3.a} \right) - \ln \left(\frac{Q-4.a}{Q-6.a} \right) \right]} \cdot \ln \left(\frac{Q-3.a}{Q-a} \right)}{\ln 3} \quad \text{Eq.5.26}$$

From Eq.5.25 and Eq.5.26, Eq.5.20 becomes:

$$\ln R_1 = \frac{\ln R_2 - \frac{(\ln R_2 - \ln R_1) - (\ln R_3 - \ln R_4)}{\left[\ln \left(\frac{Q-2.a}{Q-3.a_1} \right) - \ln \left(\frac{Q-4.a_1}{Q-6.a_1} \right) \right]} \cdot \ln \left(\frac{Q-3.a}{Q-a} \right)}{\ln 3} \cdot \ln 2 + \frac{(\ln R_2 - \ln R_1) - (\ln R_3 - \ln R_4)}{\left[\ln \left(\frac{Q-2.a_1}{Q-3.a_1} \right) - \ln \left(\frac{Q-4.a_1}{Q-6.a_1} \right) \right]} \cdot \ln \left(\frac{Q-2.a}{Q-a} \right) \quad \text{Eq.5.27}$$

Hence,

$$\frac{\ln R_2 - \frac{(\ln R_2 - \ln R_1) - (\ln R_3 - \ln R_4)}{[\ln(\frac{Q-2.a}{Q-3.a}) - \ln(\frac{Q-4.a}{Q-6.a})]} \cdot \ln(\frac{Q-3.a}{Q-a})}{\ln 3} \cdot \ln 2 + \frac{(\ln R_2 - \ln R_1) - (\ln R_3 - \ln R_4)}{[\ln(\frac{Q-2.a}{Q-3.a}) - \ln(\frac{Q-4.a}{Q-6.a})]} \cdot \ln(\frac{Q-2.a}{Q-a}) - \ln R_1 = 0$$

Eq.5.28

In Eq.5.28, Q is the only unknown. A range of Q values can be attempted in Eq.5.28 (using MathCad software) and the value that realises the equation is the correct Q value. After determining Q , m and n values can be calculated from Eq.5.25 and Eq.5.26 respectively.

5.4. Results and Discussion

5.4.1. Application of calculation method to simulated data

The calculation method was applied using four different simulated data sets. The aim was to determine the validity of the calculation method since all the parameters are known and the data are free from noise. Another aim was to determine the lowest area under the power-time curve (% data coverage) needed to recover the correct parameters. Results are summarised in Tables 5.3, 5.4, 5.5 and 5.6. $c.k$ values were calculated from Eq.5.14 as:

$$c.k = P/Q \cdot (\alpha)^n [1 - (\alpha)]^m$$

Eq.5.29

In the tables below, $c.k$ values were determined using three different values for α (0.3, 0.5 and 0.8: these values were chosen as they represent different portions of the power-time signal) and the mean value was reported alongside the standard deviation.

Table 5.3: Summary of calculation results for simulated dataset 1 ($c.k$: 5.10^{-6} , Q : 20J, n : 0.8, m : 0.5).

% data coverage	m	n	Q (J)	c.k
6	0.162	0.799	7.2	$11.0 \times 10^{-6} (\pm 1.8 \times 10^{-6})$
10	0.312-0.317	0.799	13.4-13.6	$6.5 \times 10^{-6} (\pm 0.6 \times 10^{-6})$
15	0.492-0.498	0.800	19.7-19.9	$5.0 \times 10^{-6} (\leq 0.0 \times 10^{-6})$
30	0.504-0.511	0.800	20.1-20.3	$5.0 \times 10^{-6} (\leq 0.0 \times 10^{-6})$
60	0.500	0.800	20.00	$5.0 \times 10^{-6} (\leq 0.0 \times 10^{-6})$
75	0.500	0.800	20.0	$5.0 \times 10^{-6} (\leq 0.0 \times 10^{-6})$

Table 5.4: Summary of calculation results for simulated dataset 2 (Cck : 5.10^{-6} , Q : 20J, n : 0.5, m : 0.8).

%data coverage	m	n	Q (J)	c.k
6	1.053	0.501	25.72	$4.7 \times 10^{-6} (\pm 0.6 \times 10^{-6})$
10	0.706	0.500	17.88	$5.2 \times 10^{-6} (\pm 0.2 \times 10^{-6})$
15	0.851	0.500	21.06	$4.9 \times 10^{-6} (\pm 0.1 \times 10^{-6})$
30	0.797	0.500	19.96	$5.0 \times 10^{-6} (\leq 0.0 \times 10^{-6})$
60	0.800	0.500	20.00	$5.0 \times 10^{-6} (\leq 0.0 \times 10^{-6})$
75	0.800	0.500	20.00	$5.0 \times 10^{-6} (\leq 0.0 \times 10^{-6})$

Table 5.5: Summary of calculation results for simulated dataset 3 ($c.k: 5.10^{-6}$, $Q: 20J$, $n: 0.8$, $m: 0.8$).

% data coverage	m	n	Q (J)	c.k
6	1.948	0.802	45.58	$5.5 \times 10^{-6} (\pm 2.9 \times 10^{-6})$
10	1.367	0.801	32.50	$4.7 \times 10^{-6} (\pm 1.3 \times 10^{-6})$
15	0.855	0.801	21.08	$4.9 \times 10^{-6} (\pm 0.1 \times 10^{-6})$
30	0.808	0.800	20.14	$5.0 \times 10^{-6} (\leq 0.0 \times 10^{-6})$
60	0.800	0.800	20.00	$5.0 \times 10^{-6} (\leq 0.0 \times 10^{-6})$
75	0.800	0.800	20.00	$5.0 \times 10^{-6} (\leq 0.0 \times 10^{-6})$

Table 5.6: Summary of calculation results for simulated dataset 3 ($c.k: 5.10^{-6}$, $Q: 20J$, $n: 0.5$, $m: 0.5$).

%data coverage	m	n	Q (J)	c.k
6	19.877	0.501	734.1	$6.1 \times 10^2 (\pm 1.1 \times 10^3)$
10	0.804	0.501	30.76	$4.1 \times 10^{-6} (\pm 0.6 \times 10^{-6})$
15	0.484	0.500	19.40	$5.1 \times 10^{-6} (\leq 0.0 \times 10^{-6})$
30	0.507	0.500	20.20	$5.0 \times 10^{-6} (\leq 0.0 \times 10^{-6})$
60	0.499	0.500	19.98	$5.0 \times 10^{-6} (\leq 0.0 \times 10^{-6})$
75	0.500	0.500	20.00	$5.0 \times 10^{-6} (\leq 0.0 \times 10^{-6})$

Tables 5.3, 5.4, 5.5 and 5.6 show consistent results. For all values for % data coverage (area used to carry out the calculation i.e. $a \times 6$), the correct n values were recovered. However, the correct m and Q values were only obtained at 15% data coverage and above. Another interesting observation is that when the correct values for $c.k$ were obtained, the standard deviation was very small. This can be used as an indicator for the validity of the calculations. These results demonstrate that the calculation method is valid when at least 15% of the total heat change is used and the variability of $c.k$ value can be used as a test to check the validity of the calculation method.

5.4.2. Application of calculation method to real calorimetric data

5.4.2.1. Characterisation of crystallised indomethacin with XRPD

Indomethacin crystallisation from the amorphous state was chosen as an example for solid state reactions. Amorphous indomethacin was aged in the TAM at 25°C, 30°C and 35°C. The reactions were left to proceed to completion. After the calorimetric measurements the samples were characterised with XRPD in order to determine their solid state nature. The XRPD pattern for amorphous indomethacin aged in the TAM at 30°C and 35°C are shown in Fig.5.2 along with the XRPD patterns for crystalline γ and α indomethacin. XRPD data showed that amorphous indomethacin after calorimetric measurement at 30°C and 35°C transformed predominantly to the γ crystalline form. Traces of the α -crystalline form were also present. The onset T_g of the indomethacin sample was measured with DSC at 5°C/min and found to be 44.6 (± 0.4)°C. All the experimental temperatures therefore were below the T_g of amorphous indomethacin. Yoshioka et al [109] also reported that below T_g , amorphous indomethacin crystallised to the most stable γ form. It was therefore assumed that the crystallisation process recorded with TAM originated from the emergence of only one polymorph (γ form).

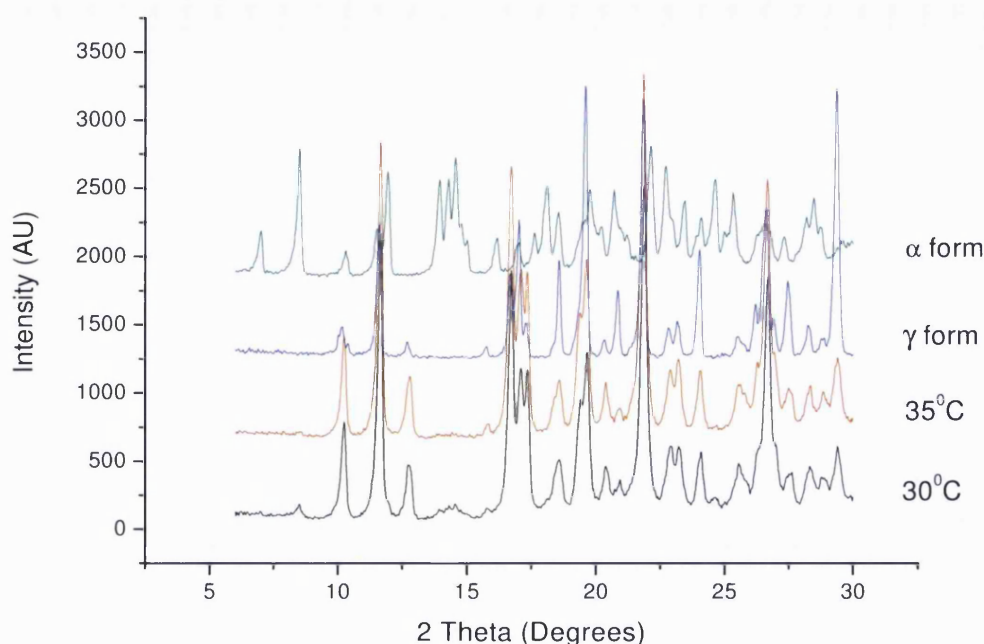


Figure 5.2: XRPD pattern for γ indomethacin, α indomethacin and for crystallised indomethacin at 30°C and 35°C.

5.4.2.2. Determination of crystallisation kinetics with model fitting approach

The reaction kinetics were first determined using the model fitting approach. This was carried out by fitting $d\alpha/dt$ versus α to the reduced Sestak-Berggren equation proposed by Perez-Maqueda et al [38] (Eq.5.5). $d\alpha/dt$ was determined from Eq.5.30:

$$\frac{d\alpha}{dt} = \frac{\frac{dq}{dt}}{Q} \quad \text{Eq.5.30}$$

The reacted fraction (α) was then calculated using Eq.5.6.

Fig.5.3 (A) shows a typical power-time signal for amorphous indomethacin at 25°C. A decay signal is first recorded. The signal then reached a low non-zero value and then it started increasing and a bell-shaped signal was then observed. The same phases were

recorded at the other experimental temperatures (30⁰C and 35⁰C). Amorphous materials tend to relax below their T_g and this process can be recorded in the calorimeter as a decaying exothermic signal [23]. This accounts for the decay signal recorded for indomethacin samples since all the experimental temperatures were below the T_g of indomethacin. After relaxation the sample starts crystallising and the calorimetric signal starts increasing. The relaxation signal was separated from the crystallisation signal by fitting the initial decay signal to the time derivative of the KWW equation (Eq.1.12, Section 1.5.2).

The KWW model provided a good fit for the data and the resulting relaxation parameters were then used to simulate the relaxation process until completion (when the signal reached zero). The simulated curve is illustrated as a red curve in Fig.5.3(A). The simulated curve was then subtracted from the total signal. The resulting signal, illustrated in Fig. 5.3 (B), was assumed to have originated solely from the crystallisation process.

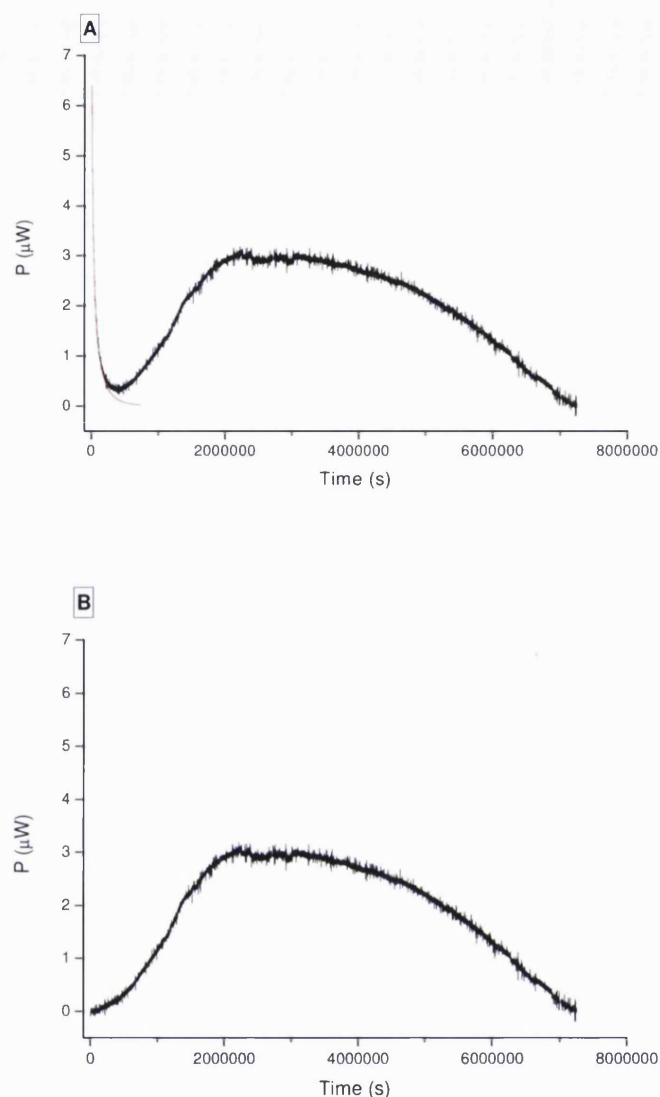


Figure 5.3: *A) Power-time signal for amorphous indomethacin at 25⁰C. Red line represents simulated relaxation curve. B) Resulting power-time signal for amorphous indomethacin at 25⁰C after subtracting the relaxation signal from the total signal in (A).*

Fig.5. 4 illustrates representative power-time data for crystallising indomethacin at 25, 30 and 35⁰C (A). The corresponding crystallisation rate ($d\alpha/dt$) as a function of reacted fraction (α) and the resulting fit curve (red) to the reduced Sestak-Berggren equation (Eq.5.5) are also illustrated in Fig.5.4 (B).

As can be seen from Fig.5.4 (B), at all three temperatures amorphous indomethacin show typical bell-shaped graph for reaction rate ($d\alpha/dt$) as a function of reacted fraction (α). The graphs were well fitted by the reduced Sestak-Berggren equation (Eq.5.5) as all fits had R^2 values greater than 0.95. The resulting fit values are summarised in Tables 5.7, 5.8 and 5.9 for calorimetric data at 25, 30 and 35°C, respectively. As the temperature changed, all the kinetic parameters also changed. One would expect that if the samples crystallised with the same mechanism only the rate constants (represented partially in $c.k$ value) would change due to changes in molecular mobility, whereas m and n values would remain constant. The results obtained from these experiments could suggest that crystallisation mechanism is temperature dependent. However, it should be remembered that the Sestak-Berggren model is purely empirical and its parameters do not possess any physical meaning and hence variation of the parameters with temperature does not necessarily reflect variation in crystallisation mechanism.

Figure 5.4: Power-time signal (A) and corresponding crystallisation rate as a function of reacted fraction (B) for amorphous indomethacin at 25, 30 and 35°C. Red curves in (B) represent fit to the reduced Sestak-Berggren equation (eq.5.5).

Characterisation of indomethacin samples after TAM measurements at 30°C and 35°C with XRPD revealed that the samples were predominantly present in the γ form

(Fig.5.2), so there is no change in the type of emerging polymorph. In order to know whether the mechanism changed with temperature below T_g , the reaction rate versus reacted fraction graphs should be fitted to multiple models and then observe whether the same model provides the best fit for all temperatures. This work, however, is mainly concerned in determining whether the calculation method developed based on the reduced Sestak-Berggren equation is valid for real calorimetric data. Comparison of fit and calculated values is therefore sufficient for this purpose. It is worth noting, however, that the Arrhenius relationship was found to relate the $c.k$ values and temperature as can be seen from Fig.5.5. An activation energy of 2.6 kJ/g was calculated from the plot.

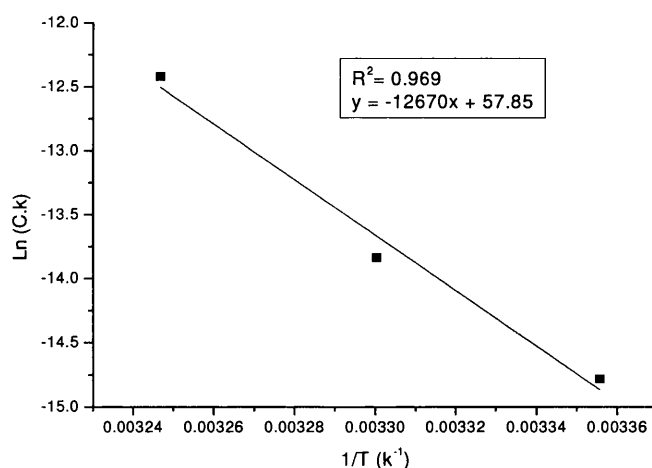


Figure 5.5: Arrhenius plot for $c.k$ as a function of temperature for the crystallisation process of amorphous indomethacin below T_g .

5.4.2.3. Determination of crystallisation kinetics with the calculation method

The calculation method described in the theoretical development section (Section 5.4.3) was applied to each calorimetric data set except for one dataset at 25⁰C since calculation was not feasible due the noisy nature of the data. Since simulated data revealed that a minimum of 15% of total heat change is needed at the end of the crystallisation process

to recover the real kinetic values, all the values used for % data coverage were higher than 15%; 30%, 50% and 80% were used. $c.k$ values were determined using three different values for α (0.3, 0.5 and 0.8). The mean and standard deviation values were then reported as shown in Tables 5.7, 5.8, and 5.9.

The calculated values for the parameters of reduced Sestak-Berggren equation for crystallising indomethacin at 25°C, 30°C and 35°C are also summarised in Tables 5.7, 5.8 and 5.9, respectively. At some values for % data coverage, the calculated parameters had no physical meaning or the Q function could not be determined. These results were reported as Not Applicable (NA). Such results are likely to have originated from significant interference of noise in the data. Results of physical meaning did not all agree with the fit values. Calculated values that agreed with fit values are underlined in the summary Tables 5.7, 5.8 and 5.9.

When the calculated values were consistent with the fit values, the variation in the calculated $c.k$ value was very small whereas this variation is relatively large when the calculated values were different from the fit values. In terms of the % data coverage that resulted in the success of the calculation method, no trend was observed. With some samples (eg. 35°C data, sample 1, Table 5.9) high % data coverage (80%) was needed to reach agreement between the differently determined kinetic parameters. With other samples (eg. 25°C data, sample1, Table 5.7) lower % data coverage value (50%) resulted in recovering the fit values whereas higher % data coverage (80%) returned significantly different calculated values. This indicates that with real calorimetric data the success of the calculation method is also affected by the level of noise in the data used to carry out the calculation. If the calculation method fails with certain % data coverage, it is therefore worth carrying out the calculation with different % data coverage. A good test to check the accuracy of the calculation is to look at the variation

in the calculated $c.k$ because as noted earlier when the fit and calculated values agreed the calculated $c.k$ value had very small variation. However, care should be taken as there was one case (30°C data, sample 1, Table 5.8) where the calculated $c.k$ value had very small variation and agreed with the fit value but the other calculated values were not consistent with the fit values.

Table 5.7: Crystallisation kinetic parameters for indomethacin at 25°C determined by fitting data to reduced Sestak-Berggren model (Eq. 5.5) and by applying calculation method.

	m	n	Q	c.k
Fit values	0.351 (±0.026)	0.496 (±0.026)	11.88 (± 2.18)	$3.80 \times 10^{-7} (\pm 0.42 \times 10^{-7})$
% data coverage	Calculated values/ sample 1			
30%	NA	NA	NA	NA
50%	<u>0.329</u>	<u>0.458</u>	<u>13.00</u>	<u>$3.90 \times 10^{-7} (\pm 0.04 \times 10^{-7})$</u>
80%	2.134	0.544	40.50	$6.60 \times 10^{-7} (\pm 4.81 \times 10^{-7})$

Table 5.8: Crystallisation kinetic parameters for indomethacin at 30°C determined by fitting data to reduced Sestak-Berggren model (Eq. 5.5) and by applying calculation method.

	m	n	Q (J)	c.k
Fit values	0.413 (±0.001)	0.908 (≤0.000)	14.70 (≤0.00)	$0.98 \times 10^{-6} (\leq 0.00 \times 10^{-6})$
% data coverage	Calculated values/ sample 1			
30%	NA	NA	NA	NA
50%	0.101	0.689	8.68	<u>$1.07 \times 10^{-6} (0.00 \pm \times 10^{-6})$</u>
80%	NA	NA	NA	NA
% data coverage	Calculated values/ sample 2			
30%	NA	NA	NA	NA
50%	<u>0.359</u>	<u>0.738</u>	<u>13.40</u>	<u>$0.88 \times 10^{-6} (0.01 \pm \times 10^{-6})$</u>
80%	NA	NA	NA	NA

Table 5.9: Crystallisation kinetic parameters for indomethacin at 35°C determined by fitting data to reduced Sestak-Berggren model (Eq. 5.5) and by applying calculation method using three different values for α (0.3, 0.5 and 0.8).

	m	n	Q (J)	c.k
Fit values	0.575 (± 0.028)	0.795 (± 0.032)	16.41 (± 0.29)	4.04×10^{-6} ($\pm 0.30 \times 10^{-6}$)
% data coverage	Calculated values/ sample 1			
30%	NA	NA	NA	NA
50%	1.369	0.815	26.80	4.22×10^{-6} ($1.26 \pm \times 10^{-6}$)
80%	<u>0.525</u>	<u>0.737</u>	<u>16.40</u>	<u>3.59×10^{-6}</u> ($0.01 \pm \times 10^{-6}$)
% data coverage	Calculated values/ sample 2			
30%	0.608	0.962	11.00	7.39×10^{-6} ($0.75 \pm \times 10^{-6}$)
50%	NA	NA	NA	NA
80%	1.397	0.939	23.10	6.21×10^{-6} ($1.95 \pm \times 10^{-6}$)

5.5. Summary

Long duration of solid-state reactions or loss of initial calorimetric data results in difficulty in determining the total heat of crystallisation. As a result, determining the crystallisation kinetics from isothermal microcalorimetric data using the model fitting approach becomes unfeasible. A calculation method based on the reduced Sestak-Berggren equation was proposed to solve this problem. Simulated calorimetric data revealed that a minimum of 15% of total reaction heat is needed to recover the correct crystallisation parameters. Small variation in the calculated $c.k$ is a good indicator of the accuracy of the calculation method.

Indomethacin crystallisation from the amorphous state was used as a model for solid-state reactions. Crystallisation was monitored using an isothermal microcalorimeter. Crystallisation kinetics were determined using both model fitting and calculation

approaches. Agreement between fit and calculated values was erratic and there was not a relationship between the % data coverage and the accuracy of calculation results. This could be attributed to inherent noise in calorimetric data. However, in most cases accurate calculation results were accompanied by small variation in calculated $c.k$ values.

The calculation method proposed in this work can be used for all solid state reactions with the condition that either the initial or final part of the calorimetric data is available.

***6) Chapter 6: Complex crystallisation
studies with IMC: amorphous
indomethacin crystallisation at 60⁰C.***

6.1. Introduction

Crystallisation from the amorphous state is controlled by different thermodynamic, molecular and dynamic factors [12]. The preparation method appears to be another important factor as amorphous samples of the same material can show different recrystallisation profiles depending on the preparation method [12]. Bhugra et al [73] showed that quench cooled samples exposed to higher levels of mechanical stress tend to show a greater tendency to recrystallise. In the first part of this study, IMC was used to investigate the effect of sample preparation on the calorimetric output upon recrystallisation. Indomethacin crystallisation from the amorphous state above the T_g was used as a model system.

In Chapter 5, determination of crystallisation kinetics with IMC was examined. Indomethacin crystallisation below T_g was used as a model system. This task was not complicated by the occurrence of multiple processes simultaneously since indomethacin crystallised predominantly into one polymorph (γ form). However, indomethacin has been reported to crystallise into different polymorphs (γ , α and δ forms) at temperatures above its T_g [73, 101]. This complication may render the analysis of calorimetric data challenging since the recorded heat flow will result from different processes of different kinetics. The second part of this study will therefore explore the feasibility of using IMC to examine complex crystallisation processes using indomethacin crystallisation above T_g as a model system. Interpretation of calorimetric data is usually best achieved when complementary techniques are used [97, 110]. X-ray powder diffraction, DSC and PLM were therefore used to aid the analysis of our calorimetric data.

6.2. Aims and objectives

- Preparation of amorphous quench cooled indomethacin by two different methods.
- Record the calorimetric output for the prepared indomethacin samples at 60⁰C and determine the effect of the preparation method on this output.
- Deconvolute the calorimetric signal for complex crystallisation processes.
- Derive quantitative information from calorimetric data for complex crystallisation processes and compare it with data obtained with XRPD and PLM.

6.3. Experimental

6.3.1. Materials

6.3.1.1. Preparation of amorphous indomethacin

- Amorphous indomethacin was prepared directly in the TAM ampoule using two different methods:

Method 1: crystalline indomethacin (Molekula, UK) (300mg) was weighed and loaded into a TAM ampoule. Ampoules were then flushed with nitrogen and crimped in a glove bag at low %RH ($\leq 5\%$). Crystalline samples were then melted at 175⁰C for 5min and immediately quench cooled with liquid nitrogen. Samples prepared by this method will be referred to in the remaining text as amorphous bulk indomethacin (ABI).

Method 2: same as method 1 except that the ampoule was rotated after melting the drug in order to form a film around the walls of the ampoules. Ampoules were then

cooled by immersing them in liquid nitrogen or under tap water (at ambient temperature). Samples prepared by this method will be referred to as amorphous film indomethacin (AFI)

- Amorphous indomethacin was also prepared by melting crystalline indomethacin on aluminium paper on a hot plate. The quenched cooled sample (with liquid nitrogen) was then gently ground using a mortar and pestle. This sample will be referred to as powdered amorphous indomethacin.

6.3.1.2. Preparation of α and δ indomethacin polymorphs

The two polymorphs are not commercially available so they were prepared as was described by Joshi [111].

- α -indomethacin was prepared by dissolving 10g of indomethacin (as purchased from Molekula) in ethanol (10ml) at 80°C. After filtering the undissolved drug, 20ml of distilled water (at ambient temperature) was added to the ethanol solution while it was maintained at 80°C.

The white crystals formed were then filtered and dried in a vacuum desiccator over P₂O₅. The melting point of the crystals obtained was determined with DSC to be 153°C in agreement with that reported by Joshi [111] for α indomethacin.

- δ -polymorph was prepared by desolvation of indomethacin methanolate for 10 days in a vacuum desiccator at 30°C. Indomethacin methanolate was prepared by dissolving indomethacin (5 g) (as purchased from Molekula) in methanol (80ml) at 80°C. The solution was then filtered and covered with perforated parafilm and allowed to evaporate gradually at ambient conditions. Crystals of indomethacin methanolate were then collected after 3-2 days.

The melting point for the prepared δ polymorph was measured by DSC and was found to be 133⁰C in agreement with the values reported by Crowley et al [112].

6.3.2. Methods

6.3.2.1. Isothermal microcalorimetry

Ampoules were loaded into the TAM channel at 60⁰C and equilibrated for 30 min. This time was referred to as time = 0 s. Ampoules were lowered to the measurement position and heat flow was recorded for at least 10 days. The calibration and measuring technique were as described in Section 2.2.3.4. Measurements were conducted at least in triplicate.

6.3.2.2. X-ray powder diffraction (XRPD)

Samples were prepared in the TAM ampoules according to Method 2 and then stored in a temperature controlled oven at 60⁰C. Ampoules were then removed at several time points and samples (present as thin films) were removed from the ampoules to be gently ground using a mortar and pestle. Diffractograms for the powdered samples were recorded as described in Section 2.2.7.2. Traces for scanning angle (2θ) from 5^o to 30^o were obtained in 0.02⁰ steps using 4 s averaging time. Measurements were conducted at least in duplicate. Peaks in the XRPD patterns were determined using the peak search program of the X'Pert HighScore (Version 1.0a, Philips Analytical B. V., The Netherlands) software by detecting the minima from the second derivative of the diffractogram.

6.3.2.3. Differential scanning calorimetry (DSC)

DSC measurements were conducted using Pyris 1 DSC (Perkin-Elmer Instruments, USA) connected to the cooling unit Intracooler 2P (Perkin-Elmer Instruments, USA) as

described in Section 2.2.5.2. Samples (about 10 mg) were loaded in non-hermetically sealed aluminium pans and then heated from 0 to 180°C at 5, 40 and 100°C/min.

6.3.2.4. Polarised light microscopy

Samples prepared by Method 2 were examined under the light microscope. Samples were stored in a temperature controlled oven and removed at different time points to be examined directly under polarised light microscope as described in section 2.2.9.2.

6.4. Results and discussion

6.4.1. Qualitative analysis of calorimetric signal for ABI and AFI samples

Amorphous indomethacin samples denoted as ABI and AFI as described above were transferred to the TAM at 60°C as soon as the cooling process was accomplished. Figs.6.1 and 6.2 illustrate the heat output for the ABI and AFI samples, respectively. For ABI samples (Fig.6.1), the power-time curve is initiated by a small decaying signal (phase “a”) which then levels off for a short while (phase “b”) at a low non-zero P value. An increasing signal is then recorded which then levels off (phase “c”) but shows another increasing pattern again in a smooth manner (phase “d”). At 5 days approximately, the signal starts decaying in an uneven manner (phase “e”). Finally the signal starts decreasing at a very slow rate at low P values (phase “f”). AFI samples showed a similar pattern (Fig.6.2) but some differences are noticed and these can be clearly seen from Fig.6.3 which illustrates representative calorimetric outputs for an ABI sample and an AFI sample. The first major difference is noticed with phase “c” which lasts for a longer period with the AFI samples compared to the ABI samples. Although phase “e” starts at the same time point (5.5 days) within experimental error, the signal at this phase proceeds in a noticeably more even manner with the AFI samples compared with the ABI samples.

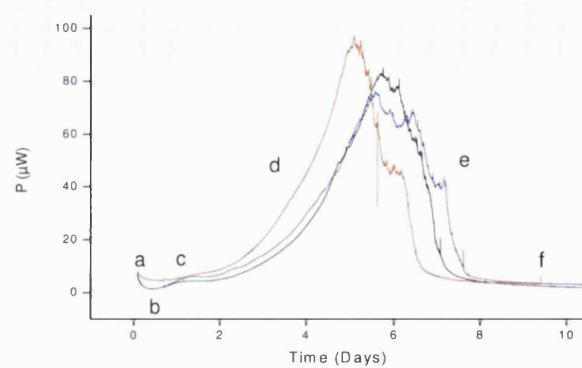


Figure 6.1: Power-time signal for three ABI samples as they crystallised at 60⁰C.

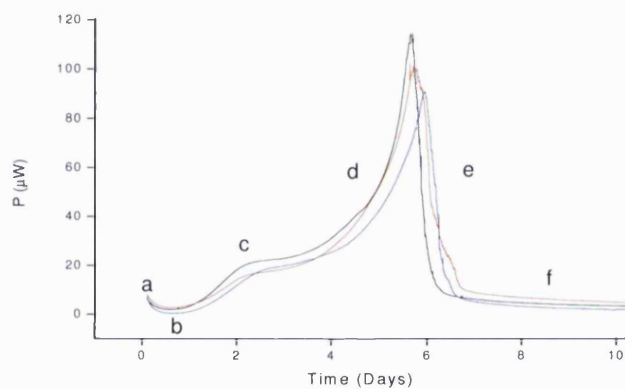


Figure 6.2: Power-time signal for three AFI samples as they crystallised at 60⁰C.

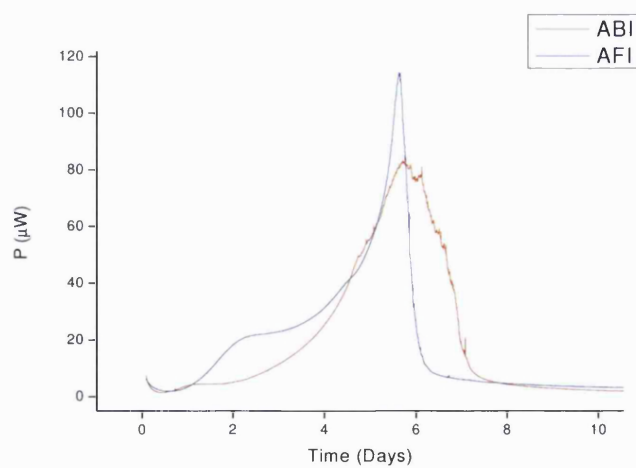


Figure 6.3: Illustration of the power-time signal for an ABI sample and an AFI sample.

From this descriptive analysis it can be concluded that the preparation method affected the progress of the calorimetric signal for amorphous indomethacin at 60°C as expected. There are different factors in the preparation of AFI and ABI samples. These include the cooling method (by inserting the ampoule in liquid nitrogen or cold water) and whether the samples are spread along the inner walls of the TAM ampoules. In order to verify which factor has mainly affected the progress of the calorimetric signal, melted indomethacin was spread inside the ampoule then cooled with liquid nitrogen. This method will exclude differences in the cooling method. Sample prepared with this method will be referred to as nitrogen cooled amorphous film indomethacin (NAFI). As can be seen from Fig.6.4, power-time signal for NAFI sample has the pattern as AFI sample, except that phase “c” starts earlier for NAFI sample. This might be due to the mechanical stress induced by quenching with liquid nitrogen resulting in the creation of cracks, which can act as nucleation sites. These results suggest that the cooling method was not the main factor resulting in differences in the progress of the calorimetric signal for AFI and ABI samples. It is therefore very likely that these differences stem from the shape of the samples (bulk or film-like).

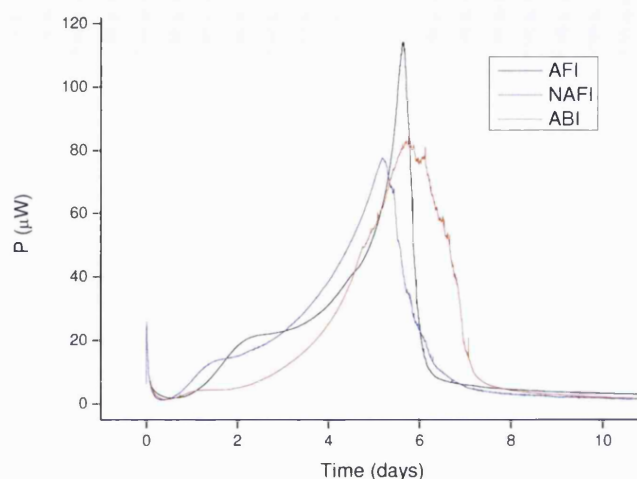


Figure 6.4: Power-time signal for a representative ABI sample, AFI sample and NAFI sample.

In a research article by Bhugra et al [63] the onset of crystallisation of amorphous indomethacin was determined with IMC at 60⁰C. The samples were also prepared *in-situ* inside the TAM ampoules by quench cooling. The same phases were reported up to phase “c” since data recording was terminated after three days as the authors were interested in recording the onset of crystallisation indicated by the sharp increase of the power signal i.e. the onset of phase “c”.

Before proceeding in interpreting the origin of the phases described above, it is important to confirm that the power signal recorded by TAM for amorphous indomethacin at 60⁰C originates from the sample itself and not from other artefacts. Bhugra et al [63] reported the presence of both exotherms and endotherms at temperatures higher than 40⁰C when glass ampoules with rubber stoppers were used. It was deduced that the rubber stoppers contributed to the power signal causing these artefacts. These effects were reported not to happen with stainless steel ampoules [63]. All our experiments were conducted using glass ampoules with rubber stoppers, but no

endotherms were observed and the signal was consistently exothermic. In order to verify whether the rubber stoppers did contribute to the power signal of our experiments, the calorimetric response from the same batch of amorphous indomethacin was recorded at 60°C using both glass and stainless steel ampoules. Powdered amorphous indomethacin (prepared as described above, Section 6.3.1.1) was used for this experiment. Results are illustrated in Fig.6.5. Samples loaded in stainless steel ampoules demonstrate an initial low positive value which then increased gradually and an intact peak was then recorded over approximately 70h. On the other hand, power signal from samples loaded in glass ampoules started from a low negative value which then gradually decreased to become positive after a short while. The positive signal then followed the same trend as that for stainless steel samples. These results indicate that the rubber closure might be contributing negatively to the power signal at 60°C. The effect of this contribution was investigated by calculating the total heat of crystallisation by integrating the power-time signal from time = 2h to t = 150h. Data before t = 2h are usually not considered when analysing data as it might contain contribution from heat of friction resulting from lowering the ampoules to the measurement position. At t = 150h, the signal for all samples was stable. Integration results are summarised in Table 6.1 and they show that the contribution from the rubber stoppers had negligible effects on the total heat of crystallisation since its value was independent of the type of ampoules used.

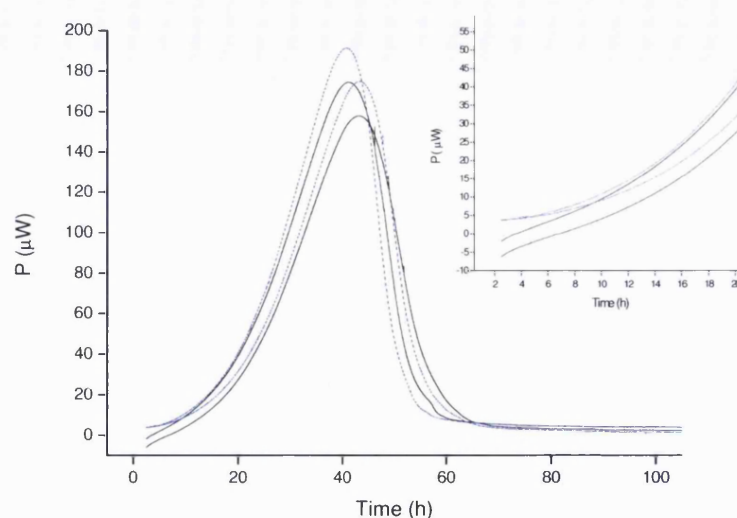


Figure 6.5: Power-time signal for powdered indomethacin samples as they crystallised in the TAM at 60⁰C using glass (solid line) and stainless steel ampoules (dashed line). Inset shows the power signal of the same samples at the beginning of the reaction.

Table 6.1: Mean total heat output from crystallisation of powdered indomethacin (300mg) (at 60⁰C) loaded either in glass or stainless steel ampoules. Standard deviation is in presented in parentheses.

	Glass ampoules (n = 2)	Stainless steel ampoules (n = 3)
Mean total heat output (J)	15.09, 14.48	15.09, 16.22, 15.21

Given that the contribution from the rubber stopper is negligible and the same phases were reported by Bhugra et al [63], our calorimetric outputs for both ABI and AFI samples are considered to originate from the samples and are weakly affected by the rubber stopper contribution.

The initial decay signal i.e. phase “a” is similar to the enthalpy relaxation signal of amorphous systems. However, the relaxation phenomenon above T_g occurs at very short times (in the microseconds range) and hence phase “a” is likely to have originated from a different phenomenon. Bhugra et al [63] hypothesised that this phase might have resulted from the decay in nucleation rate. When stable nuclei are formed, crystal growth is initiated resulting in an increasing exothermic response. The plateau phase (phase “b”) is then the sum of the decaying nucleation signal and the increasing crystal growth signal. Finally, crystal growth becomes dominant and phase “c” is recorded [63]. This explanation could be feasible knowing that the crystallisation onset for indomethacin at 60°C is about 6h as was determined with polarised light microscopy [63]. In our study, small crystals were also visualised with a polarised light microscope after 6 hours of storage at 60°C as will be discussed later.

6.4.2. Characterisation of TAM samples

6.4.2.1. XRPD

After microcalorimetric measurements, ABI and AFI samples were analysed with XRPD. The two types of indomethacin samples had the same XRPD pattern as illustrated in Fig.6.6. This indicates that the ABI and AFI samples crystallised into the same polymorphs. In an attempt to identify these polymorphs, the peak positions for the crystallised indomethacin samples (either ABI or AFI) shown in Fig.6.6 were plotted against the peak positions for the most common crystalline forms of indomethacin as shown in Figs. 6.7, 6.8 and 6.9. As can be seen from these figures, 6 peak positions from the crystallised indomethacin sample correspond to the γ polymorph (Fig.6.7), 12 positions correspond to the α form (Fig.6.8) and 5 positions correspond to the δ form (Fig.6.9). This might indicate that all three polymorphs are

present in the crystallised ABI and AFI samples. X'Pert High Score software allows matching an XRPD pattern to reference patterns for defined crystalline forms. When this function was applied on crystallised ABI and AFI samples, the software provided scores for the three polymorphs in the following order: $\alpha > \gamma > \delta$. These results are partly consistent with what was reported by Wu et al [101] who studied the crystallisation of indomethacin prepared by melt quenching crystalline indomethacin on a clean microscope cover glass. Between 50 and 100°C, it was found that more than 90% of the crystals formed were in the δ form, and the remaining crystals were of both γ and α forms.

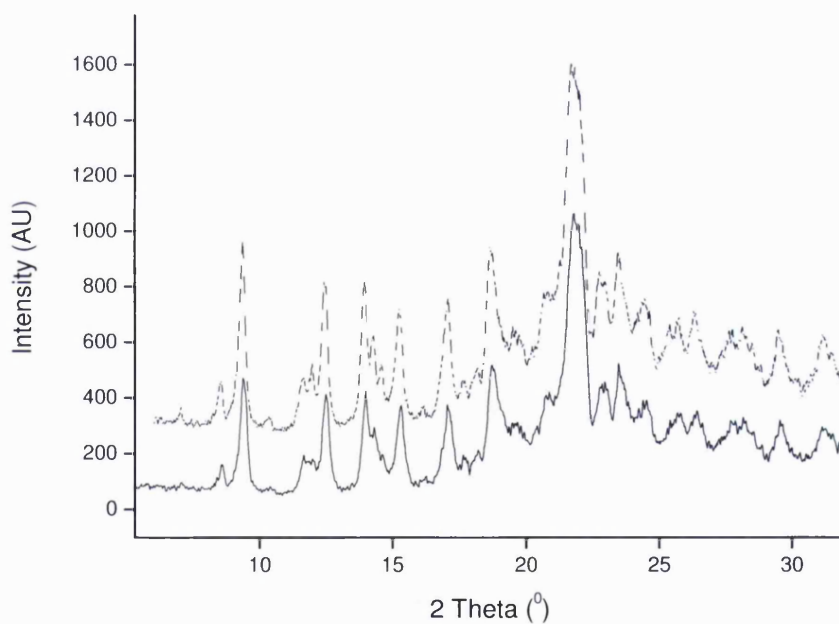


Figure 6.6: XRPD pattern for ABI (solid line) and AFI (dashed line) after microcalorimetric measurements at 60°C.

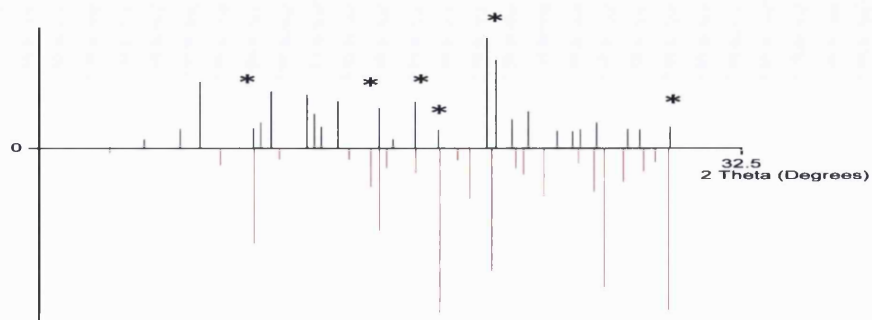


Figure 6.7: Illustration of peak positions for crystallised indomethacin samples (top black) and for gamma indomethacin (bottom red).

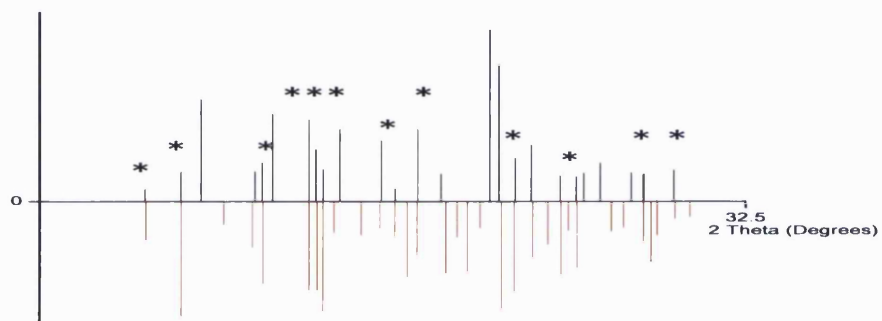


Figure 6.8: Illustration of peak positions for crystallised indomethacin samples (top black) and for alpha indomethacin (bottom red).

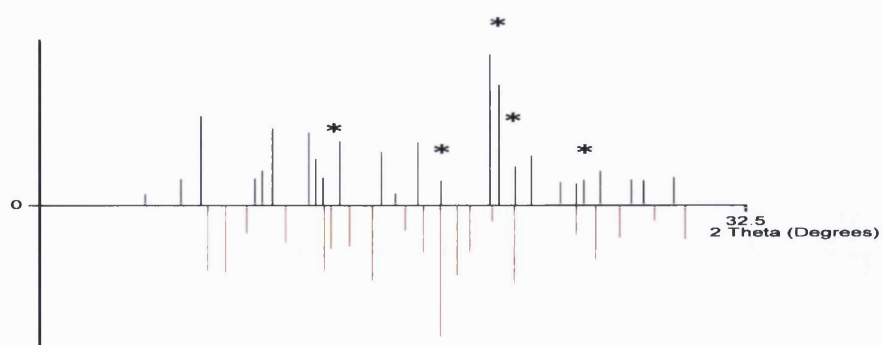


Figure 6.9: Illustration of peak positions for crystallised indomethacin samples (top black) and for delta indomethacin (bottom red).

There are, however, prominent diffraction peaks in both ABI and AFI sample diffractograms which do not correspond to any of the examined polymorphs (γ , α and δ). These are situated at diffraction angles 9.37, 12.38 and 15.25. It is speculated that there is another crystalline species that the available reference diffraction patterns do not reflect. X-ray diffractograms for the γ and the α forms are well established in the literature since their single-crystal structures are known [101]. Single-crystal structure for the δ polymorph is not known and the X-ray diffractogram for this polymorph is assumed to be that produced for a crystalline form that emerges from desolvation of indomethacin methanolate [101]. There is no record in the literature that confirms that the diffractogram for the δ form that emerges from the amorphous state is the same as the diffractogram for the δ form that emerges from indomethacin methanolate desolvation. XRPD data were, therefore, not conclusive and the use of complementary techniques was mandatory.

6.4.2.2. DSC

In order to identify further the identity of the indomethacin polymorphs that emerged at 60°C, AFI samples were also analysed by DSC by heating the samples at different heating rates. The resulting DSC scans are illustrated in Fig.6.10. As the samples were heated at 5°C/min, an endotherm was observed at 124.35°C, which was immediately followed by an exotherm. Another endotherm was then observed at 154.28°C that was also followed by a small exotherm. Finally, an endotherm at 160.02°C was recorded. The three endotherms correspond to the melting of indomethacin polymorphs δ (124.35°C), α (154.28°C) and γ (160.02°C) [101].

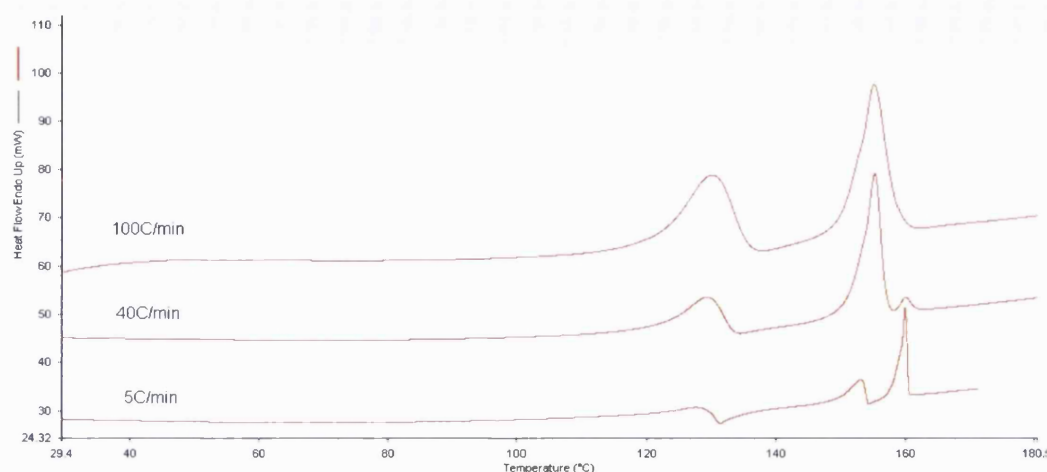


Figure 6.10: DSC scans for AFI samples after microcalorimetric measurements heated at 5, 40 and 100⁰C/min.

Crystalline indomethacin is known to be a monotropic system with the γ form being the most stable form [111]. Both α and δ forms are metastable forms and were reported to transform to the stable form after melting which is manifested in the exotherm that follows the melting endotherm [111] as it was illustrated in Fig.6.10 (5⁰C/min). However, the δ form being the least stable can transform to either the α or γ forms depending on the types of seeds present and the heating mode employed [111]. Our DSC results at 5⁰C/min therefore confirm the presence of δ form but not the other two forms since these might have originated from the conversion of the δ form.

As the heating rate was increased to 40⁰C/min, the same events in the same order were noted as for 5⁰C/min but the fusion enthalpy ratio between γ and α polymorphs was reversed so that it became higher in favour of the α form (Fig.6.10). Quantitative analysis was not possible due to the possibility of conversion between melting events of α and γ forms.

Finally, when a heating rate of $100^{\circ}\text{C}/\text{min}$ was used both the melting endotherms for δ and α forms were present whereas that for the γ form disappeared. It can be concluded that the use of higher heating rates suppressed the appearance of the γ form indicating that this form was not originally present in the recrystallised AFI samples but resulted from the conversion of the metastable polymorphs. There remain two possible scenarios: either the AFI samples recrystallised both to δ and α forms or they recrystallised totally to δ form, which transformed to α form upon heating in the DSC and this conversion was not suppressed by high heating rates. However, when pure δ indomethacin was heated at $100^{\circ}\text{C}/\text{min}$, no transformation was observed (Fig.6.11). When pure δ form was mixed with pure α form in a 1:1 ratio, the δ form clearly transformed to the α form indicated by the presence of an exotherm following the melting endotherm of the δ form (Fig.6.12). The data presented confirm that the AFI samples recrystallised at 60°C into both α and δ forms.

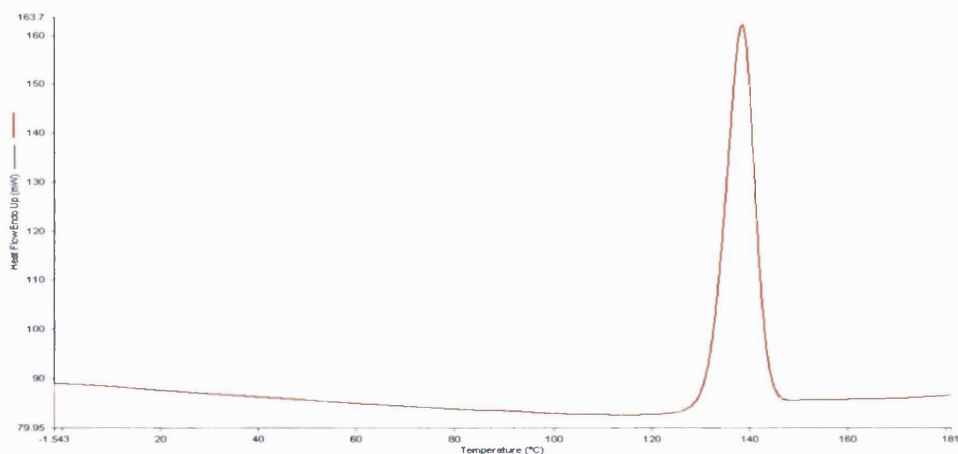


Figure 6.11: DSC scan for indomethacin δ -form at $100^{\circ}\text{C}/\text{min}$.

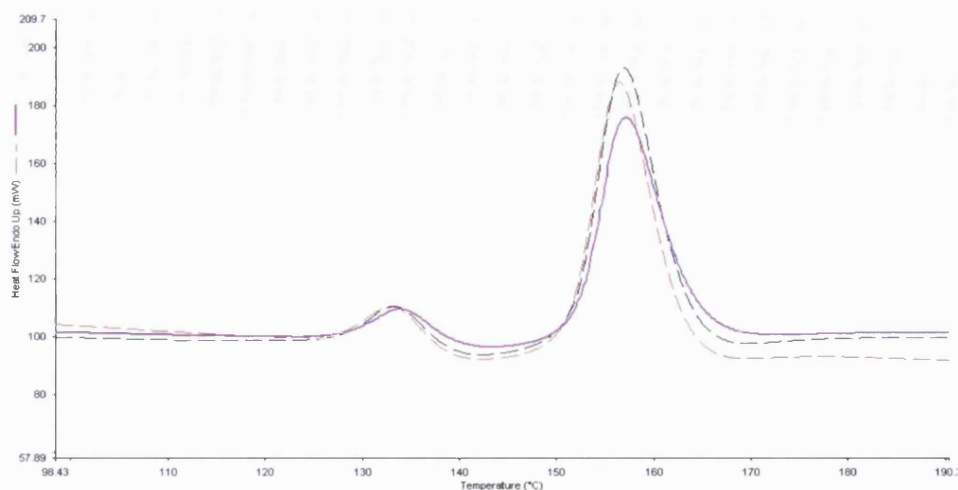


Figure 6.12: DSC scan for a 1:1 mixture of α and δ polymorphs scanned at $200^{\circ}\text{C}/\text{min}$.

In order to confirm the absence of the γ form in the recrystallised AFI and ABI samples, some γ crystals were added as seeds to an AFI sample. The sample was then allowed to recrystallise in the TAM at 60°C . The recrystallised sample was then scanned in the DSC at $200^{\circ}\text{C}/\text{min}$. The resulting DSC scan is illustrated in Fig.6.13. Unlike the non-seeded samples (Fig.6.10, $100^{\circ}\text{C}/\text{min}$), the melting endotherms for all three polymorphs are clearly seen, although the fast heating rate resulted in the partial overlap of the α and γ melting endotherms.

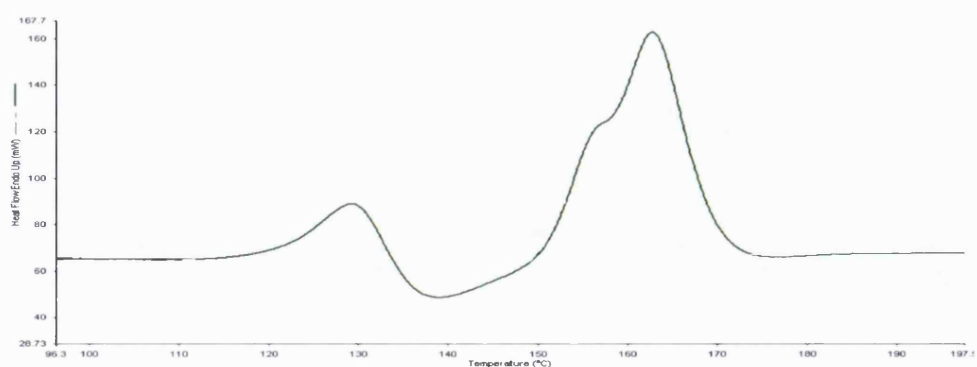


Figure 6.13: DSC scan for a gamma seeded AFI sample scanned at $200^{\circ}\text{C}/\text{min}$.

DSC analysis of AFI samples proved the presence of only two crystalline forms, α and δ . This might seem contradicting with the XRPD analysis which revealed the possibility of the presence of three or four different polymorphs. The most likely explanation for this is that the δ form that emerges from the amorphous state has a different x-ray diffractogram from the δ form that is produced from desolvation of indomethacin methanolate. The diffractogram for the δ form that emerges from the amorphous state might have diffraction peaks that overlap with those for the γ form and δ form that results from desolvation of indomethacin methanolate. This might have led to a misinterpretation of the XRPD data.

In conclusion, DSC analysis provided strong evidence that AFI and ABI samples crystallised to α and δ forms and no evidence for the presence of γ form was obtained.

6.4.3. Characterisation of AFI samples with PLM

Physical reactions such as crystallisation can be better understood if monitored visually since different crystals can have different shapes. This could be achieved with AFI samples since the thin indomethacin layer inside the ampoule could be easily visualised with a polarised light microscope after storage at 60°C.

Pictures taken under polarised light microscope for AFI samples stored at 60°C for different time periods are illustrated in Fig.6.14. It is clear that within 6 hours of storage, some formed crystals of a spherical shape can be visualised. Both Bhugra et al [73] and Wu et al [101] reported that at 60°C, the δ form emerges first as compact and fine-grained spherulites. Therefore it is very likely that the crystals seen at 6h are those for the δ form. As time proceeded, the concentration of δ crystals increased as seen in Fig.6.14 (21h). By 41h, the whole surface was covered with these crystals. At 48h,

smaller and denser crystals were observed on top of the already existing δ crystals. Subsequently, the concentration of these dense crystals increased up to the fourth day. No more monitoring could be achieved after this time point as significant crystallisation hindered light transmission through samples.

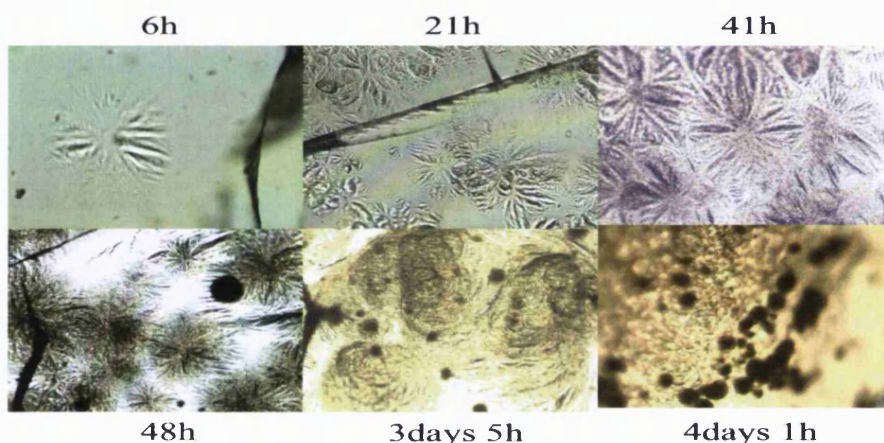


Figure 6.14: Polarised light microscope pictures for AFI samples stored at 60°C for different time periods as designated on top of each picture.

6.4.4. Characterisation of AFI samples with XRPD

X-ray powder diffraction is a standard method to monitor crystallisation processes since characteristics of the diffraction pattern are dependent on the types and quantity of crystals present in a sample. The progress of the crystallisation process for AFI samples at 60°C was also monitored using XRPD in order to understand better and interpret the calorimetric signal. XRPD patterns for the samples at different time intervals are illustrated in Fig.6.15. In the first day, a broad hump characteristic of amorphous form was observed. In the second day, some diffraction peaks started to appear. As time proceeded, the same diffraction pattern was retained with an increase in peaks' intensity up to the fifth day, where new diffraction peaks clearly corresponding to the α form appeared. From day 5 to day 7, no more new peaks appeared, and the intensity of the existing peaks grew longer.

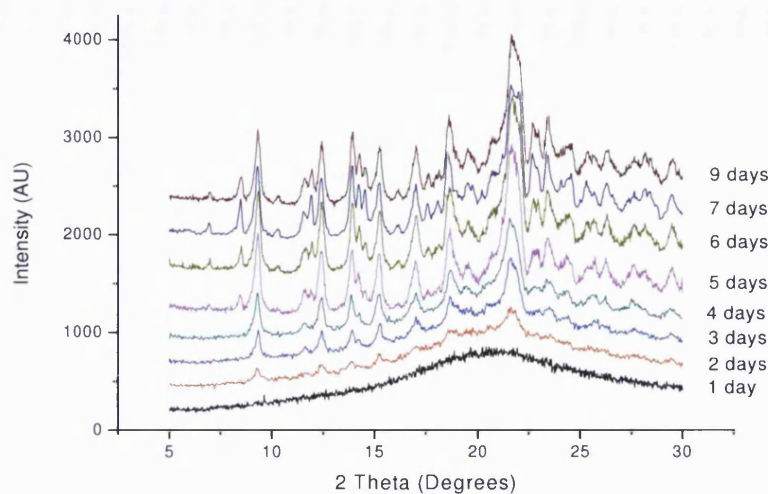


Figure 6.15: Illustration of progress of XRPD pattern for AFI samples stored at 60°C over 9 days.

The intensity of some characteristic peaks was plotted against time to provide a better interpretation of the diffraction patterns shown in Fig.6.15. Data for day 12 were also included. As it can be seen from Fig.6.16, three patterns of peak intensity evolution are present. In the first pattern (pattern 1), represented by peaks at positions 9.28° and 21.61°, peaks appeared at 2 days and their intensity increased steadily up to 4.6 days. From 4.6 days to 5 days, a sharp increase in the intensity was observed. From 5 days and 9 days, the intensity remained constant within experimental error. After 9 days, a decrease in the intensity occurred. In the second pattern (pattern 2), presented by peak positions 13.92° and 18.71°, the same trend was observed except after 9 days when the intensity remained constant (within experimental error). In the third pattern (pattern 3), represented by peak position 8.48°, peak appeared in the 5th day approximately and its intensity increased from 5 days to 7 days then remained constant (within experimental error) and finally showed some increase after 9 days.

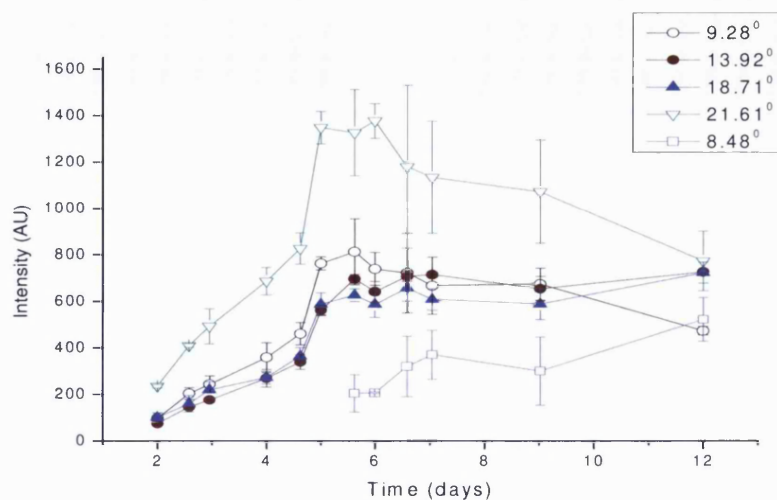


Figure 6.16: The evolution of intensity of characteristic peaks over time for AFI samples stored at 60°C.

From this analysis it appears that three different species are emerging. Each species can be hypothesised to be represented by one pattern from the three patterns described above. These species will be referred to by the number of the pattern to which they correspond.

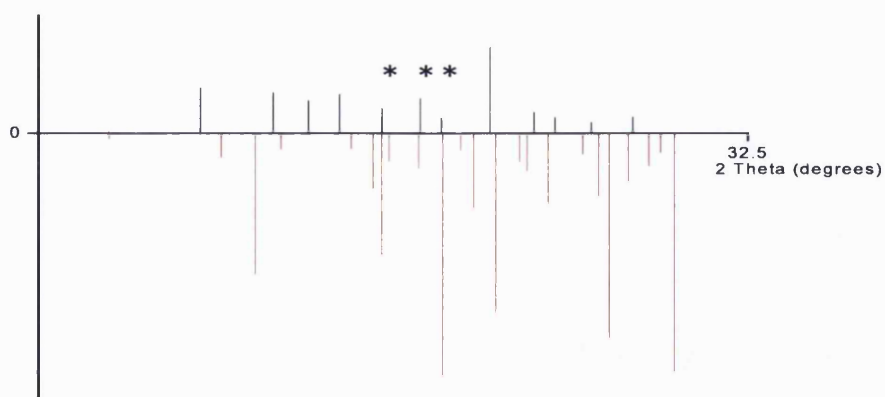


Figure 6.17: Illustration of peak positions for crystallised AFI sample after 4 days storage at 60°C (top black) and for γ indomethacin (bottom red).

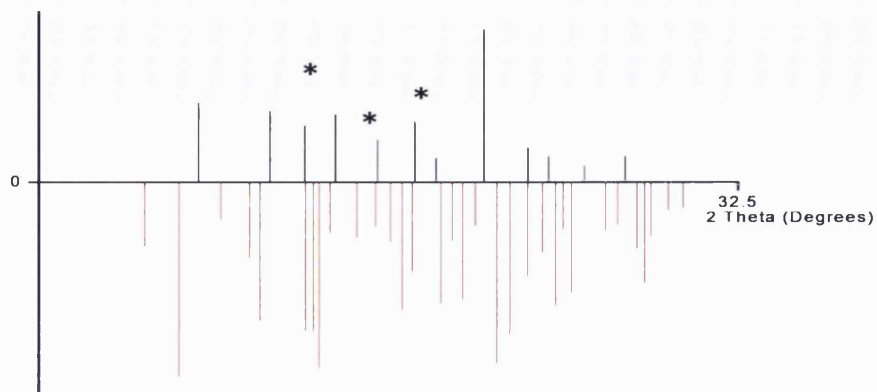


Figure 6.18: Illustration of peak positions for crystallised AFI sample after 4 days storage at 60°C (top black) and for α indomethacin (bottom red).

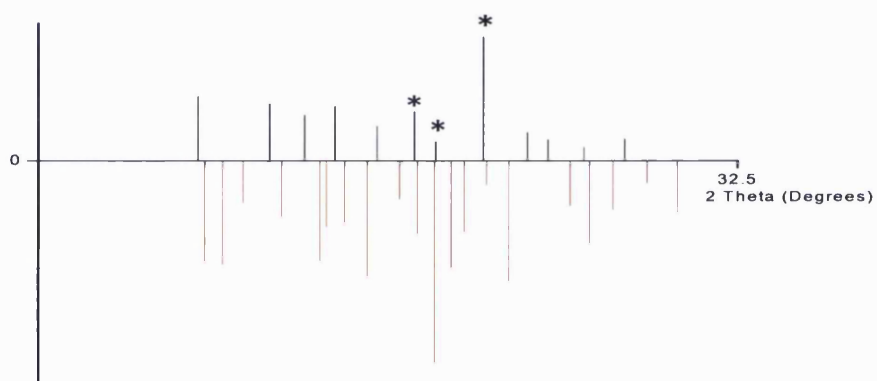


Figure 6.19: Illustration of peak positions for crystallised AFI sample after 4 days storage at 60°C (top black) and for δ indomethacin (bottom red).

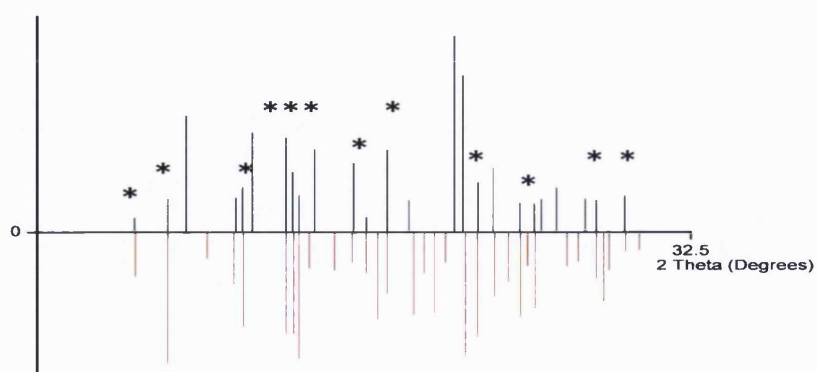


Figure 6.20: Illustration of peak positions for crystallised AFI sample after 6 days storage at 60°C (top black) and for α indomethacin (bottom red).

The XRPD pattern from 2 days to 5 days is very likely to have resulted from the presence of species 1 and species 2 since polarised light microscopy has shown that by 48h two different crystalline species were present. Unfortunately, XRPD data before 2 days do not provide sufficient information about the nature of the crystals that emerged the earliest due to weak sensitivity of the technique. In an attempt to determine the nature of crystalline forms from 2 days and 5 days, the peak positions for AFI samples at 4 days were plotted against those for γ , α and δ forms as shown in Figs.6.17, 6.18 and 6.19, respectively. For each polymorph, only three peak positions for AFI sample matched those for an indomethacin polymorph. DSC data discussed earlier have proved that the γ form was absent. Analysis of XRPD patterns after 5 days showed that the new emerging peaks matched those for the α form (Fig.6.20). This indicates that the α form represents species 3 and it only appeared after 5 days. It is therefore possible that both species 1 and 2 correspond to the δ form. Wu et al [101] reported that the thickness of the indomethacin liquid affected the morphology of δ crystals grown. More transparent δ crystals emerged from thinner liquids (Fig.6.21 a) compared with thicker liquids (Fig.6.21 b). It could be hypothesised that differences in the thickness of drug layer (with the AFI samples) along the inner walls of the TAM ampoules resulted in different growth modes of δ crystals. Trofimov et al [113] also demonstrated that film thickness can affect crystal growth kinetics. It was shown that with volume induced crystallisation, kinetics were determined by film thickness. Surface induced crystallisation kinetics are described by 2D Kolmogorov–Johnson–Mehl–Avrami (KJMA) in thin films and are linear in thick films [113].

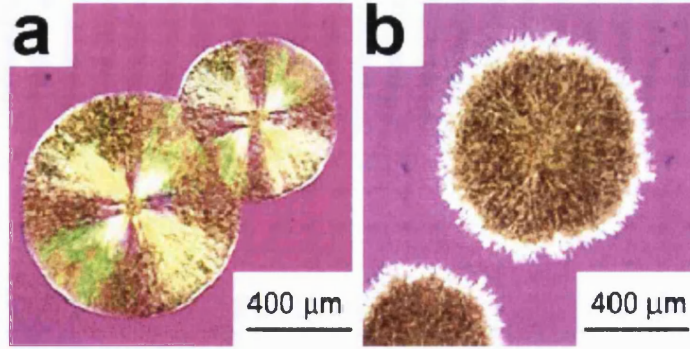


Figure 6.21: “(a and b) Typical appearances of δ IMC crystals. Both were grown at 70 °C.” Figure reproduced from Wu et al [101].

The rate of crystallisation was modelled using the Avrami model. This is the most commonly used model to derive isothermal crystallisation kinetics in different fields [99, 114]. The first assumption this model makes is that crystal growth rate is constant and linear. It also assumes that nucleation is either instantaneous (athermal) or sporadic (thermal) [114]. It is expressed mathematically by a simple equation (Eq.6.1) as follows:

$$\theta_t = 1 - \exp[-(kt)^n] \quad \text{Eq.6.1}$$

where θ_t is relative crystallinity at time t , k is the Avrami rate constant and n is the Avrami exponent. k is a first order parameter (has units of time^{-1}) and gives a quantitative indication for the stability of a system. The mechanism of nucleation and crystal growth can be deduced from the value of n which should be an integer (ranging from 1 to 4) [115]. Values for θ_t can be obtained from XRPD data as described in Eq.6.2:

$$\theta = \frac{I_t}{I_f} \quad \text{Eq.6.2}$$

where I_t is peak intensity at time t and I_f is the maximum peak intensity attained when the crystallisation process ceases. The analysis was applied using intensity evolution for representative peaks at diffraction angles 9.28° and 21.61° (pattern 1) and 13.92° and 18.71° (pattern 2). Data for peaks corresponding to pattern 3 were not sufficient to carry out the analysis, so the analysis was restricted to pattern 1 and 2 only. Whenever possible data were fitted to the Avrami model for θ_t values ranging between 0.1 and 0.8. above $\theta_t = 0.8$, it is hypothesised that the assumption of constant linear crystal growth rate is not valid [114] as at this stage an impingement effect may occur. This effect is referred to situations where two crystallisation interfaces grow from different nuclei and then impinge on each other. As a result, crystal growth might be terminated on the common interface formed [116]. Fit lines obtained by least squares minimisation and kinetic parameters are illustrated in Fig.6.22 and Table 6.2 respectively.

The Avrami model provided a fair but not a perfect description of the data as can be concluded from the relatively low values of R^2 (Fig.6.22). The model provided a better prediction of k values than n values as it is reflected in the low RSE values for k (<10%) and high RSE values for n (>10%) (Table 6.2). Quantitatively, all the peaks had a similar k value reflecting that species 1 and species 2 evolved at the same rate. Although values for the Avrami exponent n were greatly variable, they generally varied between 2 and 3 which indicates that crystallisation is characterised by two dimensional growth and both thermal and athermal nucleation mechanisms [99].

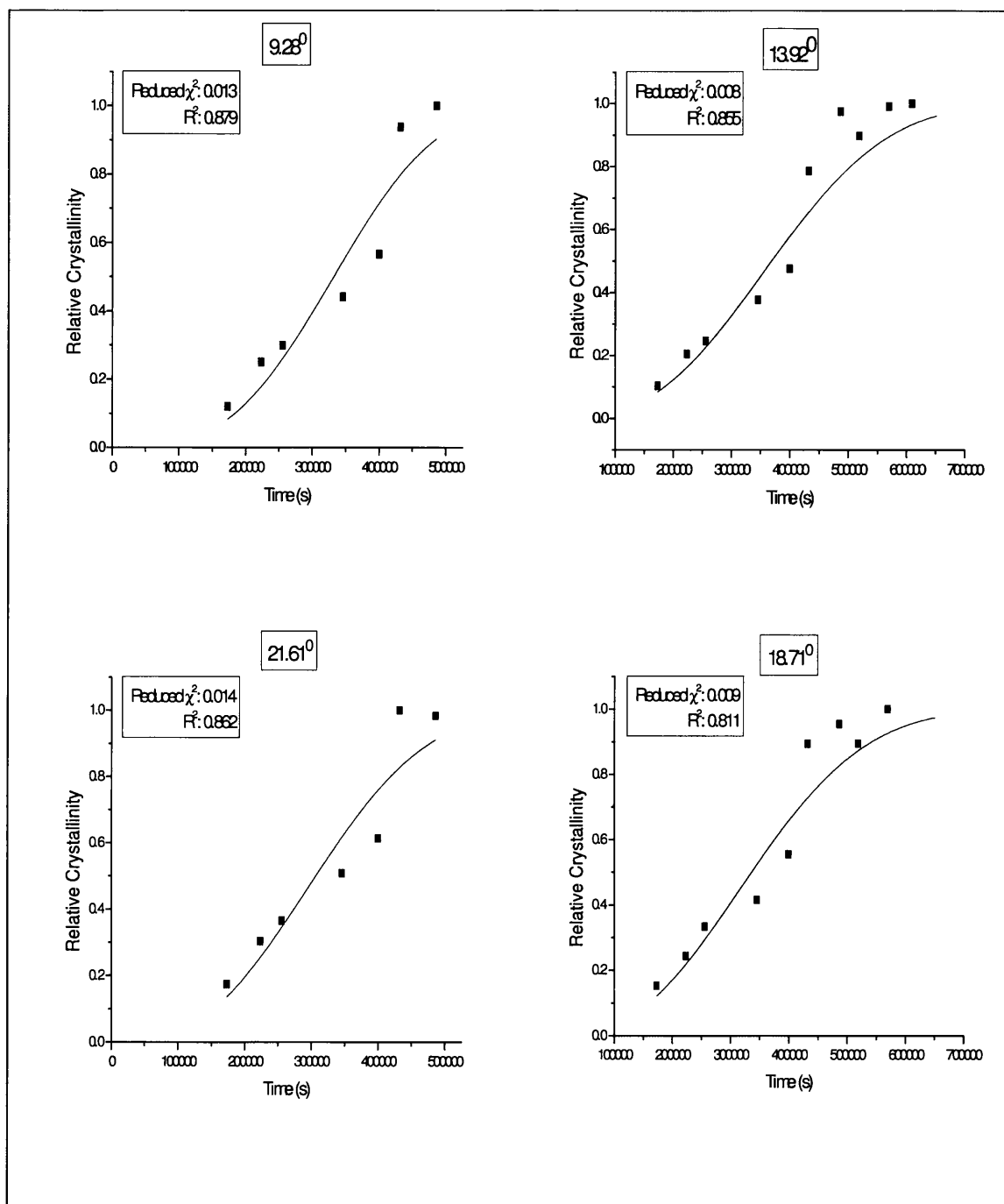


Figure 6.22: Relative crystallinity at diffraction angles 9.28° , 13.92° , 18.71° and 21.61° for AFI samples at 60°C . Solid lines represent fit lines to Avrami model.

Table 6.2: Crystallisation kinetic parameters for AFI samples at 60°C obtained by fitting XRPD data at diffraction angles (9.28°, 13.92°, 18.71° and 21.61°) to the Avrami model using least squares minimisation. Standard error is shown between parentheses. RSE stands for relative standard error.

Diffraction angle	k (s ⁻¹)	n
9.28°	2.69 (± 0.14) × 10 ⁻⁶ , RSE=5%	3.2 (± 0.8), RSE=25%
13.92°	2.37 (± 0.05) × 10 ⁻⁶ , RSE=2%	2.7 (± 0.7), RSE=26%
18.71°	2.57 (± 0.18) × 10 ⁻⁶ , RSE=7%	2.5 (± 0.7), RSE=28%
21.61°	2.85 (± 0.17) × 10 ⁻⁶ , RSE=5%	2.7 (± 0.6), RSE=22%

6.4.5. Quantitative analysis of calorimetric signal

6.4.5.1. AFI samples

Calorimetric data for crystallisation processes have been used to extract crystallisation kinetics by plotting relative crystallinity (θ_t) against time [104, 115]. The plot is then fitted to appropriate models. θ_t can be calculated as follows:

$$\theta_t = \frac{\int_0^t \left(\frac{dq}{dt}\right) dt}{\int_0^\infty \left(\frac{dq}{dt}\right) dt} = \frac{q}{Q} \quad \text{Eq.6.3}$$

where t is the elapsed time during the course of crystallisation, q is the heat change to time t and Q is the total heat of crystallisation. It should be noted that this approach is based on the assumption that there is a linear relationship between the evolution of crystallinity and the evolution of heat recorded by the calorimeter. Furthermore, this approach can only be applicable if only one crystallisation mechanism takes place. However, inspection of calorimetric data for AFI samples reveals that there at least two overlapping peaks. Quantitative analysis of such data necessitates the separation of

these peaks. Gaisford et al [115] found that a double-Lorentzian model could describe calorimetric data for the crystallisation of indomethacin to two different polymorphs. Double (2), triple (3) and quadruple (4)-Lorentzian models were employed successively to deconvolute AFI calorimetric data up to 9 days when crystallisation process is believed to have nearly finished. Results of fitting typical data for AFI samples to 2, 3, and 4-Lorentzian models are illustrated in Figures 6.23, 6.24 and 6.25, respectively. As can be seen from Figures 6.23 and 6.24, a better fit was obtained with 3-Lorentzian compared with 2-Lorentzian. This was expected since models of higher number of parameters usually provide better fits [22]. However, when data were fitted to 4-Lorentzian model, which has more parameters than 3-Lorentzian model, the fitting process failed to converge and the software reported the same crystallisation peaks returned by 3- Lorentzian (Fig.6.25). This indicates that the better fit obtained by 3-Lorentzian is not merely because the model has more parameters but because the data are best described by the overlap of three peaks. The symmetrical nature of the peaks returned by Lorentzian model might have resulted in the fit line not perfectly matching the calorimetric data. Crystallisation from the amorphous state is a complex phenomenon and tends to be described by models which take into account mechanistic factors such the impingement effect. It should be noted then that quantitative analysis (as described above with Eq.6.1) of the deconvoluted peaks is just an approximate estimation of the real kinetics of the reactions.

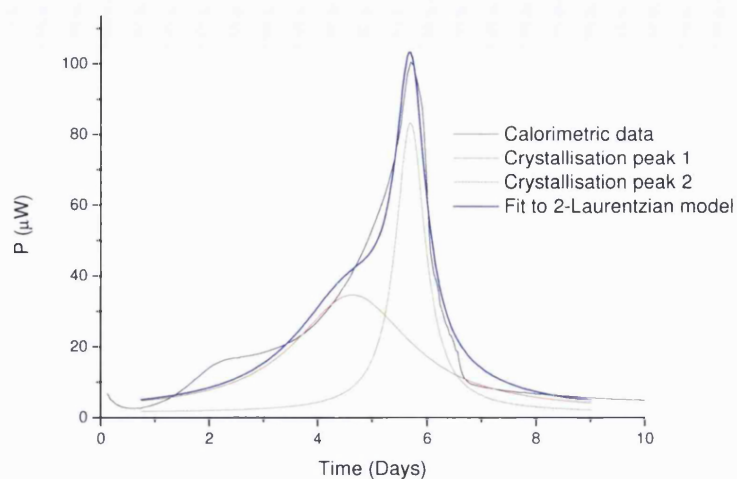


Figure 6.23: Power-time data for a typical AFI sample and the fit lines obtained by fitting to a 2-Laurentzian model.

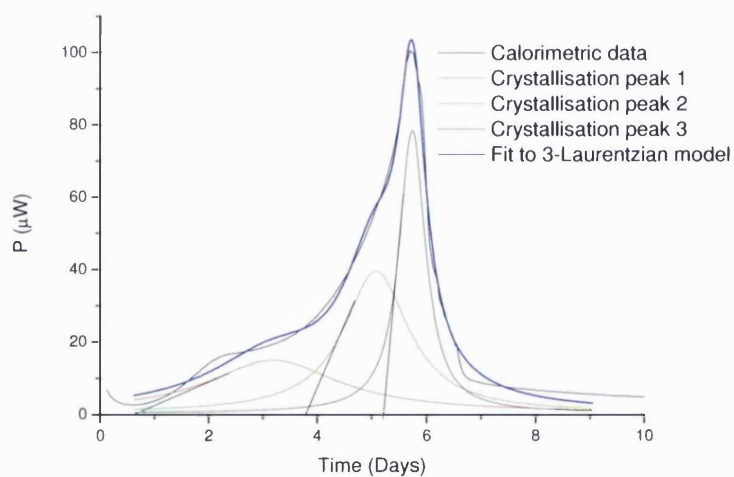


Figure 6.24: Power-time data for a typical AFI sample and the fit lines obtained by fitting to a 3-Laurentzian model.

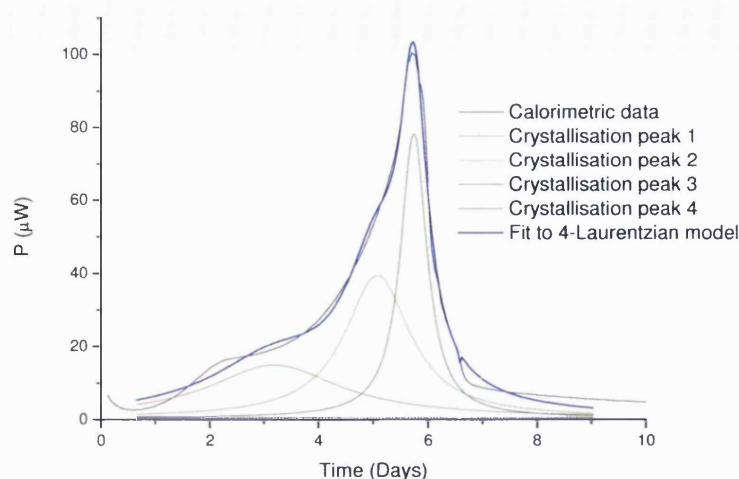


Figure 6.25: Power-time data for a typical AFI sample and the fit lines obtained by fitting to a 4-Lorentzian model.

θ_t values were calculated using Eq.6.3 for each of the three peaks (each representing a distinct phase) returned by 3-Lorentzian model. θ_t versus time plots were then constructed and data were fitted to the Avrami model for θ_t values ranging between 0.1 and 0.8. The resulting fits and kinetic parameters are illustrated in Fig.6.26 and Table 6.3. All three phases had values for the Avrami rate constant k in the same order of magnitude (Table 6.3). However, k value for phase 1 conforms quite well with the k values calculated with XRPD for species 1 and species 2 (Table 6.2). Also only phase 1 had an n value of physical meaning which also agrees quite well with the n value obtained with XRPD data for species 1 and species 2. The other two phases had n values of no physical meaning. This may reflect some flaws in the deconvolution method used rendering the quantitative analysis of crystallisation kinetics not possible to obtain.

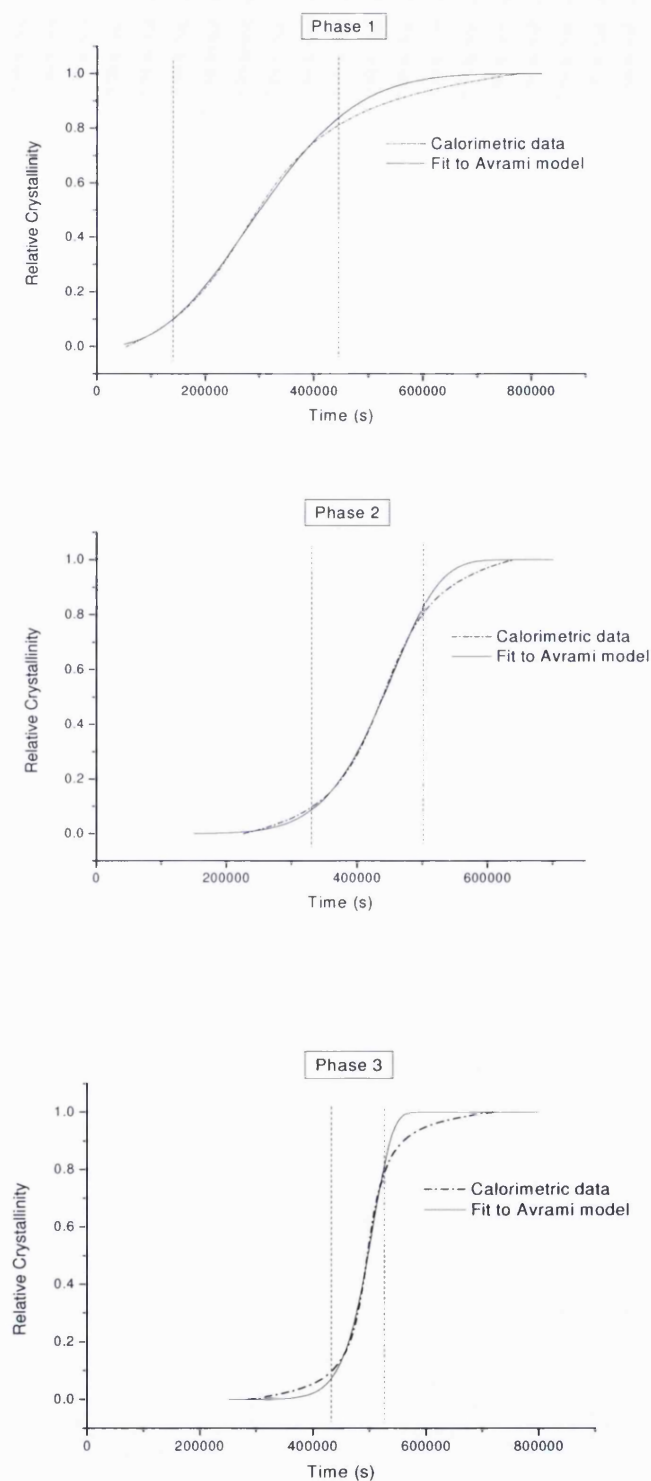


Figure 6.26: Relative crystallinity as a function of time for AFI samples (three phases) at 60°C and the fit lines obtained by fitting to the Avrami model between 0.1 and 0.8 relative crystallinity as demonstrated between the two dashed vertical lines.

Table 6.3: Kinetic parameters obtained by fitting the crystallisation data for AFI samples (three phases) at 60°C to the Avrami model with least squares minimization.

Crystallisation peak	k (s ⁻¹)	n
1	2.65 (± 0.35) × 10 ⁻⁶	2.9 (± 0.4)
2	2.04 (± 0.15) × 10 ⁻⁶	10.7 (± 3.1)
3	1.88 (± 0.11) × 10 ⁻⁶	27.2 (± 9.8)

To further relate TAM data to microscopy and XRPD data, the onset time to crystallisation for each phase (determined with 3-Lorentzian model) was estimated by drawing a tangent between the time axis and the accelerating part of each peak as illustrated in Fig.6.24. A similar approach was used by Bhugra et al [63] in order to determine the onset time to crystallisation for amorphous indomethacin using TAM data. Results are summarised in Table 6.4. The analysis revealed that phase 1 appeared after approximately one day of storage. This does not agree with microscopy data which showed that indomethacin crystals were present after 6 hours. The same conclusion was drawn by Bhugra et al [63]. TAM data are also not consistent with microscopy data in regard to the onset of phase 2 since microscopy images showed that the second crystalline species appeared after 2 days whereas the onset of phase 2 (from TAM data) was found to be 4.4 days. Finally, the onset of phase 3 (5.65 days) was more consistent with XRPD data (5.5 days). The inconsistency between TAM and microscopy data could have resulted from the superior sensitivity (i.e. ability to detect initial crystallisation) of microscopy technique relative to TAM [63]. Alternatively, the deconvolution process of the crystallisation peaks did not reflect quantitatively the

actual or real peaks. This could be again due to the symmetrical nature of Lorentzian peaks, which might not be the case with the actual crystallisation peaks.

Table 6.4: Onset time to crystallisation determined for peaks deconvoluted by 3-Lorentzian model for AFI samples at 60°C.

	Phase 1	Phase 2	Phase 3
Onset time (days)	0.94 (\pm 0.32)	4.43 (\pm 0.61)	5.65 (\pm 0.45)

6.4.5.2. ABI samples

The same analysis with Lorentzian model was carried out with calorimetric signal for ABI samples illustrated in Fig.6.1. The signal appears to be composed of at least two peaks; the first peak (phase “c” in Fig.6.1) is noticeably small relative to the second peak composed of phases “d” and “e” (Fig.6.1). The broad, uneven and variable nature of the second peak (phases “d-e”) resulted in the creation of artefacts in data fitting. It was noted that increasing the parameters of the model resulted in a better or comparable fit as it can be concluded from the values of reduced χ^2 and R^2 . This can be seen from Fig.6.27 which illustrates an example of calorimetric signal for an ABI sample fitted to Lorentzian models of increasing number of parameters. It was not possible therefore to determine the model that best describes the data. This reflects one of the main challenges and drawbacks of IMC when it comes to quantitative analysis of complex power-time data.

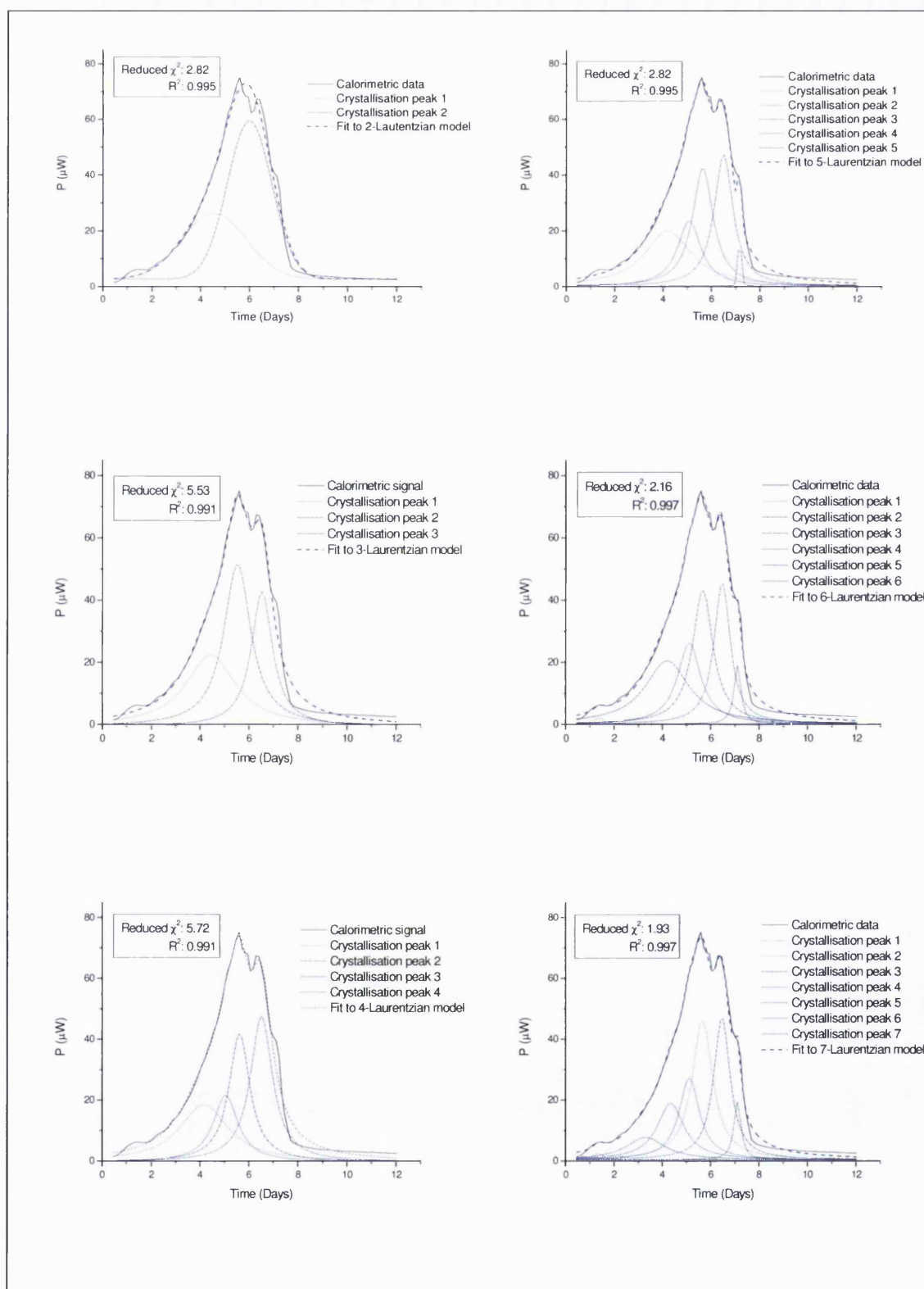


Figure 6.27: Calorimetric signal for a representative ABI sample fitted to Lorentzian models as illustrated in the legends.

6.5. General discussion

Indomethacin crystallisation from the amorphous state has been widely studied [73, 96, 101, 102, 117]. Indomethacin was shown to crystallise to three different polymorphs (two metastable forms and one stable form) at temperatures above the T_g (44.2°C)[64, 73, 101, 109]. Bhugra et al [73] have demonstrated that the level of mechanical stress applied during the preparation process can greatly affect the crystallisation behaviour. The aim of this study had two facets: 1) explore the feasibility of using isothermal microcalorimetry to study the complex crystallisation of indomethacin at 20°C above T_g and 2) examine if isothermal microcalorimetry can be used to detect differences in the crystallisation behaviour of two differently prepared indomethacin samples above T_g .

The first objective was approached using film-like amorphous indomethacin samples (AFI) since these showed a “neat” isothermal microcalorimetry signal (Fig.6.2) unlike bulky amorphous indomethacin samples (ABI) which showed an uneven signal. Moreover, AFI samples were more easily analysed with the complementary techniques as the samples were transparent enabling microscopy inspection and easily removed from TAM ampoule enabling analysis with XRPD.

Analysis of AFI samples after microcalorimetry measurements (when the signal stabilised at low values) with DSC revealed the presence of both the α and the δ polymorphs based on the recorded melting points. This agrees only partly with what has been reported in the literature as several studies reported the presence of the γ form as well. The appearance of the metastable forms is consistent with the Ostwald step rule which hypothesises that during crystallisation crystal forms emerge successively in the order of decreasing entropy [96]. This explains why the δ form appeared before the α form as was revealed by microscopy and XRPD analysis. However, microscopy revealed the emergence of two different crystalline species before the appearance of the

α form. These two species were speculated to represent the δ form grown by two different modes, which were reflected in the shape of the calorimetric signal that was best fitted by 3-Lorentzian model. Although quantitative analysis of the deconvoluted peaks provided some non-physical values for the Avrami exponent n , qualitative analysis and rate constants were in reasonable agreement with microscopy and XRPD data. In drug stability assays determination of rate constants is more important than the determination of process mechanism since the former enables comparison between formulations and determination of product shelf life. Moreover, microcalorimetry appeared to be more sensitive than XRPD in terms of detecting early crystallisation.

Other interesting information can be obtained from the last phase (phase “f” Fig.6.2) of the power-time signal starting after 6.5 days of measurement. It is noted that after phase “e” (Fig.6.2) the low non-zero calorimetric signal starts decreasing at a very slow rate (phase “f”). This might indicate that the crystallisation process did not cease completely after phase “e” but proceeded at a slow rate. Alternatively, phase “f” might have arisen from a solid-solid transformation. This could be explained by the drop in peak intensity at diffraction angles 9.28° and 21.61° corresponding to crystalline species 1 after approximately 7 days (Fig.6.16). This occurred simultaneously with an increase in peak intensity at diffraction 8.48° corresponding to species 3 (or α form), which can be clearly seen at day 12. This means that the δ form could be transforming to the α form at 60°C .

Regarding the second objective of the study IMC was used to examine differences in the crystallisation behaviour of amorphous indomethacin prepared by cooling a bulk of melted material (ABI samples) or thin layer of indomethacin (AFI samples). Although both materials showed the same XRPD pattern, their calorimetric signals were significantly different reflecting differences in the crystallisation behaviour. Although

phase “c” (Fig.6.1 and Fig.6.2) was present for both AFI and ABI samples, it is significantly shorter for ABI samples. It could be therefore deduced that this phase of crystallisation is related to the free surface of the sample since the major difference one can think of in terms of the structure of AFI and ABI samples is the area of the free surface. AFI samples have greater free surface area and their phase “c” lasted longer. It was shown that indomethacin crystallisation at the surface was two orders of magnitude faster than that at the bulk below T_g [102]. Wu et al [118] showed that surface crystallisation was suppressed by depositing a ultrathin (a few nanometers thick) coating of gold or polyelectrolytes. It was speculated that this supports the notion that coating inhibits the mobility of a thin layer of surface molecules responsible for enabling surface crystallisation [118]. In the field of metallic glasses, Laudisio et al [119] found that powdered potassium heptagermanate glass samples crystallise initially to a metastable crystal form which then transform to a stable crystal form, whereas bulk potassium heptagermanate samples crystallised directly to the stable crystal form. The differences between the calorimetric signals for AFI and ABI samples have important implications in term of crystallisation studies from the amorphous state. Polarised light microscopy is widely used for this purpose and samples are usually prepared as a glob on top of a microscope glass. Although this glob simulates the film-like structure, results are usually generalised to bulk crystallisation as it was, for example, in Ref [63]. Furthermore, care should be taken when comparing different studies employing different preparation methods.

6.6. Summary

Isothermal microcalorimetry has been shown to be a useful tool to study the complex crystallisation processes of indomethacin above its T_g at 60°C. This technique provided both qualitative and quantitative information regarding this process especially for film-like amorphous samples. Quantitative analysis carried out with Lorentzian model to deconvolute the calorimetric signal was reasonably consistent with the analysis undertaken with light microscopy and XRPD. IMC was shown to be more sensitive than XRPD in detecting early crystallisation but less sensitive than PLM. This shows that the elegant characteristics of IMC can be exploited to study even complex crystallisation processes.

Qualitative analysis of calorimetric signal revealed significant differences in the crystallisation behaviour of film-like and bulky amorphous indomethacin samples. These differences were speculated to have originated from difference in the free surface area between the two differently prepared samples. Analysis of the final re-crystallised material with XRPD failed to reveal these differences as the two samples had the same polymorphic composition. This suggested that the preparation method should be taken into consideration when comparing crystallisation kinetics even if the same cooling method was used and same mechanical stress was applied.

Chapter 7: Conclusion and future work

Ensuring physical stability is a paramount requirement for the usage of amorphous pharmaceuticals. This thesis aimed at exploring different aspects of the stability of the amorphous state using mainly isothermal microcalorimetry. The main aims of the thesis were to:

- Compare enthalpy relaxation profile for a hydrophobic drug using IMC and DSC.
- Explore the feasibility of using TAM to assess enthalpy relaxation profiles for two-phase amorphous systems.
- Explore the effect of the anomeric composition of amorphous lactose on some aspects of its physical properties.
- Develop a calculation method to determine the reaction parameters for solid-state reactions using IMC.
- Assess the complex crystallisation processes with IMC
- Explore the effect of the preparation method on the crystallisation process of amorphous indomethacin above T_g using IMC.

Enthalpy relaxation studies are routinely undertaken to determine the stability of amorphous materials. DSC and IMC are both established techniques in enthalpy relaxation studies. The enthalpy relaxation profile for an amorphous hydrophobic drug, indomethacin, was determined using both DSC and IMC. The same relaxation profile was obtained from the two techniques when the same material was used. The value used for T_g to calculate $\Delta_r H(\infty)$ was found to affect the determined relaxation profile. Good agreement between DSC and IMC results was obtained when T_g at zero heating rate was used. This clarified the potential source of contradictory results present in the literature regarding whether DSC and IMC measure the same type of molecular

mobility. Our results suggest that the two techniques “look” at the same type of molecular mobility (α -relaxation). This conclusion can be verified further by comparing enthalpy relaxation profiles for other different pharmaceutical materials using the method proposed in this thesis.

Enthalpy relaxation of two-phase amorphous pharmaceutical systems was explored using IMC. The model fitting approach was employed to analyse the power-time data. The analysis was based on the assumption that the calorimetric output from the relaxation of a two-phase amorphous system is the sum of the outputs from the relaxation of each phase; and hence can be described by the sum of two models that described relaxation, namely the KWW and MSE models. Analysis of simulated data with the time derivative of the 2-KWW equation revealed that the model can successfully recover the correct relaxation parameters for each phase given that no phase predominates the signal. With real calorimetric data, the 2-KWW model appeared to be sensitive to inherent noise and failed to return the correct relaxation parameters. The 2-MSE model, on the other hand, appeared to be more robust and less sensitive to noise. The 2-MSE recovered the expected relaxation parameters for a sucrose-indomethacin system but not for a sucrose-lactose system likely due to possible interaction between sucrose and lactose. These findings suggest that IMC can be used to detect the effect of co-existence of amorphous pharmaceuticals on their relaxation profile.

The physical properties of an amorphous material depend on several factors. The effect of the anomeric composition was examined using amorphous lactose, a widely used pharmaceutical excipient. Amorphous α -lactose and β -lactose were prepared using ball milling. Some of the physical properties of the two materials were identified and

compared. Enthalpy relaxation studies using IMC revealed that the two anomers have different relaxation profiles with β -lactose relaxing at a faster rate.

The anomers, however, had similar T_g widths as was measured by DSC. This could have arisen from significant mutarotation during the DSC scan. Discrepancy between the relaxation and T_g widths studies could also have resulted from differences in the type of molecular mobility being measured by each study. An interesting, but erratic, phenomenon was observed when analysing ball-milled lactose with DSC. This was the emergence of low-temperature exotherm as well as the expected high-temperature recrystallisation exotherm. This could be a crystal defect rearrangement as it occurs at lower temperature i.e. it consumes lower energy than a high-temperature recrystallisation exotherm.

The effect of the anomeric composition on the interaction of amorphous lactose with moisture was also investigated. It appeared that, physically, the two anomers interacted similarly with moisture below 40% RH as they absorbed the same amounts of moisture. Above 40% RH, β -lactose crystallised more readily than α -lactose. Calculations using the Gordon-Taylor equation revealed that at 40% RH the amount of moisture absorbed results in decreasing the T_g of lactose to experimental temperature (25°C). Therefore, above T_g β -lactose has a greater tendency to crystallise than α -lactose. The anomeric composition affected greatly the type of polymorph that lactose crystallised to. α -lactose crystallised predominantly to α -lactose monohydrate, whereas β -lactose crystallised mainly to anhydrous β -lactose.

Although this study achieved the pre-defined aims, some aspects merit further investigation. For example, further work is needed to elucidate the nature of the pre- T_g exotherm and how ball-milling conditions affect it. This will have significant impact in

terms of improving the current understanding of the milling process and its effects on product properties and performance.

Water-solid interaction studies were sufficient to determine macroscopic differences between amorphous α -lactose and β -lactose. However, further comparison can be undertaken to determine the thermodynamic equilibrium constants (equilibrium constant (K), Van't Hoff enthalpy change (ΔH_v), Gibbs free energy for sorption (ΔG) and the entropy change for sorption (ΔS)) as was proposed by Willson and Beezer [120]. Such a study will allow a better understanding regarding the effect of the anomeric form on the properties of amorphous lactose.

Crystallisation from the amorphous state represents a significant stability issue. This solid-state reaction was examined using IMC. Often the process can be very slow or the initial, or final, parts of IMC data are missing. This renders analysis using the model fitting approach unachievable since the parameters of the universal Sestak-Berggren equation are not integral and analysis of calorimetric data would require the total heat output to be known. In order to solve this problem, a calculation method based on the universal solid state equation, Sestak-Berggren equation, was developed. The calculation method was applied to simulated power-time data for a solid state reaction. The method was found to be successful if only 15% of the total reaction heat is available. The calculation method was then applied to real calorimetric data that resulted from the crystallisation of amorphous indomethacin at three different temperatures (25⁰C, 30⁰C and 35⁰C). These were also analysed using the model fitting approach to get reference values for crystallisation parameters. Agreement between calculated and fit values was erratic and this is likely to be due to inherent noise associated with real calorimetric data. However, it was noted that narrow variation was

obtained for the calculated $c.k$ value when the correct reference values were obtained from the calculation method. This could be used as a test to verify the accuracy of the calculation method. This work provided successfully a calculation method to determine the parameters for solid-state reactions using calorimetric data given that the initial or final part of the reaction was recorded. Further work in this aspect might consider the development of new calculation strategies applicable to data when both the initial and final parts of the reaction are missing.

The calculation method proposed in Chapter 5 is applicable to calorimetric data when only one solid-state reaction is taking place. When multiple processes are occurring simultaneously, a different analysis approach should be adopted. Crystallisation of amorphous indomethacin above T_g (at 60°C) was a good case scenario as the drug crystallised into more than one crystal form. Indomethacin samples were prepared directly in the TAM ampoules as film-like (AFI) and bulk samples (ABI). Qualitatively, the two types of indomethacin samples showed different power-time profiles. This indicated that the preparation method had an impact on the crystallisation behaviour. This difference is partially attributed to differences in the total free surface area between AFI and ABI samples. Deconvolution of the calorimetric signal was not achievable for ABI samples as the signal was complex reflecting complexity of the crystallisation process. The signal for the AFI sample was simpler and could be deconvoluted to three different peaks. This suggests that amorphous indomethacin crystallised to three different crystalline species. AFI samples crystallisation was also monitored using XRPD and PLM. IMC appeared less sensitive than PLM at detecting onset of crystallisation but more sensitive than XRPD. After IMC analysis, AFI samples were also analysed with DSC. DSC analysis revealed the presence of only two crystalline polymorphs, namely α and δ . XRPD and IMC data revealed that the α form

appeared after 5 days of storage at 60°C. PLM and IMC data showed that two different crystalline species appeared within 2 days of storage at 60°C. These two crystalline species were speculated to be two different crystal habits for the δ form.

This work demonstrated that IMC can be used to monitor complex crystallisation processes. Deconvolution of the signal is the main challenge in analysing the resulting calorimetric output. Chemometric analysis has been suggested as a possible approach to deconvolute complex calorimetric data [22, 54, 56]. This method can offer a great advantage since it is model-free [56]. It was applied successfully to deconvolute simulated calorimetric data for the solution-state reactions [56]. It was identified that at least $2n+2$ repeats for the experimental are needed to form a matrix where n is the total number of processes taking place. Time and power are two readily available from the calorimetric data, whereas a third variable can be obtained from variation in sample weight.

The effect of the preparation method can be examined further using other pharmaceutical materials and systems such as amorphous solid dispersions. Gaisford et al [115] demonstrated that IMC can be used to monitor the crystallisation of indomethacin oral films and obtained both qualitative and quantitative information about the kinetics of the process.

In this thesis, it was shown that IMC can be used to explore different aspects of the stability of the amorphous state. The technique is highly sensitive to detect both relaxation and crystallisation processes. It also requires minimal sample preparation and allows direct monitoring of the material's behaviour. However, one should be aware of the challenges involved with use of IMC. For example, relaxation studies require good control of the sample's thermal history. Data analysis can be challenging when different processes occur simultaneously. A model-free approach should be used

to analyse the data whenever possible. Further work is needed to develop this approach of calorimetric data analysis.

References

- [1] Roberts CJ, Debenedetti PG. Engineering pharmaceutical stability with amorphous solids. *AIChE Journal*. 2002;48(6):1140-4.
- [2] Byrn SR, Pfeiffer RR, Stowell JG. *Solid-state chemistry of drugs*. 2nd ed. Indiana: SSCI 1999.
- [3] Aulton ME. *Pharmaceutics: the science of dosage form design*. 2nd ed. London: Churchill Livingstone 2002.
- [4] Hancock BC, Zografi G. Characteristics and significance of the amorphous state in pharmaceutical systems. *J Pharm Sci*. 1997 Jan;86(1):1-12.
- [5] Cui Y. A material science perspective of pharmaceutical solids. *Int J Pharm*. 2007;339:3-18.
- [6] Yoshioka S, Aso Y. Correlations between molecular mobility and chemical stability during storage of amorphous pharmaceuticals. *J Pharm Sci*. 2007 May;96(5):960-81.
- [7] Hancock BC, Parks M. What is the true solubility advantage for amorphous pharmaceuticals? *Pharm Res*. 2000 Apr;17(4):397-404.
- [8] Sebhatu T, Elamin AA, Ahlneck C. Effect of moisture sorption on tableting characteristics of spray dried (15% amorphous) lactose. *Pharm Res*. 1994;11:1233-8.
- [9] Suzuki T, Imamura K, Yamamoto K, Satoh T, Okazaki M. Thermal stabilisation of freeze-dried enzymes by sugars. *Journal of Chemical Engineering of Japan*. 1997;30:609-13.
- [10] Yu Z, Rogers TL, Hu J, Johnston K, Williams III RO. Preparation and characterisation of microparticles containing peptide produced by a novel process: spray freezing into liquid. *Eu J Pharm Biopharm*. 2002;54:221-8.
- [11] Hinrichs WLJ, Prinsen MG, Frijlink HW. Inulin glasses for the stabilisation of therapeutic proteins. *Int J Pharm*. 2001;215:163-74.
- [12] Bhugra C, Pikal MJ. Role of thermodynamic, molecular, and kinetic factors in crystallization from the amorphous state. *J Pharm Sci*. 2008 Apr;97(4):1329-49.
- [13] Ward GH, Schultz RK. Process-induced crystallinity changes in albuterol sulfate and its effect on powder physical stability. *Pharm Res*. 1995;12:773-9.
- [14] Mackin LA, Sartnurak S, Thomas I, Moore S. The impact of low levels of amorphous material (< 5%) on the blending characteristics of a direct compression formulation. *Int J Pharm*. 2002;231:213-26.
- [15] Pikal MJ, Lukes AL, Lang JE. Thermal decomposition of amorphous beta-lactam antibacterials. *J Pharm Sci*. 1977;66(13):12-1316.
- [16] Oberholtzer ER, Brenner GS. Cefoxitin sodium: solution and solid-state chemical stability studies. *J Pharm Sci*. 1979;68:863-6.
- [17] Guo Y, Byrn SR, Zografi G. Physical characteristics and chemical degradation of amorphous quinapril hydrochloride. *J Pharm Sci*. 2000;89:128-43.
- [18] Ahlqvist MUA, Taylor LS. Water diffusion in hydrated crystalline and amorphous sugars monitored using H/D exchange. *J Pharm Sci*. 2002;91(3):690-8.
- [19] Atkins PW. *The elements of physical chemistry*. Oxford: Oxford University Press 1992.
- [20] Yu L. Amorphous pharmaceutical solids: preparation, characterisation and stabilisation. *Adv Drug Deliv Rev*. 2001;48:27-42.
- [21] Ediger MD, Angell CA, Nagel SR. Supercooled liquids and glasses. *J Phys Chem* 1996;100:13200-12.
- [22] Gaisford S, O'Neill MAA. *Pharmaceutical Isothermal Calorimetry*. New York: Informa Healthcare 2006.
- [23] Kawakami K, Pikal MJ. Calorimetric investigation of the structural relaxation of amorphous materials: evaluating validity of the methodologies. *J Pharm Sci*. 2005 May;94(5):948-65.
- [24] Hancock BC. Disordered drug delivery: destiny, dynamics and the Deborah number. *JPP*. 2002;54:737-46.
- [25] Aso Y, Yoshioka S, Kojima S. Explanation of the relaxation rate of nifedipine and phenobarbital from their molecular mobility as measured by ¹³C nuclear magnetic resonance

relaxation time and the relaxation time obtained from the heating rate dependence of the glass transition temperature. *J Pharm Sci.* 2001;90:798-806.

[26] Shamblin SL, Hancock BC, Pikal MJ. Coupling between chemical reactivity and structural relaxation in pharmaceutical glasses. *J Pharm Res.* 2006;23:2254-68.

[27] Liu J, Rigsbee DR, Stotz C, Pikal MJ. Dynamics of pharmaceutical amorphous solids: the study of enthalpy relaxation by isothermal microcalorimetry. *J Pharm Sci.* 2002 Aug;91(8):1853-62.

[28] Shamblin SL, Hancock BC, Dupuis Y, Pikal MJ. Interpretation of relaxation time constants for amorphous pharmaceutical systems. *J Pharm Sci.* 2000;89:417-27.

[29] Hilden LR, Morris KR. Physics of amorphous solids. *J Pharm Sci.* 2004 Jan;93(1):3-12.

[30] Ahlneck C ZG. The molecular basis of moisture effects on the physical and chemical stability of drugs in the solid state. *Int J Pharm.* 1990;62:87-95.

[31] Buckton G. Interfacial phenomena in drug delivery and targeting. Singapore: Harwood academic publishers 1995.

[32] Hancock BC, Zografi G. The relationship between the glass transition temperature and the water content of amorphous pharmaceutical solids. *Pharm Res.* 1994 Apr;11(4):471-7.

[33] Buckton G, Darcy P. Water mobility in amorphous lactose below and close to the glass transition temperature. *Int J Pharm.* 1996;136:141-6.

[34] Buckton G, Darcy P. The use of gravimetric studies to assess the degree of crystallinity of predominantly crystalline powders. *Int J Pharm.* 1995;123:265-71.

[35] Buckton G, Darcy P, Mackellar A. The use of isothermal microcalorimetry in the study of small degrees of amorphous content of powders. *Int J Pharm.* 1995;117:253-6.

[36] Lacmann R, Herden A, Mayer C. Kinetics of nucleation and crystal growth. *Chem Eng Technol.* 1999;22:279-89.

[37] Khawam A, Flanagan DR. Solid-state kinetic models: basics and mathematical fundamentals. *J Phys Chem B.* 2006;110:17315-28.

[38] Perez-Maqueda LA, Criado JM, Sanchez-Jimenez PE. Combined kinetic analysis of solid-state reactions: a powerful tool for the simultaneous determination of kinetic parameters and the kinetic model without previous assumptions on the reaction mechanism. *J Phys Chem A.* 2006;110:12456-62.

[39] Zhou D, Zhang GG, Law D, Grant DJW, Schmidt EA. Physical stability of amorphous pharmaceuticals: importance of configurational thermodynamic quantities and molecular mobility. *J Pharm Sci.* 2002;91:1863-72.

[40] Siniti M, Carre J, Ietto JM, Bastide JP, Claudy P. The thermal behaviour of hexitols: part1. Vitrification and crystallisation of iditol, mannito, sorbitol and dulcitol. *Thermochim Acta.* 1993;224:97-104.

[41] Carpentier L, Desprez S, Descamps M. Crystallisation and glass properties of pentitols: Xylitol, adonitol, arabitols *J Therm Anal Cal.* 2003;73:577-86.

[42] Aso Y, Yoshioka S, Kojima S. Explanation of the crystallisation rate of amorphous nifedipine and phenobarbital from their molecular mobility as measured by ¹³C nuclear magnetic resonance relaxation time and the relaxation time obtained from the heating rate dependence of the glass transition temperature. *J Pharm Sci.* 2001;90:798-806.

[43] Masuda K, Tabata S, Sakata Y, Hayase T, Yonemochi E, Terada K. Comparison of molecular mobility in the glassy state between amorphous indomethacin and salicin based on spin-lattice relaxation times. *Pharm Res.* 2005;22:797-805.

[44] Alie J, Menegotto J, Cardon P, Duplaa H, Caron A, Lacabanne C, et al. Dielectric study of the molecular mobility and the isothermal crystallisation kinetics of an amorphous pharmaceutical drug substance. *J Pharm Sci.* 2004;93:218-33.

[45] Beezer AE, S G, Hills AK, Willson RJ, Mitchell JC. Pharmaceutical microcalorimetry: applications to long-term stability studies. *Int J Pharm.* 1999;179:159-65.

[46] Spray Drying Information from GEA Niro. [cited 14/06/2010]; Available from: <http://www.niro.com/niro/cmsdoc.nsf/WebDoc/ndkk5hmc6zSprayDryersSprayDryers>

- [47] Mio H, Kano J, Saito F, Kaneko K. Effects of rotational direction and rotation-to-revolution speed ratio in planetary ball milling. *Mat Sci Eng A*. 2002;332:75-80.
- [48] Gaisford S. Calorimetry as a process analytical tool for micronising pharmaceuticals. *Eu Pharm Rev*. 2009(1):28-30.
- [49] Wadsö I. Isothermal microcalorimetry near ambient temperature: An overview and discussion. *Thermochim Acta*. 1997;294:1-11.
- [50] Wadsö I. Isothermal microcalorimetry: current problems and prospects. *Thermal Anal Calorim*. 2001;64:75-84.
- [51] Angberg M, Nyström C. Evaluation of heat-conduction microcalorimetry in pharmaceutical stability studies. *Acta Pharm Suec* 1988;25:307-20.
- [52] Willson RJ, Beezer AE, Mitchell JC, Loh W. determination of thermodynamic and kinetic parameters from isothermal heat conduction microcalorimetry: Applications to long-term reaction studies. *J Phys Chem A*. 1995;99:7108-13.
- [53] Bakri A, Janssen LHM, Wilting J. Determination of reaction rate parameters using heat conduction microcalorimetry. *J Therm Anal Cal*. 1988;33:185-90.
- [54] Beezer AE, O'Neill M, Urakami K, Connor JA, Tetteh J. Pharmaceutical microcalorimetry: recent advances in the study of solid-state materials. *Thermochim Acta*. 2004;420:19-22.
- [55] O'Neill M, Beezer AE, Morris AC, Urakami K, Willson RJ, Connor JA. Solid-state reactions from isothermal heat conduction microcalorimetry: theoretical approach and evaluation via simulated data. *J Therm Anal Cal*. 2003;73:709-14.
- [56] O'Neill M, Beezer AE, Tetteh J, Gaisford S, Dhuna M. Application of chemometric analysis to complexity in isothermal calorimetric data. *J Phys Chem B*. 2007;111:8145-9.
- [57] Craig DQM, Reading M. *Thermal analysis of pharmaceuticals*. London: CRC Press 2007.
- [58] Hill VL, Craig DQM, Feely LC. Characterisation of spray-dried lactose using modulated differential scanning calorimetry. *Int J Pharm*. 1998;161:95-107.
- [59] Yu X, Kappes SM, Bello-Perez LA, Schmidt SJ. Investigating the moisture sorption behaviour of amorphous sucrose using a dynamic humidity generating instrument. *J Food Sci*. 2008;73(1):25-35.
- [60] Lane RA, Buckton G. The novel combination of dynamic vapour sorption gravimetric analysis and near infra-red spectroscopy as a hyphenated technique. *Int J Pharm*. 2000;207:49-56.
- [61] Dincer TD, Parkinson GM, Rohl AL, Ogden MI. Crystallisation of α -lactose monohydrate from dimethyl sulfoxide (DMSO) solutions: influence of β -lactose. *J Cryst Growth*. 1999;205:368-74.
- [62] Willart JF, Caron V, Lefort R, Danede F, Prevost D, Descamps M. Athermal character of the solid state amorphization of lactose induced by ball milling. *Solid State Commun*. 2004;132:693-6.
- [63] Bhugra C, Shmeis R, Krill SL, Pikal MJ. Prediction of onset of crystallisation from experimental relaxation times. II. Comparison between predicted and experimental onset times. *J Pharm Sci*. 2008;97(1):455-72.
- [64] Bhugra C, Shmeis R, Krill SL, Pikal MJ. Prediction of onset of crystallisation from experimental times I-Correlation of molecular mobility from temperatures above the glass transition to temperatures below the glass transition. *Pharm Res*. 2006;23(10):2277-90.
- [65] Van den Mooter G, Augustijns P, Kinget R. Stability prediction of amorphous benzodiazepines by calculation of the mean relaxation time constant using the Williams-Watts decay function. *Eur J Pharm Biopharm*. 1999 Jul;48(1):43-8.
- [66] Haque MK, Kawai K, Suzuki T. Glass transition and enthalpy relaxation of amorphous lactose glass. *Carbohydr Res*. 2006 Aug 14;341(11):1884-9.
- [67] Hancock BC, Shamblin SL, Zografi G. Molecular mobility of amorphous pharmaceutical solids below their glass transition temperatures. *Pharm Res*. 1995 Jun;12(6):799-806.

- [68] Hasegawa S, Ke P, Buckton G. Determination of the structural relaxation at the surface of amorphous solid dispersion using inverse gas chromatography. *J Pharm Sci.* 2009 Oct 3;98:2133-9.
- [69] Shamblin SL, Zografi G. Enthalpy relaxation in binary amorphous mixtures containing sucrose. *Pharm Res.* 1998 Dec;15(12):1828-34.
- [70] Matsumoto T, Zografi G. Physical properties of solid molecular dispersions of indomethacin with poly(vinylpyrrolidone) and poly(vinylpyrrolidone-co-vinyl-acetate) in relation to indomethacin crystallization. *Pharm Res.* 1999 Nov;16(11):1722-8.
- [71] Aso Y, Yoshioka S, Kojima S. Molecular mobility-based estimation of the crystallization rates of amorphous nifedipine and phenobarbital in poly(vinylpyrrolidone) solid dispersions. *J Pharm Sci.* 2004 Feb;93(2):384-91.
- [72] Korhonen O, Bhugra C, Pikal MJ. Correlation between molecular mobility and crystal growth of amorphous phenobarbital and phenobarbital with polyvinylpyrrolidone and L-proline. *J Pharm Sci.* 2008 Sep;97(9):3830-41.
- [73] Bhugra C, Shmeis R, Pikal MJ. Role of mechanical stress in crystallization and relaxation behavior of amorphous indomethacin. *J Pharm Sci.* 2008 Oct;97(10):4446-58.
- [74] Craig DQM, Barnes M, Royall PG, Kett VL. An evaluation of the use of modulated temperature DSC as a means of assessing the relaxation behaviour of amorphous lactose. *Pharm Res.* 2000;17(6):696-700.
- [75] Zografi G, Grandolfi GP, Kontny MJ, DW. M. Prediction of moisture transfer in mixtures of solids: transfer via the vapour phase. *Int J Pharm.* 1988;42:77-88.
- [76] Skaria CV, Gaisford S, O'Neill MA, Buckton G, Beezer AE. Stability assessment of pharmaceuticals by isothermal calorimetry: two component systems. *Int J Pharm.* 2005 Mar 23;292(1-2):127-35.
- [77] Burnett DJ, Thielmann F, Sokoloski T, Brum J. Investigating the moisture-induced crystallisation kinetics of spray-dried lactose. *Int J Pharm.* 2006;313:23-8.
- [78] Lefort R, Caron V, Willart JF, Descamps M. Mutarotational kinetics and glass transition of lactose. *Solid State Commun.* 2006;140:329-34.
- [79] Buckton G, Chidavaenzi OC, Koosha F. The effect of spray-drying feed temperature and subsequent crystallization conditions on the physical form of lactose. *AAPS PharmSciTech.* 2002;3(4):1-6
- [80] Otsuka M, Ohtani H, Kaneniwa N, Higuchi S. Isomerization of lactose in solid-state by mechanical stress during grinding. *J Pharm Pharmacol.* 1991;43:148-53.
- [81] Diogo HP, Pinto SS, Ramos JJM. Thermal behaviour and slow molecular mobility in two isomers of biphenylmethanol DSC and TSDC study. *J Therm Anal Cal.* 2006;83(2):361-6.
- [82] Diogo HP, Pinto SS, Ramos JJM. Slow molecular mobility in the crystalline and amorphous solid states of pentitols: a study by thermally stimulated depolarisation currents and by differential scanning calorimetry. *Carbohydr Res.* 2007;342:961-9.
- [83] Crowley KJ, Zografi G. The use of thermal methods for predicting glass-former fragility. *Thermochim Acta.* 2001;380:79-93.
- [84] Hancock BC, Dalton CR, Pikal MJ, Shamblin SL. A pragmatic test of a simple calorimetric method for determining the fragility of some amorphous pharmaceutical materials. *Pharm Res.* 1998;15(5):762-7.
- [85] Moynihan CT, Lee SK, Tatsumisago M, Minami T. Estimation of activation energies for structural relaxation and viscous flow from DTA and DSC experiments. *Thermochim Acta.* 1996;280/281:153-62.
- [86] Pikal MJ, Chang LL, Tang XC. Evaluation of glassy-state dynamics from the width of the glass transition: results from theoretical simulation of differential scanning calorimetry and comparisons with experiment. *J Pharm Sci.* 2004;93:981-94.
- [87] Chidavaenzi OC. The effect of spray drying on the physicochemical properties of products. London: School of Pharmacy, University of London; 1999.

- [88] Angberg M, Nyström C, Castensson S. Evaluation of heat-conduction microcalorimetry in pharmaceutical stability studies. III. Crystallographic changes due to water vapour uptake in anhydrous lactose powder. *Int J Pharm*. 1991;73:209-20.
- [89] Kedward CJ, MacNaughtan W, Mitchell JR. Crystallisation kinetics of amorphous lactose as a function of moisture content using isothermal differential scanning calorimetry. *J Food Sci*. 2000;65(2):324-8.
- [90] Willart JF, Caron V, Descamps M. Transformations of crystalline sugars upon milling. *J Therm Anal Cal*. 2007;90(1):125-30.
- [91] Feng T, Pinal R, Carvajal MT. Process induced disorder in crystalline materials: differentiating defective crystals from the amorphous form of griseofulvin. *J Pharm Sci*. 2008;97(8):3207-21.
- [92] Burnett DJ, Thielmann F, Booth J. Determining the critical relative humidity for moisture-induced phase transitions *Int J Pharm*. 2004;287:123-33.
- [93] Haque MK, Roos YH. Crystallisation and X-ray diffraction of spray-dried and freeze-dried amorphous lactose. *Carbohydr Res*. 2005;340:293-301.
- [94] Ambarkhane AV, Pincott K, Buckton G. The use of inverse gas chromatography and gravimetric vapour sorption to study transitions in amorphous lactose. *Int J Pharm*. 2005;294:129-35.
- [95] Sacchetti M. Thermodynamic analysis of moisture sorption isotherms. *J Pharm Sci*. 1998;87(8):982-6.
- [96] Andronis V, Yoshioka M, Zografi G. Effects of sorbed water on the crystallisation of indomethacin from amorphous state. *J Pharm Sci*. 1997;86(3):346-51.
- [97] Lehto VP, Laine E. A kinetic study on crystallization of an amorphous lubricant. *Pharm Res*. 1997 Jul;14(7):899-904.
- [98] Kawakami K, Miyoshi K, Tamura N, Yamaguchi T, Ida Y. Crystallization of sucrose glass under ambient conditions: evaluation of crystallization rate and unusual melting behavior of resultant crystals. *J Pharm Sci*. 2006 Jun;95(6):1354-63.
- [99] Supaphol P. Application of the Avrami, Tobin, Malkin, and Urbanovici-Segal macrokinetic models to isothermal crystallisation of syndiotactic polypropylene. *Thermochim Acta*. 2001;370:37-48.
- [100] Zhou D, Schmitt EA, Zhang GG, Law D, Vyazovkin S, Wight CA, et al. Crystallisation kinetics of amorphous nifedipine studied by model-fitting and model-free approaches. *J Pharm Sci*. 2003;92(9):1779-92.
- [101] Wu T, Yu L. Origin of enhanced crystal growth kinetics near T_g probed with indomethacin polymorphs. *J Phys Chem B*. 2006 Aug 17;110(32):15694-9.
- [102] Wu T, Yu L. Surface crystallization of indomethacin below T_g. *Pharm Res*. 2006 Oct;23(10):2350-5.
- [103] Otsuka M, Kato F, Matsuda Y. Physicochemical stability of cimetidine amorphous forms estimated by isothermal microcalorimetry. *AAPS PharmSciTech*. 2002;3(4):1-13.
- [104] Aso Y, Yoshioka S, Kojima S. Feasibility of using isothermal microcalorimetry to evaluate the physical stability of amorphous nifedipine and phenobarbital. *Thermochim Acta*. 2001;380:199-204.
- [105] Latsch S, Selzer T, Fink L, Kreuter J. Crystallisation of estradiol containing TDDS determined by isothermal microcalorimetry, X-ray diffraction, and optical microscopy. *Eu J Pharm Biopharm*. 2003;56:43-52.
- [106] Latsch S, Selzer T, Fink L, Kreuter J. Determination of the physical state of norethindrone acetate containing transdermal drug delivery systems by isothermal microcalorimetry, X-ray diffraction, and optical microscopy. *Eu J Pharm Biopharm*. 2004;57:383-95.
- [107] Schubert MA, Schicke BC, Muller-Goymann CC. Thermal analysis of the crystallization and melting behavior of lipid matrices and lipid nanoparticles containing high amounts of lecithin. *Int J Pharm*. 2005 Jul 14;298(1):242-54.

- [108] Beezer AE, Morris AC, O'Neill MAA, Willson RJ, Hills AK, Mitchell JC, et al. Direct determination of equilibrium thermodynamic and kinetic parameters from isothermal heat conduction microcalorimetry. *J Phys Chem B*. 2001;105:1212-5.
- [109] Yoshioka M, Hancock BC, Zografi G. Crystallization of indomethacin from the amorphous state below and above its glass transition temperature. *J Pharm Sci*. 1994 Dec;83(12):1700-5.
- [110] Phipps MA, Mackin LA. Application of isothermal microcalorimetry in solid state drug development. *PSTT*. 2000;3(1):9-17.
- [111] Joshi V. Physical transformations in solvated pharmaceuticals. IN: Purdue University; 1998.
- [112] Crowley KJ, Zografi G. Cryogenic grinding of indomethacin polymorphs and solvates: assessment of amorphous phase formation and amorphous phase physical stability. *J Pharm Sci*. 2002 Feb;91(2):492-507.
- [113] Trofimov VI, Trofimov IV, Kim J. The effect of finite film thickness on the crystallisation kinetics of amorphous film and microstructure of crystallised film. *Thin Solid Films*. 2006;495(1-2):398-403.
- [114] Narine SS, Humphrey KL, Bouzidi L. Modification of the Avrami model for application to the kinetics of the melt crystallisation of lipids. *JAOCs*. 2006;83(11):913-21.
- [115] Gaisford S, Verma A, Saunders M, Royall PG. Monitoring crystallisation of drugs from fast-dissolving oral films with isothermal calorimetry. *Int J Pharm*. 2009;380:105-11.
- [116] Vazquez J, Gonzalez-Palma R, Lopez-Aleman PL, Villares P, Jimenez-Garay R. Impingement effect on the glass-crystal transformation kinetics by using DSC under non-isothermal regime. Application to the crystallisation of the several semiconducting alloys of the Sb-As-Se and Ge-Sb-Se glassy systems. *J Phys Chem Solids*. 2005;66(7):1264-73.
- [117] Crowley KJ, Zografi G. The effect of low concentrations of molecularly dispersed poly(vinylpyrrolidone) on indomethacin crystallization from the amorphous state. *Pharm Res*. 2003 Sep;20(9):1417-22.
- [118] Wu T, Sun Y, de Villiers MM, Yu L. Inhibiting surface crystallisation of amorphous Indomethacin by Nanocoating. *Langmuir*. 2007;23(9):5148-53.
- [119] Laudisio G, Catauro M. Bulk and surface crystallisation of potassium heptagermanate glass. *Physics and Chemistry of glasses*. 1997;38(5):244-5.
- [120] Willson RJ, Beezer AE. The determination of equilibrium constants, ΔG , ΔH and ΔS for vapour interaction with a pharmaceutical drug, using gravimetric vapour sorption. *Int J Pharm*. 2003 Jun 4;258(1-2):77-83.